

“INSITU ROCK MODULUS APPARATUS”

**Contract No. BC-354
RPWO No. 13**

Submitted To:

Mr. Richard Long, Research Center Director
Mr. Peter Lai, PE, Project Manager
Florida Department of Transportation
605 Suwannee Street, M.S.30
Tallahassee, FL 32399-0450

23 August 2004

Submitted By:

University of Florida
Department of Civil and Coastal Engineering
365 Weil Hall
PO Box 116580
Gainesville, FL 32611

Paul J. Bullock, PhD, PE, Asst. Professor

1. Report No.		2. Government Accession No.		3. Recipient's Catalog No.	
4. Title and Subtitle Insitu Rock Modulus Apparatus				5. Report Date 23 August 2004	
				6. Performing Organization Code	
				8. Performing Organization Report No. 4910-4504-721-12	
7. Author(s) Paul J. Bullock, PhD, PE				10. Work Unit No. (TRAIS) RPWO 13	
9. Performing Organization Name and Address University of Florida Department of Civil and Coastal Engineering 365 Weil Hall / P.O. Box 116580 Gainesville, FL 32611-6580				11. Contract or Grant No. BC-354	
				13. Type of Report and Period Covered Final Report 30 September 1999 - 23 August 2004	
				14. Sponsoring Agency Code	
12. Sponsoring Agency Name and Address Florida Department of Transportation Research Management Center 605 Suwannee Street, MS 30 Tallahassee, FL 32301-8064					
15. Supplementary Notes FDOT Project Manager Mr. Peter Lai					
16. Abstract <p>Drilled shaft foundations socketed into limestone support many Florida structures and bridges through weak overburden soils. The current design method for side shear capacity of drilled shafts in the highly variable Florida limestone uses compressive and tensile strength tests of rock cores. However, these tests represent only the recovered, intact portion of the rock core, not the rock mass. The pressuremeter measures rock strength insitu and should accurately reflect the properties of the rock mass while reducing lab-testing effort. The research described herein includes pressuremeter tests in both laboratory and field tests to estimate the strength and stiffness of Florida limestone. It also includes the measurement of modulus and strength on rock core samples by the Florida Department of Transportation and the University of Florida (UF). It also includes Probex-1 and Texam pressuremeter tests performed by UF, eight tests in the lab in "Gatorock", a synthetic limestone developed for this research, and 31 tests in the field at the SR20 Blountstown Bridge adjacent to two test shafts. This report compares the pressuremeter modulus, yield pressure, and limit pressure to similar core test results. It presents a database of 419 comparisons of q_u vs. q_t and 173 comparisons of q_u vs. E_i based on limestone core tests from six bridge sites. Pressuremeter tests in the lab proved successful, but tests using the Probex-1 in the field compared poorly with core tests and with the capacity of the adjacent test shafts. Site variability and weak rock affected these comparisons. An empirical design method, published by Laboratoire des Ponts et Chaussees (LPC), provided the best estimate of the drilled shaft unit side shear, but it requires further calibration before design use in Florida.</p>					
17. Key Words Drilled Shaft Capacity, Deep Foundation, Florida Limestone, Side Shear, Modulus, Unconfined Compression, Split Tensile, Rock Pressuremeter, Limit Pressure, Yield Pressure, Cracking			18. Distribution Statement No restrictions.		
19. Security Classif. (of this report) Unclassified		20. Security Classif. (of this page) Unclassified		21. No. of Pages 146	22. Price

DISCLAIMER

The opinions, findings and conclusions expressed in this publication are those of the author and not necessarily those of the Florida Department of Transportation or the U.S. Department of Transportation. This publication was prepared in cooperation with the State of Florida Department of Transportation and the U.S. Department of Transportation.

Final Report Contract #BC354 RPWO #13

SI* (MODERN METRIC) CONVERSION FACTORS					
Property	Symbol	When You Know	Multiply By	To Find	Symbol
APPROXIMATE CONVERSIONS TO SI UNITS					
LENGTH	in	inches	25.4	millimeters	mm
	ft	feet	0.305	meters	m
	yd	yards	0.914	meters	m
	mi	miles	1.61	kilometers	km
AREA	in ²	square inches	645.2	square millimeters	mm ²
	ft ²	square feet	0.093	square meters	m ²
	yd ²	square yards	0.836	square meters	m ²
	ac	acres	0.405	hectares	ha
VOLUME	mi ²	square miles	2.59	square kilometers	km ²
	fl oz	fluid ounces	29.57	milliliters	ml
	gal	gallons	3.785	liters	l
	ft ³	cubic feet	0.028	cubic meters	m ³
MASS	yd ³	cubic yards	0.765	cubic meters	m ³
	oz	ounces	28.35	grams	g
	lb	pounds	0.454	kilograms	kg
TEMPERATURE (exact)	T	short tons (2000lb)	0.907	megagrams	Mg
	°F	Fahrenheit temperature	(°F-32)/1.8	Celsius temperature	°C
IILLUMINATION	fc	foot-candles	10.76	lux	lx
	fl	foot-Lamberts	3.426	candela/m ²	cd/m ²
FORCE	lbf	poundforce	4.45	Newtons	N
PRESSURE	psi	poundforce/square inch	6.89	kiloPascals	kPa
APPROXIMATE CONVERSIONS FROM SI UNITS					
LENGTH	mm	millimeters	0.039	inches	in
	m	meters	3.28	feet	ft
	m	meters	1.09	yards	yd
	km	kilometers	0.621	miles	mi
AREA	mm ²	square millimeters	0.0016	square inches	in ²
	m ²	square meters	10.764	square feet	ft ²
	m ²	square meters	1.195	square yards	yd ²
	ha	hectares	2.47	acres	ac
	km ²	square kilometers	0.386	square miles	mi ²
VOLUME	ml	milliliters	0.034	fluid ounces	fl oz
	l	liters	0.264	gallons	gal
	m ³	cubic meters	35.71	cubic feet	ft ³
	m ³	cubic meters	1.307	cubic yards	yd ³
MASS	g	grams	0.035	ounces	oz
	kg	kilograms	2.202	pounds	lb
	Mg	megagrams	1.103	short tons (2000lb)	T
TEMPERATURE (exact)	°C	Celsius temperature	1.8°C + 32	Fahrenheit temperature	°F
IILLUMINATION	lx	lux	0.0929	foot-candles	fc
	cd/m ²	candela/m ²	0.2919	foot-Lamberts	fl
FORCE	N	Newtons	0.225	poundforce	lbf
PRESSURE	kPa	kiloPascals	0.145	poundforce/square inch	psi

* SI is the symbol for the International System of Units.

(Revised August 1992)

Appropriate rounding should be made to comply with Section 4 of ASTM E380

ACKNOWLEDGEMENTS

The author wishes to thank the Florida Department of Transportation for funding and supporting this research. In particular, Project Manager Mr. Peter Lai, District 3 Geotechnical Engineer Mr. Sam Weede, and District 3 Drilling Supervisor Mr. Mike Suggs are recognized for their valuable assistance during this project.

Many at UF deserve recognition and thanks. Dr. Bjorn Birgisson, Dr. Michael McVay, and Dr. Ching Kuo started this research and provided assistance during the work. UF graduate students Mr. Carlos Cepero and Mr. Scott Jacobs performed and analyzed many tests at the UF laboratory and the SR20 site. UF Assistant-in-Engineering Mr. Chris Kohlhof and UF machinist Mr. Danny Brown helped prepare the lab samples and lab equipment for testing. The geotechnical faculty and the staff, and administration of the UF Civil and Coastal Engineering Department and the UF College of Engineering, supported this work indirectly, and deserve thanks as well.

ABSTRACT

Drilled shaft foundations socketed into limestone support many Florida structures and bridges through weak overburden soils. The current design method for side shear capacity of drilled shafts in the highly variable Florida limestone uses compressive and tensile strength tests of rock cores. However, these tests represent only the recovered, intact portion of the rock core, not the rock mass. The pressuremeter measures rock strength insitu and should accurately reflect the properties of the rock mass while reducing lab-testing effort. The research described herein includes pressuremeter tests in both laboratory and field tests to estimate the strength and stiffness of Florida limestone. It also includes the measurement of modulus and strength on rock core samples by the Florida Department of Transportation and the University of Florida (UF). It also includes Probex-1 and Texam pressuremeter tests performed by UF, eight tests in the lab in "Gatorock", a synthetic limestone developed for this research, and 31 tests in the field at the SR20 Blountstown Bridge adjacent to two test shafts. This report compares the pressuremeter modulus, yield pressure, and limit pressure to similar core test results. It presents a database of 419 comparisons of q_u vs. q_t and 173 comparisons of q_u vs. E_i based on limestone core tests from six bridge sites. Pressuremeter tests in the lab proved successful, but tests using the Probex-1 in the field compared poorly with core tests and with the capacity of the adjacent test shafts. Site variability and weak rock affected these comparisons. An empirical design method, published by Laboratoire des Ponts et Chaussées (LPC), provided the best estimate of the drilled shaft unit side shear, but it requires further calibration before design use in Florida.

TABLE OF CONTENTS

	Page
ACKNOWLEDGEMENTS	v
ABSTRACT	vi
1. INTRODUCTION	1
1.1 Purpose	1
1.2 Scope.....	2
1.3 Report Outline.....	3
2. LITERATURE SEARCH AND SURVEY	4
2.1 Florida Limestone	4
2.1.1 Geology of Florida.....	4
2.1.2 Variable Composition	6
2.1.3 Mechanical Properties.....	7
2.1.4 Limestone Drainage Conditions	8
2.2 Pressuremeter	8
2.2.1 History of the Pressuremeter	10
2.2.2 Pressuremeters Used in this Research.....	11
2.2.3 Pressuremeter Test Data	15
2.2.4 Insitu Horizontal Stress and Yield Pressure	16
2.2.5 Pressuremeter Modulus	18
2.2.6 Interpretation of Limit Pressure	19
2.2.7 Tensile and Compressive Strength	21
2.2.8 Shear strength.....	24
2.2.9 Unconfined compressive strength.....	26
2.2.10 Limitations of the PMT	26
2.3 Drilled Shaft Design with the PMT	27
2.3.1 Unit Side shear.....	28
2.3.2 Strength Parameter Method	29
2.3.3 LPC Method	31
2.3.4 Proposed Side Shear Method	33

Final Report Contract #BC354 RPWO #13

2.4	Survey of State Drilling Practice	34
3.	LABORATORY TESTS OF FLORIDA LIMESTONE	36
3.1	Sample Preparation	36
3.2	Lab Tests	37
3.3	Compressive Strength	38
3.3.1	Compressive Modulus.....	38
3.3.2	Splitting Tensile Strength	40
3.3.3	Gatorock Trial Mix Samples	41
3.3.4	FDOT and Gatorock Cores	42
3.3.5	SR20 PMT Cores	43
4.	PRESSUREMETER DESIGN.....	44
5.	LABORATORY AND FIELD PMT TRIALS	45
5.1	Pressuremeter Lab Tests.....	45
5.1.1	Gatorock Sample Preparation	45
5.1.2	Gatorock Core Tests.....	47
5.1.3	PMT Lab Setup.....	48
5.1.4	PMT Lab Results.....	50
5.1.5	Comparison of Lab PMT and Core Tests.....	52
5.2	Pressuremeter Field Tests.....	57
5.2.1	SR20 Stratigraphy	57
5.2.2	PMT Corehole Preparation	63
5.2.3	PMT Results	69
5.2.4	PMT - Core Correlation	73
6.	CORRELATION OF FLORIDA LIMESTONE PROPERTIES.....	78
6.1	Compressive Strength vs. Modulus	78
6.2	Compressive Strength vs. Tensile Strength.....	80
6.3	Validity of Correlations	83
7.	DRILLED SHAFT SIDE SHEAR FROM SR20 PMT	84
7.1	LPC Method.....	84
7.2	Strength Parameter Estimates.....	84
7.3	Comparison of f_{su} Results	85

Final Report Contract #BC354 RPWO #13

7.4	Site Variability at SR20	89
8.	CONCLUSIONS AND RECOMMENDATIONS.....	93
8.1	Conclusions	93
8.1.1	Limestone Property Measurements in the Laboratory.....	93
8.1.2	Pressuremeter Tests in the Laboratory	93
8.1.3	Pressuremeter Tests in the Field	94
8.1.4	Unit Side Shear Predictions	95
8.2	Recommendations.....	96
	REFERENCES.....	97
	APPENDIX	101

1. INTRODUCTION

1.1 Purpose

The Florida Department of Transportation (FDOT) utilizes drilled shafts for deep foundation support in three basic design situations: 1) sites with strong subsurface materials, usually limestone, at relatively shallow depth, 2) in urban areas to eliminate the noise and vibration associated with driven piles, 3) to increase lateral capacity and strength for ship impact or wind loading. Many drilled shafts in Florida include a socket drilled into the limestone. Current FDOT design methods for shafts drilled into limestone rely on a combination of Standard Penetration Testing and laboratory strength tests of core samples extracted from the rock mass.

Though significantly stronger than soil, Florida limestone does not have the strength of the more competent limestone formations found in other parts of the United States. It typically contains variable zones of weakness resulting from weathering, solution features, fissures, voids, and inclusions of soil and unconsolidated carbonates. As a result, cores obtained from Florida limestone generally have lower recoveries, retrieving only the most competent limestone for laboratory testing. Designers often conservatively assign zero strength to the material lost during the coring process. Research performed at the University of Florida (UF) Civil and Coastal Engineering Department and described herein, seeks to improve drilled shaft design procedures for Florida limestone through the use of insitu testing, obtaining design parameters from direct tests performed within rock mass, rather than from core tests. Testing all of the rock, both weak and strong, should provide for safe shaft design, with better efficiency and reduced construction costs.

Different types of insitu tests may be used to characterize a rock mass. Geophysical methods provide information from which to identify stratigraphic changes and to infer changes in density and stiffness, but they do not directly measure the engineering properties required for drilled shaft design. Florida limestone is generally much stronger than soil, which makes most penetration tests impractical. Although the FDOT often reports Standard Penetration Test results in limestone, this dynamic test

provides a better model for the behavior of driven piles than drilled shafts, and has a substantial inherent variability as well. Therefore, on a practical basis, only insitu tests performed from within a borehole can provide the rock properties desired. Previous FDOT work has demonstrated a possible correlation between the strength and stiffness of Florida limestone, which this project will attempt to develop further for use in drilled shaft design. Among several possible borehole tests, the pressuremeter test (PMT) seems to provide the strongest theoretical and practical direct measurement of rock stiffness for use with a strength-stiffness correlation. In addition, by using a high-pressure probe, the PMT can also measure the strength of the rock directly. This research has the primary goal of applying pressuremeter test results to the design of drilled shafts.

1.2 Scope

The research described herein attempts, through laboratory and field tests, to correlate the strength and stiffness of Florida limestone, with the primary objective of developing a drilled shaft design method based on the insitu measurement of stiffness. It includes results from modulus, compressive, and split tensile core tests performed both by the FDOT and by UF. "Gatorock", a synthetic limestone developed for this research, provided additional test results across a wide range of strength values. UF also prepared large specimens cast from Gatorock for the laboratory evaluation of pressuremeter equipment before conducting field tests. Strength and modulus tests on cores from these specimens were compared with the pressuremeter test results. UF and FDOT personnel then performed field tests with the PMT at the Blountstown SR20 bridge site. Pressuremeter tests in core borings adjacent to two of the test shafts (5 and 7) provided comparisons of PMT results with both core tests and the side shear measured during the shaft load tests.

This report summarizes and compares the results of the research program, and provides recommendations for the use of PMT results for drilled shaft design. Two UF Master's Theses, Jacobs (2003) and Cepero (2002), provide additional details of the lab and field tests.

1.3 Report Outline

This report presents the results of the UF research program as follows:

- Literature Search and Survey
- Laboratory Tests of Florida Limestone
- Pressuremeter Design
- Laboratory and Field Pressuremeter Trials
- Correlation of Florida Limestone Properties
- Drilled Shaft Side Shear from SR20 PMT
- Conclusions and Recommendations

2. LITERATURE SEARCH AND SURVEY

The literature review presented below addresses the nature of Florida limestone, tests of core samples, pressuremeter tests and their interpretation, and current drilled shaft design methods.

2.1 Florida Limestone

2.1.1 Geology of Florida

The near-surface geomaterials of Florida consist mostly of sand over limestone, with lesser quantities of clay and mixed soils. However, due to its relatively low surface elevation, Florida has experienced many geomorphic changes that complicate this simplified stratigraphy, mostly through the action of water. Ice ages and other climatic events caused changes in the sea level, alternately submerging and then exposing the Florida platform. Periods of marine inundation lead to the deposition of carbonate sediments that formed limestone, while periods of exposure included both the deposition of outwash sediments from the Appalachian Mountains and erosion and weathering processes.

Geologists currently believe that the basement geology of Florida, 3 to 4 km beneath the ground surface, includes a sub-continental convergence, originating from the west coast of Africa and which has escaped significant deformation or metamorphism. Borehole evidence indicates an early Cambrian granitoid batholith in the Florida basement, with associated felsic volcanic rocks, and an overlying sequence of early Paleozoic sedimentary rocks. Superimposed on the Paleozoic features are a series of Mesozoic grabens and one or more Jurassic transform faults (possibly of late Paleozoic origin). Above these older units, from the Cretaceous until the present, high sea level stands have deposited the thick sequence of carbonates and evaporites (Shmidt, 1997) familiar to many engineers.

A blanket of Cenozoic sediments, ranging in age from Miocene to Holocene, covers virtually the entire carbonate platform. Cuts made by rivers, streams, and sinkholes, often expose older sediments, mostly deposited under marine conditions, but

also by fluvial and eolian deposition. The younger, surface sediments range from less than 1 m thick in parts of the west-central peninsula and the north-central panhandle to more than 300 m thick in southern Florida. The Miocene to Holocene sediments consist of carbonates, sands, clays, shell material, heavy minerals, and phosphate. They act as a confining unit above the Florida aquifer system, a thick sequence of water-bearing limestone, dolomite, and evaporates that are the source of most of Florida's potable water supply (Randazzo, 1997). Minor uplift forces have also affected Florida limestone, resulting in the oldest outcrops occurring in the Ocala Arch, northwest of Ocala, FL.

The highlands of the northern peninsula and panhandle of Florida consist of the dissected, sedimentary remains of Neogene (late Tertiary period) fluvial, deltaic, and shallow-water marine systems. Transported southward by water from the southeastern coastal plain and the southern Appalachians, siliciclastic sediments filled the Gulf trough and spilled onto the carbonate platform of Florida. This siliciclastic invasion into the clear, carbonate-producing, shallow waters, covered the limestone platform and formed a spine of clayey sand on the peninsula (Randazzo, 1997). "Subsequent sea level fluctuations and associated near-shore, coast-parallel currents reworked and reshaped these deposits, leaving the elongate system of upland ridges we see today" (Schmidt, 1997).

The Florida peninsula acquired its present shape during the last ice age, some 15,000-20,000 years ago. A North to South river orientation dominates the peninsula, reflecting the near-shore marine environment that contributed to the basic landform present today. Relict beach ridges separate swales previously occupied by shallow lagoons. "When the sea level dropped, these lagoons became valleys, and streams eroded the sands and clays, creating several coast-parallel river systems seen today as the St. Johns, Kissimmee, and Withlacoochee Rivers" (Schmidt, 1997). The topography of south Florida is typical of peninsular Florida's general geology. Biscayne Bay separates Miami Beach, located on the Atlantic Ridge, from the mainland (downtown Miami sits on a western ridge). To the west of southeastern coastal counties of Dade,

Broward, and Palm Beach and to the east of the gulf coast of Florida (where the Gulf Coast ridge is located) sits the immense “shallow lagoon” of the Everglades. Similar features, on a smaller scale, occur in many other areas of Florida.

2.1.2 Variable Composition

Sedimentary rocks, including Florida limestone, form as wind, water (predominant), and ice transport minerals, fragmented rock, and the remains of certain organisms and then deposit them in sedimentary layers. As sediments accumulate, pressure and/or chemical reactions harden the deposits. The sedimentary rocks include two major divisions, detrital and chemical. Pressure on the deposited solid products of chemical and mechanical weathering forms detrital sedimentary rocks. Limestone belongs to the chemical sedimentary rocks derived from solids precipitated out of solution, in lakes and seas, through biochemical and inorganic processes. It is the most abundant chemical sedimentary rock, composed primarily of the mineral calcite (calcium carbonate, CaCO_3) hardened underwater by chemical cementing action, rather than pressure. Limestone represents about 10% of all sedimentary rocks, and most formations, including Florida limestone, have a marine biochemical origin. However, individual Limestone formations in Florida may exhibit little apparent visual or physical difference, and Florida geologists often identify the contacts by relying on the fossil record within the rock.

Because of the varied deposition and erosion processes that occurred during Florida's geologic history, Florida limestone has a highly heterogeneous nature. Even within the same formation, it may include coral, shell, chert, strongly cemented carbonates, crystalline deposits, oolites, and lime mud. It may also include zones of weak cementation, poor consolidation, detrital weathering products, and inclusions of clay, sand, and organic matter deposited in karst features and/or interbedded layers. The carbonate matrix may also contain many impurities, including iron, silica, and magnesium. The dolomitic limestone (dolomite, $\text{CaMg}(\text{CO}_3)_2$) sometimes found in Florida forms when magnesium ions, transported through limestone beds by groundwater, replace some of the calcium in the calcite matrix. Groundwater may

convey carbonic acids (dissolved carbon dioxide) and organic acids that dissolve the calcite matrix, forming karst features such as cavities and fissures. Because of the greater influence of weathering processes and lesser consolidation stresses, Florida limestone found near the ground surface tends to be weaker than that found at depth. **Figures 2.1 and 2.2** show exposed stratigraphy at two Florida mines that illustrates the potential variability of near-surface limestone formations.



Figure 2.1 Ocala Limestone Exposed in Newberry, FL Mine



Figure 2.2 Tampa Limestone Exposed in Lecanto, FL Mine

2.1.3 Mechanical Properties

Generally weaker than many other sedimentary rocks, and often including zones of unconsolidated carbonates and karst features, the mechanical properties of Florida limestone vary significantly. Properties may vary between and within recognized formation units, and both laterally and vertically at any given site, often almost randomly. Because of this inherent variability, the FDOT performs a detailed investigation of the limestone at each site when it may affect the structure under design. This investigation typically consists of the Standard Penetration Test and strength tests of core samples. The competency of the limestone also plays an important role in core retrieval and in the excavation of a borehole in which to perform insitu tests, both of which may affect the quality of the respective test results. Testing and sampling techniques add further variation. Reported parameters usually include the SPT N-value (ASTM D1586), core recovery (%), rock quality designation (%), and laboratory tests.

Laboratory tests are usually limited to the unconfined compressive strength, q_u (ASTM D2938) and splitting tensile strength, q_t (ASTM D3967). Unconfined compressive strengths vary from less than 100 psi to as much as 10,000 psi, but the majority of values fall between 500 psi and 2,000 psi. A few projects have included pullout tests of small diameter (<6") concrete plugs used to model the shaft side shear. Drilled shafts designed using these test results typically have high capacity, and the FDOT routinely performs load tests during the construction phase of each project to verify design assumptions.

2.1.4 Limestone Drainage Conditions

Many engineers assume Florida limestone behaves as a drained material. Limestone typically has permeability similar to very fine sand, in the range of 10^{-2} to 10^{-4} cm/sec, and a porosity of 5 to 15%. According to Johnston and Chiu (1981) the dissipation of porewater pressure caused by loading “may be described by the coefficient of consolidation, c_v ,” which varies inversely with the coefficient of volume change, m_v , and directly with permeability. For a relatively incompressible material like soft limestone, the coefficient of volume change (m_v), the reciprocal of the constrained modulus, may be several orders of magnitude smaller than for a clay. This combination results in “a c_v value that is several orders of magnitude larger than for clays” (Johnston and Chui, 1981) and leads to a more rapid porewater dissipation rate. Johnston and Chiu (1981) further indicate that their laboratory “specimens did not contain the fissures, joints and seams encountered in the field”, which will lead to a further increase in drainage. Of course, the presence of clay in the limestone matrix, a common occurrence in Florida, will significantly reduce drainage.

2.2 Pressuremeter

The pressuremeter test (PMT) provides an insitu measurement of both strength and stiffness. After placing a flexible, cylindrical probe into the ground, an operator then expands it in the lateral direction (see **Figure 2.3**). The stress field created around the probe has a vertical axis of symmetry, and a probe of sufficient length creates an approximately plane strain condition perpendicular to its axis. This relatively unique

combination provides boundary conditions that simplify the analysis of the test data. The lateral pressure applied by the probe, p , (radial stress, σ_{rr} , at the cavity wall) plotted versus the relative increase in probe radius, $\Delta R_0/R_0$ (at the cavity wall) provides an insitu stress-strain curve that the engineer may interpret to obtain the lateral insitu stress, stiffness, and strength. From tests performed at various depths, the engineer may develop a depth profile of these parameters for design use.

Engineers currently use one of four main types of pressuremeter probes categorized by the method of insertion: preboring pressuremeters, self-boring pressuremeters, the pushed or driven cone pressuremeter, and the pushed Shelby tube pressuremeter. Each PMT type has both advantages and disadvantages and provides different stress-strain curves in the same geomaterial. Because of the potential for damage to the probe and the variable disturbance caused by penetration, pushed or driven probes will not provide reliable tests in soft rock, the main goal of this project. To obtain accurate test results from a preboring pressuremeter, test personnel have to prepare a borehole with minimal disturbance of the geomaterial and its insitu stress field. The engineer must then assess disturbance effects during analysis of the test. Only the self-boring pressuremeter approaches undisturbed testing, but it combines the pressuremeter with a cutting device and has not proven effective in strong materials.

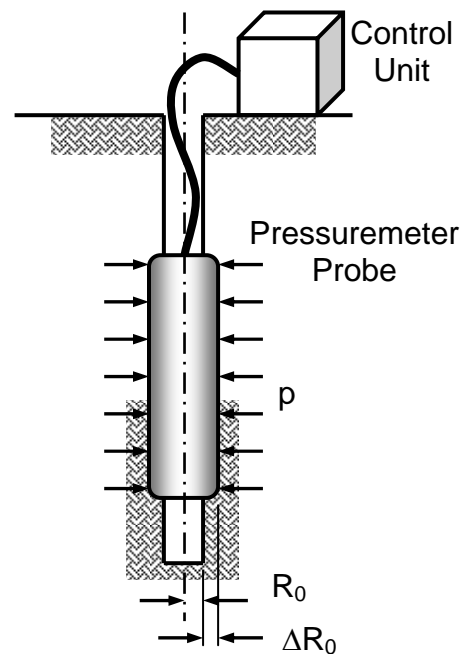


Figure 2.3 PMT in Borehole

2.2.1 History of the Pressuremeter

The roots of the pressuremeter extend back to Kogler, who developed the first preboring pressuremeter in Germany in 1933. Due to the limitations of the available materials, Kogler achieved only partial success. However, the French engineer Louis Menard made significant advances in the pressuremeter device, its analysis, and its acceptance. Menard's initial pressuremeters included guard cells at the top and bottom of the probe to minimize vertical deflection at the ends of the measurement cell and better confine the probe expansion to the horizontal direction. Returning to France after studies at the University of Illinois, Menard started a company to promote its use, the Centre d'Etudes Louis Menard. In 1963, he published the first equations and charts relating pressuremeter results directly to foundation settlement and bearing capacity, from the field experience gathered through hundreds of tests.

The French engineer, Jezequel, developed the first self-boring pressuremeter, the PAF, at the Laboratoire des Ponts et Chaussées (LPC). In England, C.P. Wroth and J.M.O. Hughes developed another self-boring pressuremeter, the Camkometer, in 1971 at the University of Cambridge in England. Engineers from Japan have developed numerous pressuremeters, including the preboring Lateral Load Tester and the Elastometer series. Researchers in Russia created an automatic pressuremeter, the PA108, and the French Petroleum Institute produced the self-boring PAM for offshore investigation. More recently, in 1982, Jean-Louis Briaud and his co-workers at Texas A&M University investigated end effects and simplified Menard's preboring probe to a mono-cell device called the Texam probe.

Pressuremeters used in rock generally have thicker, stronger membranes to apply higher pressure than those used in soil. Because of the extra strength, they also have less sensitivity, less expansion capability, and reduced accuracy for testing softer materials. The operator must carefully control the diameter of the borehole to avoid over-expansion and bursting of the membrane. Engineers often refer to high-pressure probes as "dilatometers". Oyo's Elastometer II can apply pressures up to 2,900 psi (20 MPa), as is the borehole dilatometer designed by Cambridge Insitu. This pressure

may induce yielding in soft rock, e.g. shale and weak limestone, but not competent rock. A few dilatometers, for example the Probex-1 distributed by Roctest, Inc., can apply pressures up to 4,350 psi (30 MPa)

Major works published about the use of the pressuremeter for foundation design include those by Baguelin, Jezequel and Shields (1978), Mair and Woods (1987), Briaud (1992), and Clarke (1995). Numerous international conferences on insitu testing and site characterization have included the pressuremeter, as have four international symposia dedicated to it, the last in Canada in 1995. ASTM published the "Standard Test Method for Pressuremeter Testing in Soils" (ASTM D4719) in 1988. Briaud (1992) states that "...progress has been made in the interpretation of the pressuremeter data in France, England, Japan, Canada, and more recently in Italy, Norway and the United States." As the popularity of the pressuremeter increases, further studies should improve and expand correlations between pressuremeter tests and soil/rock parameters.

2.2.2 Pressuremeters Used in this Research

All pressuremeter tests performed in rock, including those in this project, require a borehole. Preboring soil pressuremeters generally exert a maximum pressure of less than 1,450 psi (10 MPa) on the borehole wall, generally insufficient to yield the rock and obtain a limit pressure. However, they will provide the slope of the linear portion of the PMT curve for calculation of the modulus of deformation (after correction for the system compressibility). This project includes PMT data from the Texam and Probex-1 pressuremeters, both distributed by Roctest, Inc.

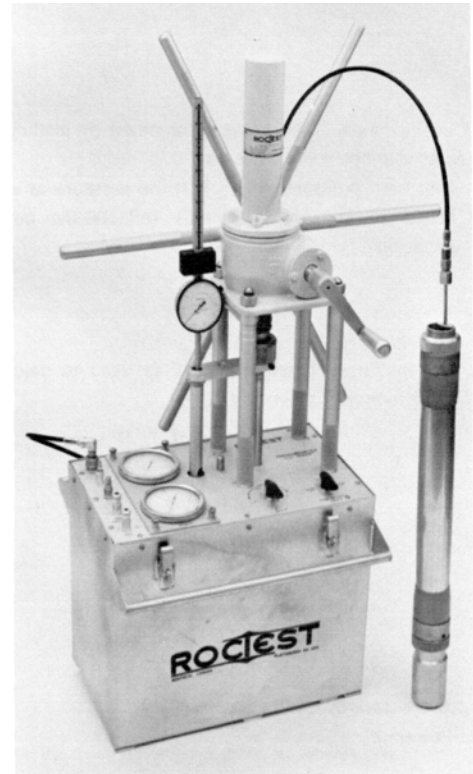


Figure 2.5 Texam Pressuremeter (Roctest, Inc. photo)

The Texam, shown in **Figure 2.5**, can test both very stiff soils and soft rock. Developed at Texas A&M by Dr. Jean-Louis Briaud,

we chose it for the initial trial measurements made during this project because of its wide acceptance, relative simplicity, durability, and the compatibility of its 2.75" diameter x 18" long probe with current drilling practice. The Texam PMT requires a nominal N-size borehole, approximately 2.875" in diameter, and it has a single measuring cell (monocell) with a length to diameter ratio of $L/D = 6.5$, long enough to minimize end effects. A screw-jack piston in the control unit inflates the probe by injecting water with the volume of water calibrated to the number of revolutions of the screw-jack. Bourdon tube pressure gauges indicate the system pressure. The main features of the Texam include:

Advantages

- Water used to inflate the probe.
- Self-contained, relatively simple, and robust control unit applies pressure using a screw-jack piston.
- Maximum pressure of 1,450 psi (10 MPa), maximum 73 in^3 ($1,200 \text{ cm}^3$) expansion
- Designed for volume control test but also capable of pressure control test
 - Relatively easy to control unload/reload portion of the PMT test.
- Available with stainless steel lantern sheath to minimize membrane punctures

Disadvantages

- Maximum pressure possibly inadequate to measure the yield and limit
- Volume losses and calibration are relatively large compared to rock stiffness because of compliance of hoses and control unit.
- Relatively thin membrane, possibility of rupture

The Probex-1 borehole dilatometer (**Figures 2.6 and 2.7**) used in this project can apply pressures of up to 4,350 psi (30 MPa). As shown in **Figure 2.7**, the Probex-1 has a slightly larger probe diameter (2.9") than the Texam, but it has three times the working pressure. The thick membrane used in the Probex-1 is a composite of vulcanized rubber and plastic stiffeners and is unlikely to puncture. The higher working pressure should allow estimation of a limit pressure for nominal strength Florida limestone. The main features of the Probex-1 include:

Advantages

- A piston, located just above the probe and activated by a hand pump at the surface, injects water into the probe to inflate it during the test. A pressure transducer measures the system pressure at the hand pump. A Bourdon tube gage also confirms the system pressure.
- A linear variable displacement transducer (LVDT) measures the movement of the hydraulic piston, which is correlated with volume of water injected into the probe.
- Measurement of the injected volume at the probe eliminates correction for expansion of the tubing leading to the probe and inside of the control unit.
- Maximum pressure of 4,500 psi (30 MPa), maximum 664 cc expansion.
- A data acquisition unit digitizes and stores the applied pressure and injected volume during the test.



Figure 2.6 Probex-1 Rock Dilatometer (Roctest, Inc.)

Disadvantages

- Poor pressure release control (could be improved with a better vent valve).
- The expansion of the probe is limited due to the thickness of the membrane, thus placing extra emphasis on proper borehole size.
- The assembled probe unit with downhole piston and pressure transducer is heavy (~80 lbs), long (~ 6 ft), and is best handled with drill rig.

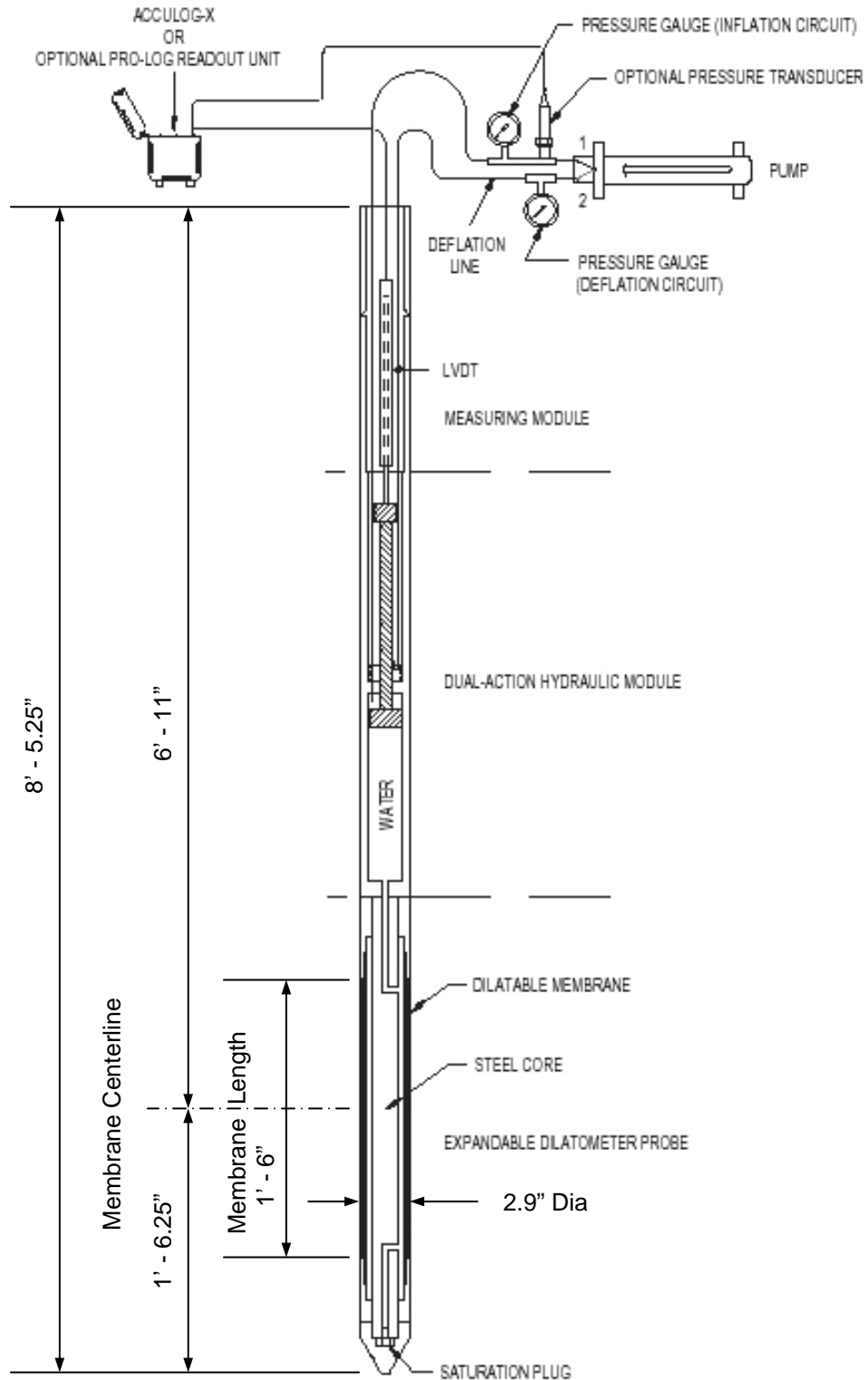


Figure 2.7 Probex-1 Schematic (Roctest, Inc., dimensions added)

2.2.3 Pressuremeter Test Data

Pressuremeter tests generally include test increments during which the operator holds either the pressure or the volume constant for a specified period of time, usually 30 to 60 seconds. Readings taken at different times during each pressure or volume increment (30 and 60 seconds during this research) provide a measurement of creep. The measured pressure and volume from water-filled probes, such as used during this research, require correction for:

- volume lost to the expansion of the tubing in the control unit and leading to the probe, compression of the probe membrane, and compressibility of the system fluid due to trapped or dissolved air
- pressure added to overcome the inertia of the membrane
- the difference in probe fluid pressure due to the elevation difference between the pressure gage and the saturated probe

Figure 2.4 shows a typical "s-shaped" plot of the corrected volume and pressure measurements at the same elapsed time for each increment of a pressuremeter test, either volume- or pressure-controlled. The initial curvature between points A and B brings the probe into solid contact with the boring sidewall and, at point B, replaces the insitu horizontal stress ($p_0 = \sigma_h$) removed

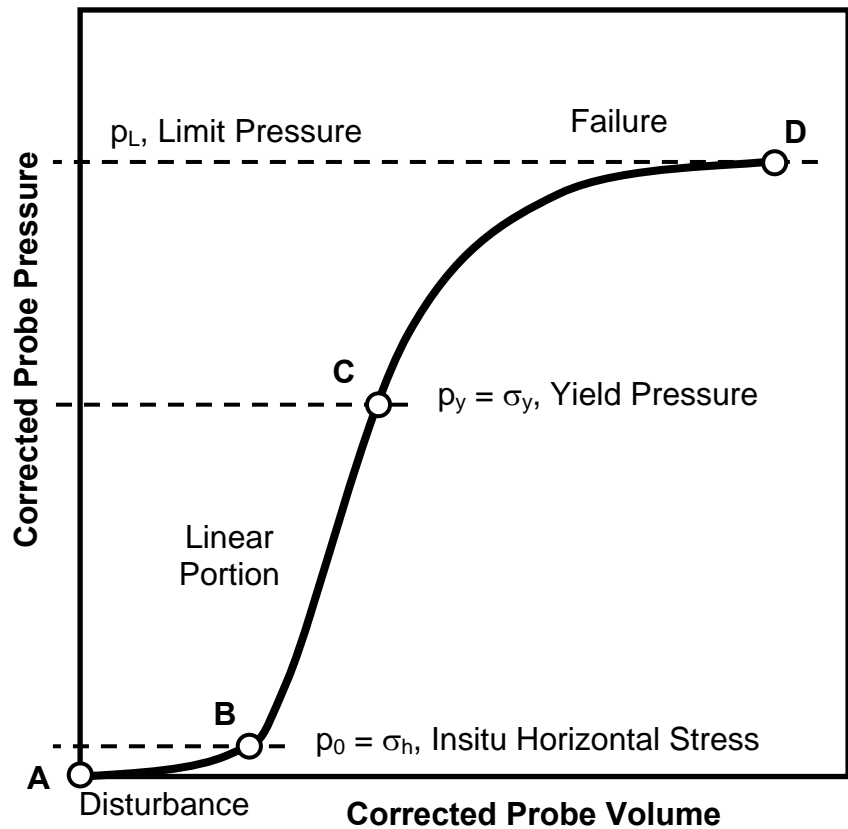


Figure 2.4 Typical Pressuremeter Curve

during preparation of the borehole. Self-boring and pushed pressuremeters may eliminate this portion of the curve depending on disturbance. The linear portion of the

pressuremeter curve, from point B to the yield pressure at point C ($p_y = \sigma_y$) represents the linear stiffness of the geomaterial. The final curved portion from points C to D, results from plastic failure, and, after applying sufficient pressure, it reaches a maximum resistance at the limit pressure, p_L . Many authors also use the net limit pressure, $p_L^* = (p_L - \sigma_h)$, in strength correlations.

The pressuremeter curve provides several test results that the engineer may correlate with the properties of the geomaterial, or use directly in various design problems. These properties include the pressuremeter modulus (E_m), yield pressure (p_y), the limit pressure (p_L), tensile strength (σ_t), unconfined compressive strength (q_u), and shear strength (c_u). The following sections describe analyses for these parameters.

2.2.4 Insitu Horizontal Stress and Yield Pressure

Figure 2.4 showed the PMT pressure plotted as a function of volume, but many engineers plot the same pressure as a function of the ratio of the change in probe radius, ΔR , to the initial radius, R_0 . Because the probe length remains constant, we can calculate the radius of the probe at any point during the test from the corrected total volume of the probe, V , equal to the initial volume plus the injected volume. **Figure 2.8** shows a plot of the corrected probe pressure versus the ratio $\Delta R/R_0$. Because of the disturbance created by drilling the borehole, a sharp break in slope seldom occurs at point B, making the insitu horizontal stress difficult to determine. As a result, the engineer must interpret the test curve to estimate p_0 , possibly using one of several different methods: the point of maximum curvature, the beginning of the linear portion of the test curve, the intersection of the initial (A to B) and elastic (B to C) straight-line portions of the curve, or interpretation of a creep curve. **Figure 2.8** shows the last two of these methods, used predominantly during this research.

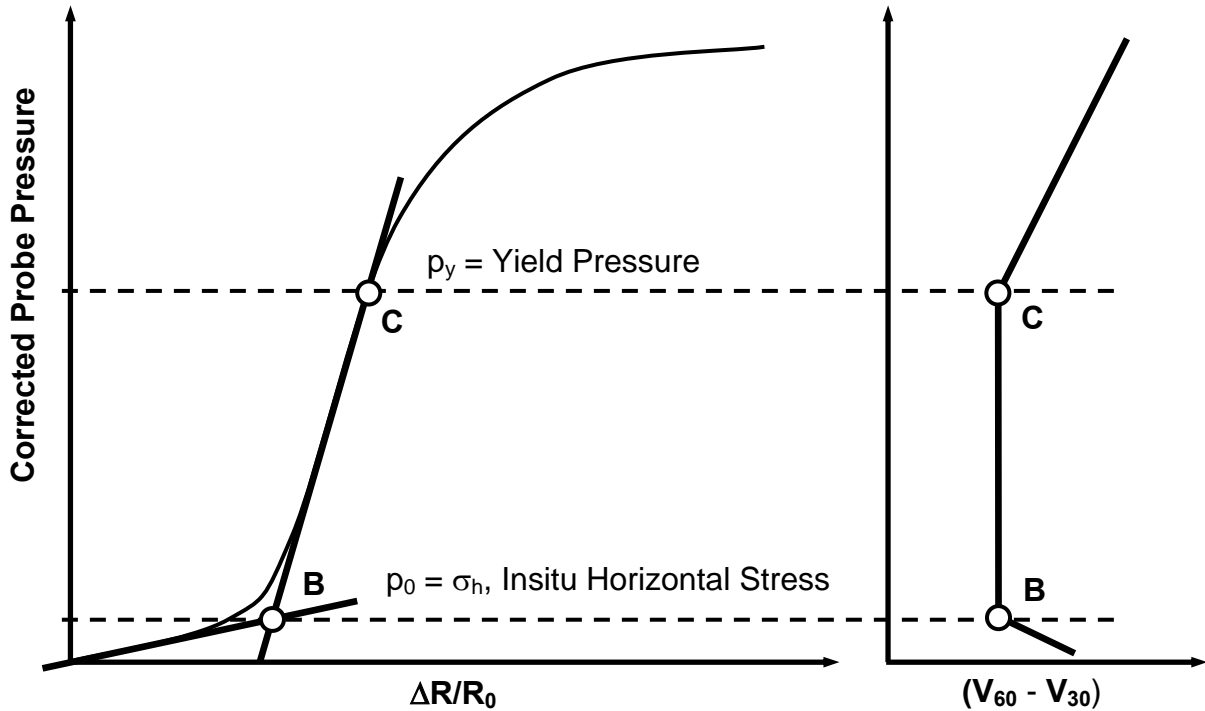


Figure 2.8 Determination of Insitu Horizontal stress and Yield Pressure

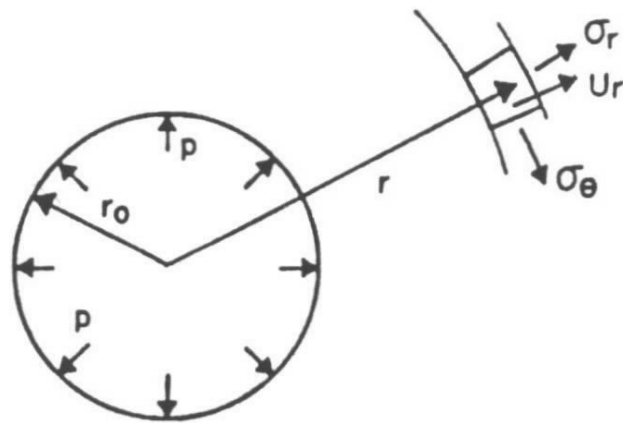
The difference between the 60-second and 30-second volume readings, $(V_{60} - V_{30})$, during a pressure-controlled test provides a relative measurement of creep for each pressure increment, as shown in the creep plot on the right side of **Figure 2.8**. Because significant plastic deformation occurs during both the initial phase of the test (A to B) and the final phase above the yield limit (C to D), the creep varies with the probe pressure. However, during the linear portion of the test (B to C), the volume creep remains relatively constant, and typically small. When plotted versus the test pressure, the larger creep values during the initial and final test phases trend to intersect with the relatively constant creep during the linear phase. As shown in **Figure 2.8**, the intersecting lines from these three test phases provide an estimate of the insitu horizontal stress at point B and the yield pressure at point C. The onset of non-linearity also provides a relatively simple determination of the yield pressure from the test curve as shown at point C on the left sides of **Figure 2.8**.

2.2.5 Pressuremeter Modulus

The expansion of the pressuremeter lends itself readily to theoretical analysis. Ignoring end effects, the probe expansion is axisymmetrical about the central (vertical) axis and plane strain in any plane perpendicular to the central axis. With these initial assumptions, only the behavior of the geomaterial significantly affects the radial expansion of the probe. As shown in **Figure 2.9** using cylindrical coordinates, the radial stress, σ_r , and the circumferential stress, σ_θ , in the stress field perpendicular to the probe axis are both principal stresses, at least for practical intents. For analysis purposes at low strain levels, many interpretation methods model the geomaterial as isotropic and linear elastic. Ignoring crack formation, these assumptions seem reasonable over the pressure range starting at the insitu horizontal stress, σ_h , and ending at the yield pressure, σ_y , at which point plastic deformation begins at the cavity wall and progresses into the material as indicated on the volume-pressure curve by the departure from linearity.

The assumptions of linear elasticity and low strain levels result in several important observations (Briaud, 1992):

- changes in radial and circumferential stresses are equal and opposite, $\sigma_r = -\sigma_\theta$
- radial and circumferential strains are equal and opposite, $\varepsilon_r = -\varepsilon_\theta$
- no volumetric strain, $\varepsilon_v = (\Delta V/V) = \varepsilon_r + \varepsilon_\theta + \varepsilon_z = 0$
- initial linear slope of the radial stress, σ_r , vs. circumferential strain, ε_θ is twice the shear modulus ($= 2G$)
- both stresses and strains vary as the inverse of radius squared, thus limiting the zone of influence of the test



p cavity pressure
 r_0 cavity radius
 σ_r radial stress at radius r
 σ_θ circumferential stress at radius r
 U_r radial displacement at radius r

Figure 2.9 Pressuremeter Stress Field (Haberfield, 1987)

The above assumptions also result in a correlation for the pressuremeter modulus of the geomaterial, E_m , calculated from the linear portion of the test curve (B to C) using either the volume or relative change in probe radius:

$$E_m = 2(1 + \mu) \left(\frac{V_2 + V_1}{2} \right) \left(\frac{P_2 - P_1}{V_2 - V_1} \right) \dots\dots\dots (2.1)$$

$$E_m = (1 + \mu)(p_2 - p_1) \frac{\left(1 + \left(\frac{\Delta R}{R_0} \right)_2 \right)^2 + \left(1 + \left(\frac{\Delta R}{R_0} \right)_1 \right)^2}{\left(1 + \left(\frac{\Delta R}{R_0} \right)_2 \right)^2 - \left(1 + \left(\frac{\Delta R}{R_0} \right)_1 \right)^2} \dots\dots\dots (2.2)$$

where: V_1, V_2 = total volumes (initial + injected) at the endpoints
 P_1, P_2 = corresponding pressures at the endpoints
 R_0 = the initial probe radius
 ΔR = change in probe radius (from R_0)
 μ = Poisson's ratio, assumed = 0.25 for soft rock

Note that because the bulk stress (mean stress) and volume do not change during this elastic phase, drainage conditions do not affect the resulting modulus (see Clarke, 1995). Also, as discussed below, radial cracks may propagate from the borehole wall during a pressuremeter test. In this case the modulus from the pre-crack portion of the elastic phase should more closely model the stress-strain behavior of the intact rock mass.

2.2.6 Interpretation of Limit Pressure

The limit pressure describes the point at which the geomaterial continues to deform without an increase in applied pressure. Theoretically, the limit pressure requires an infinite expansion of the rock cavity. However, many authors, including Briaud (1992), define the limit pressure at a volume expansion equal to twice the volume of the initial cavity, V_c , or a cavity strain of 100%. Therefore, p_L occurs at:

$$(\Delta V_c / V_c) = \frac{V - V_c}{V_c} = 1 \dots\dots\dots (2.3)$$

where: V_c = the initial volume of the cavity (at p_0)
 ΔV_c = the change in cavity volume with respect to the initial volume of the cavity

Based on eqn. 2.3, Briaud (1992) provides the following relationship:

$$\left(\frac{\Delta R}{R_0}\right)_L = 0.41 + 1.41\left(\frac{\Delta R}{R_0}\right)_c \dots\dots\dots(2.4)$$

where: $(\Delta R/R_0)_L$ = relative change in radius at the limit pressure
 $(\Delta R/R_0)_c$ = relative change in radius at the initial volume of the cavity

Both of these radial changes occur with respect to R_0 , the initial radius of the probe. For a well-prepared borehole with $(\Delta R/R_0)_c = 0.05$ to 0.10 , eqn. 2.4 indicates $(\Delta R/R_0)_L = 0.48$ to 0.55 . However, due to the limited available expansion of the Probex-1, tests performed for this research never exceeded $(\Delta R/R_0) = 0.2$. Therefore, we also used curve-fitting techniques and a method proposed by Gibson and Anderson Method to determine the limit pressure. Based on least-squares regression the following type of curve provided the best nonlinear relationship between the probe pressure, p , and the relative change in probe radius $(\Delta R/R_0)$:

$$p = A \cdot e^{-B\left(\frac{\Delta R}{R_0}\right)} + C \dots\dots\dots(2.5)$$

After determining the best-fit curve constants (A, B, C), eqn. 2.5 allows an extrapolation for p_L . The extrapolation method proposed by Gibson and Anderson, and described by Mair and Woods (1987), estimates the limit pressure in a fashion similar to the curve-fitting described above, by plotting the probe pressure versus the natural log of the cavity strain, $\ln(\Delta V_c/V_c)$. As shown in **Figure 2.10**, this semilog plot of the pressuremeter data typically results in a straight line above the yield pressure. Extrapolating the straight-line portion of the test curve in **Figure 2.10** to $\ln(\Delta V_c/V_c) = 1.0$, or approximately $(\Delta R/R_0) = 0.5$, estimates the limit pressure.

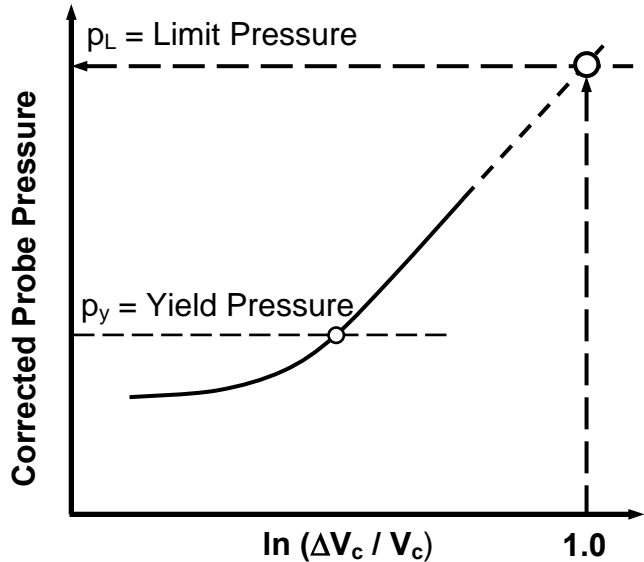


Figure 2.10 Gibson and Anderson Limit Pressure Extrapolation

2.2.7 Tensile and Compressive Strength

Briaud (1992) and Haberfield (1987) both show how the pressuremeter may induce radial tension cracks within the material tested. Haberfield and Johnston (1989, 1990) researched this topic extensively in soft rock. As shown in **Figure 2.11** for an elastic-plastic material, after applying/replacing the lateral stress (shown as $p_0 = \sigma_h$), the radial pressuremeter stress, σ_r , at the cavity wall increases with increasing pressure (applied by the pressuremeter) while the circumferential stress, σ_θ , decreases at the same rate.

As the geomaterial yields at the applied stress σ_m , volume changes alter the direction of the circumferential stress according to the plasticity model chosen.

The ideal stress diagram shown in **Figure 2.11** assumes that the tensile strength and the compressive strength have equal and opposite magnitudes, an

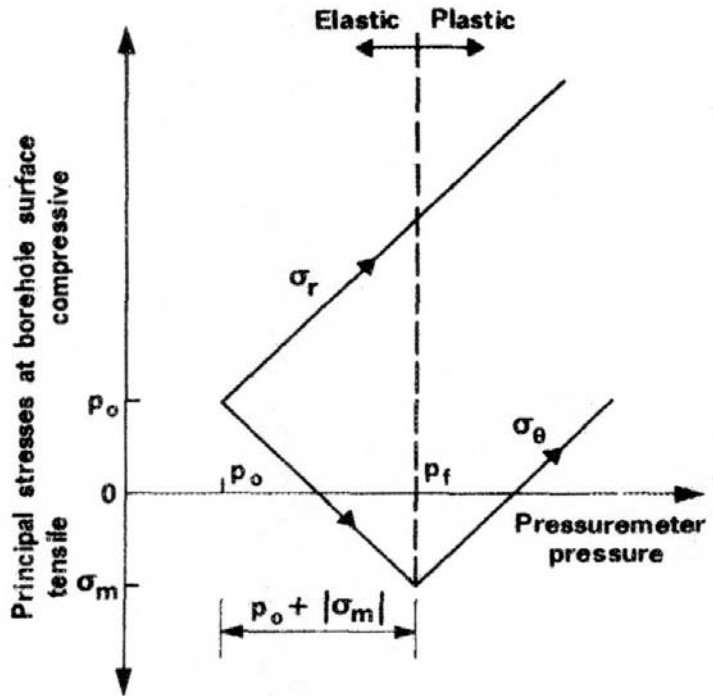


Figure 2.11 Pressuremeter Stress Diagram (Haberfield, 1989)

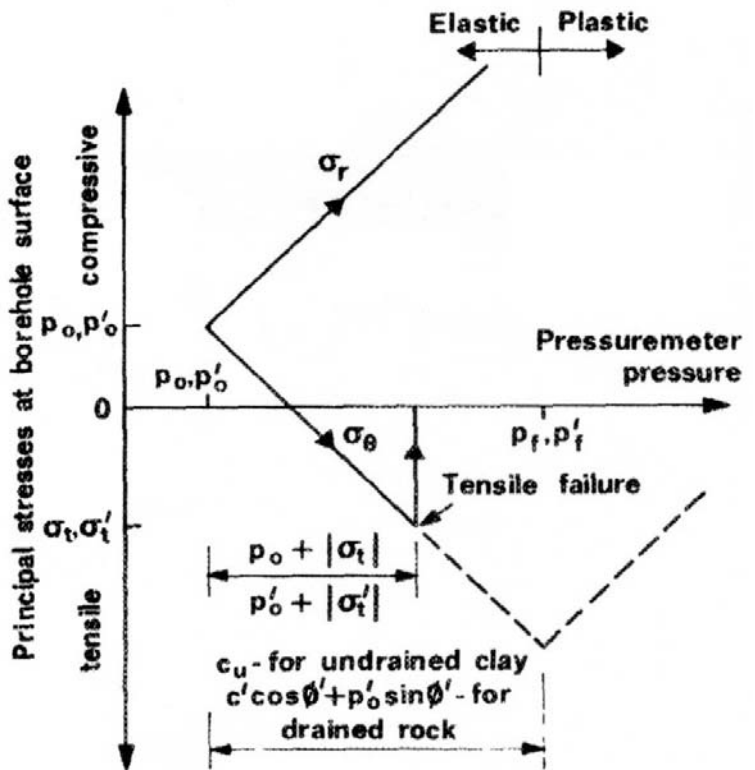


Figure 2.12 Pressuremeter Tensile Failure (Haberfield, 1987)

invalid assumption for many geomaterials, including soft rock, which often have significantly less tensile than compressive strength. Indeed, Haberfield (1987) concluded that for most pressuremeter tests in soft rock, tensile cracks form before attaining the compression yield pressure. These cracks initiate near the wall of the borehole and may propagate extensively into the rock mass. The stress diagrams presented in **Figures 2.11 and 2.12** may represent either drained or undrained, depending on the geomaterial. Using **Figure 2.12**, the following equations show the similar relationships between the tensile strength, σ_t or σ_t' , the pressuremeter pressure, p or p' , and the insitu lateral stress, σ_h or σ_h' :

$$p - \sigma_h = \sigma_h + |\sigma_t| \quad \text{for undrained geomaterial} \dots\dots\dots (2.6)$$

$$p' - \sigma_h' = \sigma_h' + |\sigma_t'| \quad \text{for drained geomaterial} \dots\dots\dots (2.7)$$

Florida limestone without inclusion of clay most likely behaves as a drained material. Substituting the pressuremeter pressure at the onset of cracking for $p' = \sigma_{cr}$, eqn. 2.7 allows the calculation of the drained tensile strength as:

$$|\sigma_t'| = \sigma_{cr} - 2\sigma_h' \dots\dots\dots (2.8)$$

This tensile strength may correlate with the splitting tensile strength measured on rock core specimens. Note that the insitu lateral stress, typically small by comparison to the cracking pressure, should generally have a secondary effect on the calculated tensile strength.

Figure 2.13 shows the progression of the Mohr circle for a stress path beginning at $\sigma_r = \sigma_\theta = p_0$ with $\Delta\sigma_r = -\Delta\sigma_\theta$. Failure occurs at yield when the applied pressure $p = p_y$, causing the Mohr circle shown in **Figure 2.13** to expand to the Mohr-Coulomb failure envelope with a radius of $(p - \sigma_h)$. At this point:

$$(p - \sigma_h)/\cos \phi = c + \sigma_h \tan \phi \dots\dots\dots (2.9)$$

and rearranging eqn. 2.9 provides:

$$p - \sigma_h = c_u \quad \text{for undrained geomaterial} \dots\dots\dots (2.10)$$

$$p' - \sigma_h' = c'(\cos\phi') + \sigma_h' (\sin\phi') \quad \text{for drained geomaterial} \dots\dots\dots (2.11)$$

The lateral stress may again have only minor significance compared to the other parameters in these equations. However, inclusion of the friction angle may prove important for interpretation of the drained strength of Florida limestone.

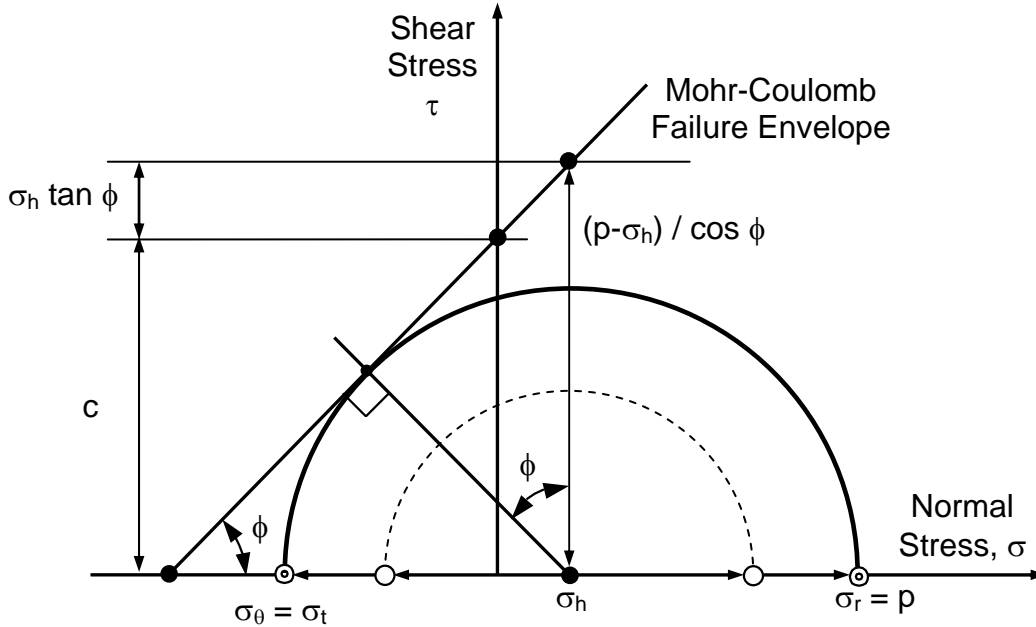


Figure 2.13 Mohr Circle at PMT Compression Yield

Combining eqns. 2.8 and 2.9, as shown in **Figure 2.12**, cracking will occur when:

$$|\sigma_t'| + \sigma_h' \leq c'(\cos\phi') + \sigma_h'(\sin\phi') \quad \text{for drained geomaterial (2.12)}$$

After reaching the tensile strength, the circumferential stress in the cracked zone reduces to zero as the pressure in the probe continues to increase. The radial stress will then continue to increase while the circumferential stress remains at zero, loading the rock wedges in a manner analogous to an unconfined compressive test of a rock core specimen. The response of the rock wedges should remain elastic until reaching the rock's unconfined compressive strength $q_u \approx p_y$. Thus, the PMT results may correlate directly with both the splitting tensile strength and the unconfined compressive strength of rock cores, parameters already used for drilled shaft design. Alternatively, a correlation between the splitting tensile strength and the unconfined compressive strength, possibly determined from a relationship with the pressuremeter, may prove viable.

2.2.8 Shear strength

Traditional analyses of the PMT to determine shear strength may also prove useful for drilled shaft design. In general, the analysis for shear strength focuses on the plastic failure that occurs following the yield pressure. Florida limestone generally exhibits drained behavior during the elastic phase of the PMT, but probably undrained conditions with excess pore pressure during the plastic failure. Drained behavior during failure would imply volume change, reduced excess porewater pressure, and the addition of a frictional component, ϕ , to the shear strength. This frictional component might increase the overall shear strength above that predicted from an undrained analysis (Haberfield, 1987). In addition, the volume change associated with drained loading could introduce dilatant behavior, which Baguelin (1978) states can cause the net limit pressure to more than double. However, due to the likelihood of excess pore pressure during plastic failure, this research primarily uses shear strength analyses based on undrained behavior.

Briaud (1992) describes several methods for determining the undrained shear strength, c_u , from the pressuremeter curve. These include the yield pressure method, the limit pressure method, the Gibson-Anderson method, and the subtangent method. The simplest of the four, the yield pressure method recognizes that plastic failure begins at the yield pressure so that:

$$c_u = p_y - \sigma_h \dots \dots \dots (2.13)$$

Briaud (1992) does not recommend this method, as it tends to overestimate c_u .

The limit pressure method uses a theoretical expression based on the limit pressure, and then approximates the ratio of shear modulus to undrained shear strength (G/c_u) to obtain a relatively simple expression based on the "constant" β :

$$c_u = \frac{(p_L - p_0)}{1 + \ln(G/c_u)} = \frac{p_L^*}{\beta} \dots \dots \dots (2.14)$$

In general, stiffer geomaterial will give a higher β coefficient. Briaud (1992) found that (G/c_u) typically varies from 100 to 600, which leads to a range of β from 5.6 to 7.4 and

an average $\beta = 6.5$. Briaud (1992) also fit a power curve to the mostly clay database of c_u and p_L^* assembled by Baguelin et al. (1978), and proposed:

$$c_u = 0.67 \cdot p_L^{*0.75} \dots\dots\dots (2.15)$$

Because eqns. 2.14 and 2.15 provide very similar results, we did not use the latter.

Gibson and Anderson (1961) looked at the semilog-linear behavior of the PMT curve above the yield pressure and proposed the following relationship:

$$p = p_y + c_u \ln\left(\frac{G}{c_u} \times \frac{\Delta V_c}{V_c}\right) \dots\dots\dots (2.16)$$

As shown in **Figure 2.14**, for a constant G/c_u ratio, the slope of the pressure versus cavity strain plot after attaining the yield pressure represents the shear strength, $c_{u\ pk}$. Also shown in **Figure 2.14**, some geomaterials, including the rock tested during this research, may exhibit additional curvature above the yield pressure.

Mair and Wood (1987) describe this curvature as a strain-softening response, resulting in a lower, ultimate shear strength, $c_{u\ ult}$, at larger strain. They favor this ultimate shear strength because “less uncertainty surrounds the determination of the apparent large strain strength given.... at large deformations.”

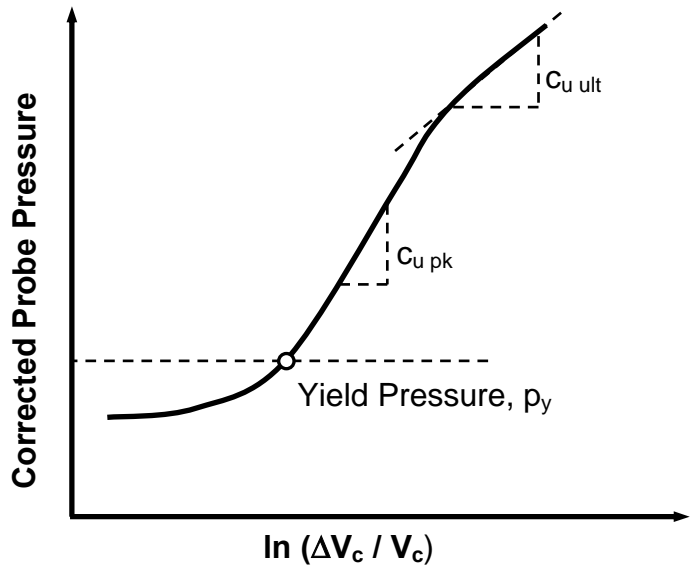


Figure 2.14 Comparison of Peak to Ultimate Shear Strength

The subtangent method results from an analysis of the shear stress-strain curve, wherein a peak value of c_u is determined graphically, usually at or just above the yield pressure. Briaud (1992) discounts this method as providing much too high c_u values for preboring pressuremeters. We did not use this method, primarily because the presence of cracks invalidates the continuum assumption necessary to develop the shear curve.

2.2.9 Unconfined compressive strength

As described above, after cracking reduces the circumferential stresses to near zero, the applied radial stress becomes analogous to an unconfined compressive test. Haberfield (1997) states that the response of the rock after cracking should remain elastic until reaching the unconfined compressive strength, q_u . After attaining q_u , the tensile cracks continue to propagate, but plastic shearing brings about a curved response with decreased stiffness (Mair and Wood, 1987). Haberfield (1997) suggests that plastic shearing begins only after surpassing the unconfined compressive strength, probably above the yield pressure. He states “the curvature in the load deformation response of a pressuremeter in weak rock at pressures below q_u is therefore likely to be the result of gradual crack propagation rather than yielding of the rock.” Therefore, either p_y or p_L may correlate directly with q_u . Also, assuming undrained post-yield behavior, any of the methods used above to calculate the undrained shear strength, c_u , could provide an estimate of q_u using:

$$q_u = 2 c_u \dots\dots\dots(2.17)$$

Finally, a correlation using the pressuremeter modulus to calculate q_u may prove viable (inverse of modulus-strength relationship used for reinforced concrete design).

2.2.10 Limitations of the PMT

The preparation of a satisfactory test hole presents the most significant obstacle to the quality and usefulness of a pressuremeter test. The driller must control the rotational rate of the drill bit, the down-pressure on the rods, the drill fluid pressure, and the flow rate provided to the drill bit to flush the cuttings. The type of drill bit used (preferably bottom discharge), the type of drill fluid, and the annular clearance between the borehole wall and the drill rods also affect the borehole quality. Different geomaterials require adjustments to all of these parameters to avoid excessive erosion and disturbance of the side of the borehole, the area that the pressuremeter probe will test. For an over-sized hole, the most common test difficulty, the limited expansion of the probe may prove inadequate to contact the sidewall and/or insufficient to reach a limit pressure. In the latter case, researchers such as Mair and Wood (1987) suggest

assuming the limit pressure as twice the yield pressure. They emphasize that this approximation provides a lower bound estimate and “a conservative assessment of strength.” Briaud (1992) suggests that although the quality of the borehole may significantly affect the pressuremeter modulus, it has less effect on the limit pressure.

The horizontal orientation of the pressuremeter test results in its most obvious limitation. Depending on insitu stresses and anisotropy, the modulus of rock measured in the horizontal direction can vary significantly from that in the vertical direction. The probe may also not expand adequately to contact discontinuities in the rock sidewall, testing less of the rock volume than assumed. Lastly, to a lesser extent, the experience level and test techniques of the user may also affect the test results and their evaluation.

2.3 Drilled Shaft Design with the PMT

Drilled shafts typically support design foundation loads exceeding 500 tons. Although driven piles may penetrate Florida limestone, they typically develop little side shear in the rock, and depend mostly on end bearing and side shear in the soil. Drilled shafts however may have a diameter of 3 to 10 ft in and penetrate as deep as 200 ft. Drilled shaft excavation through soil and/or rock usually requires a combination of augers, core barrels, and excavation and bailing buckets. Shaft construction in Florida also typically requires wet methods, using water or slurry, and possibly steel casing, to help support the excavation because of the high water table. After removing the cuttings, the contractor sets a reinforcement cage in the excavation and places a high-slump, slow-setting concrete using a pump line or tremie starting at the shaft bottom, displacing the shaft fluid out the top. Stress removal during excavation, disturbance, construction technique, and the type and strength of foundation soil and rock all have a significant effect on the final support capacity of the constructed shaft. As shown in eqn. 2.18, the ultimate shaft capacity, Q_u , results from a combination of side shear, Q_s , and end bearing, Q_p , less the buoyant weight of the shaft:

$$Q_u = Q_s + Q_p - W \dots\dots\dots (2.18)$$

The ultimate side resistance depends on the side area and the unit side shear capacity, f_s , and the ultimate end bearing resistance depends on the unit bearing capacity, q_p , and the end area of the shaft. Some designers rely primarily on side shear, some rely on end bearing, and many rely on a combination of both. This research focuses on the estimation of the unit side shear using the results from a pressuremeter test. Engineers may also use the pressuremeter to estimate the end bearing capacity, settlement, and lateral pile capacity. The pressuremeter modulus is commonly used for settlement calculations and the net limit pressure for unit side shear and end bearing.

2.3.1 Unit Side shear

The design procedures for drilled shafts are different from driven piles, primarily due to installation differences. Where driven piles benefit from the greater lateral stresses and densification caused by soil displacement during driving, drilled shafts cause a reduction in the lateral stress and shear strength due to excavation disturbance. The fluid concrete may replace the reduced lateral stress, but the net disturbance effect depends on many factors including the time of excavation, drill fluid, side roughness, shaft cleanliness, and type of soil or rock. To full utilize the available shear capacity of the rock and avoid costly conservatism (larger diameter, longer length, or more shafts), the engineer must accurately assess the side shear and control the construction process. Rock formations that have highly variable properties in either the axial or lateral direction, like Florida limestone, complicate shear strength and shaft capacity calculations. Insitu tests, like the pressuremeter, help assess this variability.

This section presents two methods for the determination of unit side shear for drilled shaft design. The strength parameter method, derived from the Mohr-Coulomb failure criteria, utilizes strength parameters from unconfined compressive tests and splitting tensile tests. The empirical LPC method uses the pressuremeter test results more directly.

2.3.2 Strength Parameter Method

The FDOT and many other designers in Florida currently use the strength parameter method. It estimates the side shear capacity of the rock from laboratory strength tests on field core specimens. The designer must obtain a sufficient number of core samples to assess the strength variability. In Florida limestone, the shaft concrete is usually both stronger and stiffer than the rock. Therefore, failure along the rock-shaft interface of a properly constructed shaft depends mostly on the shear strength of the rock. As shown in **Figure 2.15**, from McVay et al. (1992), at the relatively low stress conditions typical of drilled shafts, the cohesion component of the shear strength dominates the side shear capacity. McVay et al. (1992) define the Mohr-Coulomb failure plane, and in turn, the rock's cohesion intercept.

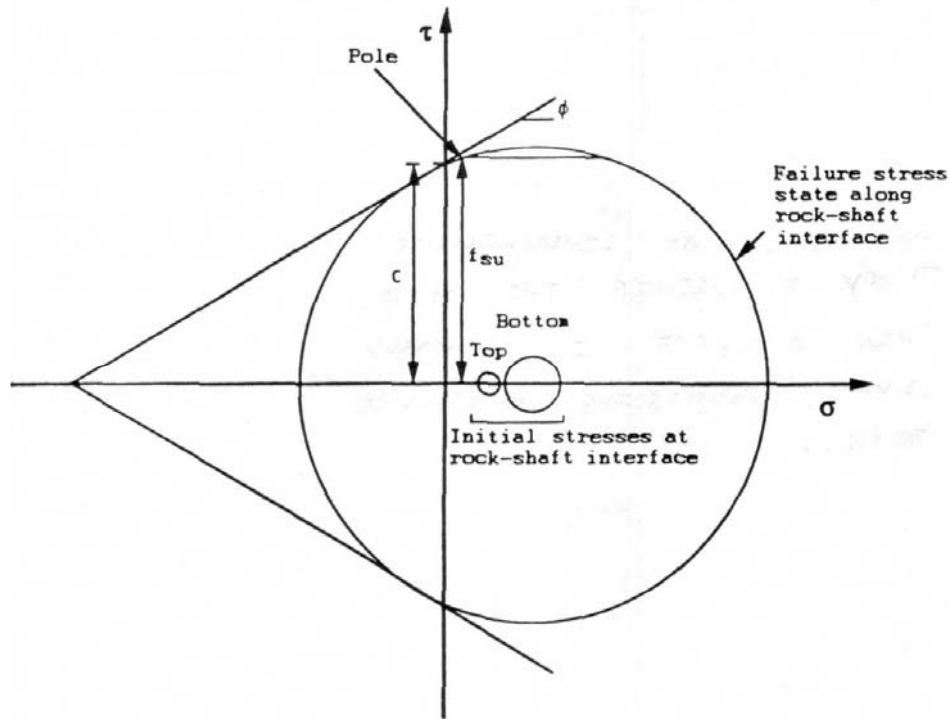


Figure 2.15 Rock-Shaft Interface Strength (McVay et al., 1992)

The designer can define the failure plane using multiple triaxial tests at different confining pressures or, more easily, using the unconfined compressive and splitting tensile strengths. As shown in **Figure 2.16**, McVay et al. (1992) derives an approximate equation relating the ultimate shear strength, f_{su} , of the limestone to these latter tests:

$$f_s = f_{su} = \frac{1}{2} \sqrt{q_u} \sqrt{q_t} \dots\dots\dots (2.19)$$

The next step in this design process involves the selection of q_u and q_t values for eqn. 2.19. For the randomly variable Florida limestone, the recommended procedure requires a distribution of q_u and q_t values representative of the entire bridge site, obtained either from extensive testing or by using a Monte-Carlo simulation. The latter method generates a fully populated distribution of q_u and q_t , then selects a random

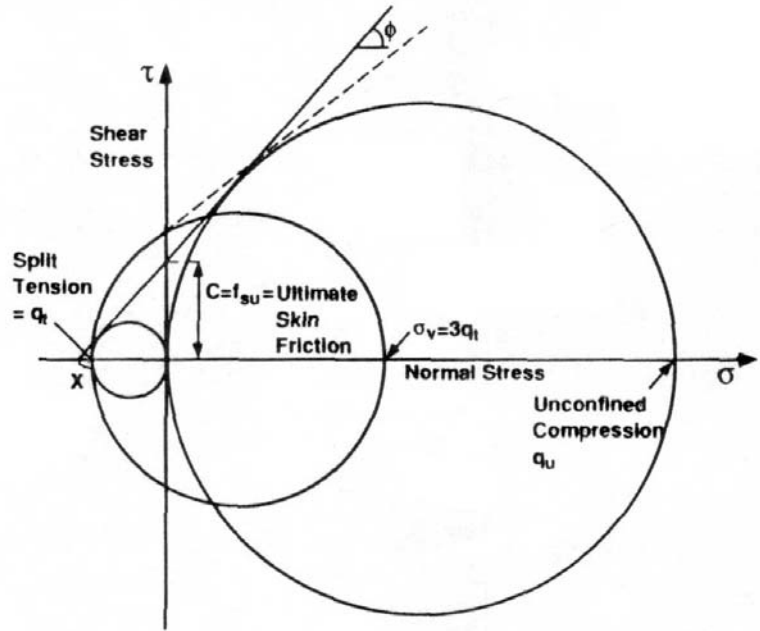


Figure 2.16 Strength Envelope Approximation from q_u and q_t (McVay et al., 1992)

group (5 to 10 values) of paired q_u and q_t values from which to calculate an average unit shear strength. This estimated unit shear strength is also multiplied by the average core recovery (or some would use the RQD) to account for voids in the rock formation. This selection process is repeated to obtain a distribution of unit shear strength values, defined by a mean and a standard deviation to identify the site variability.

An important consideration when obtaining parameters, such as q_u and q_t , is site variability. Practical economic limits usually restrict the number of cores retrieved from the field and the number of lab tests performed on them. The low recoveries typical of Florida limestone further complicate the sampling process. These issues affect the standard deviation and mean for the unit shear strength distribution. If more samples are tested, the degree of dispersion will be better defined, which would lower the sampling error associated with the standard deviation and mean for the q_u and q_t populations. This in turn will decrease the confidence interval for the unit shear strength chosen for the design. Confidence in a design parameter, such as unit shear strength,

results in a lower factor of safety, and will ultimately decrease material and construction costs while still providing a safe design.

2.3.3 LPC Method

Briaud (1992) reports that Menard introduced the use of the pressuremeter to estimate unit side shear for drilled shaft design in 1963 with correlations from a database of eight plate load tests and six short piles in sand and silt. Since then, the load test database has grown considerably, but the basic concepts developed by Menard remain the same. Briaud (1992) summarizes the current design method published by the Laboratoire des Ponts et Chaussees (LPC). The LPC method, keyed to the design curves of f_s versus p_L described in **Table 2.1** and shown in **Figure 2.17**, considers different types of soil and rock for both driven piles and drilled shafts, and their method of insertion. If averaging test results for a homogenous layer, Briaud (1992) suggest using an equivalent limit pressure, p_{Le} , given as:

$$p_{Le} = \frac{1}{2a} \int_{-a}^{+a} p_{L(z)} dz \dots\dots\dots (2.20)$$

For drilled shafts with a diameter, B, greater than 3.3 ft, $a = B/2$, and for lesser diameters, $a = 1.65$ ft. Using **Figure 2.17**, the designer can assign an average unit side shear value to each “layer”, and then sum the results along the length, z, and perimeter, P, of the shaft to calculate the ultimate side resistance as:

$$Q_s = P \int_0^h f_{su} dz \dots\dots\dots (2.21)$$

The designer may also use the Monte Carlo simulation described above to address the variability in the **limit** pressures from the pressuremeter tests. After generating a fully populated distribution of limit pressures and calculating the corresponding side shear for each, a random group of side shear values (5-10) may be used to generate the average unit side shear for a single shaft. Then, after generating multiple random groups and average unit side shear values, the mean and standard deviation of the average side shear distribution can be use for design.

Table 2.1
Pressuremeter Design
Curve Selection
(Briaud, 1992)

Pile	Soil	Clay/Silt	Sand	Gravel	Chalk	Marl/marly limestone	Weathered or fractured rock
Drilled - dry	Q1*	Q2(2) Q3(3)			Q3* Q6 (2)	Q4* Q5 (2)	Q6*
Drilled - with mud	Q1*	Q1*(6) Q2	Q2 (6) Q3		Q3* Q6 (2)	Q4* Q5 (2)	Q6*
Drilled - with casing (casing retrieved)	Q1* Q2(4)	Q1*(6) Q2	Q2(6) Q3		Q3* Q4(4)	Q4	
Drilled - with casing (casing left in place)	Q1	Q1	Q2		Q2	Q3*	
Caissons (1)	Q2 Q3(5)				Q4*	Q5	Q6*
Driven - metal (closed end)	Q1* Q2(5)	Q2	Q3		Q4	Q4	Q4*(7)
Driven - concrete	Q2	Q3	Q3		Q4*	Q4*	Q4*(7)
Driven - molded (10)	Q2	Q2*	Q3		Q4	Q4	
Driven - coated (11)	Q2	Q3*	Q4		Q5*	Q4*	
Injected - low pressure	Q2*	Q3*	Q3*		Q5*	Q5*	Q6*
Injected - high pressure (8)	Q5*	Q5*	Q6*		Q6*	Q6*	Q7*(9)

(1) Without casing left in place (rough contact).
 (2) Reaming and grooving before pouring concrete.
 (3) Reaming and grooving before pouring concrete, for very stiff clays only ($p_t \geq 1.5$ MPa or 15.7 tsf).
 (4) Drilling in the dry without twisting the casing.
 (5) Stiff clays ($p_t > 1.5$ MPa or 15.7 tsf).
 (6) Long piles (> 30 m or 98.4 ft).
 (7) If driving is possible.
 (8) Selective and repetitive injection at a low rate of flow.
 (9) (8) and proper grouting of the fissured mass. Especially for micropile for which load tests are recommended.
 (10) Driven closed-end casing, once at final penetration the casing is filled with concrete, the point is left in place and the casing is retrieved.
 (11) Driven pipe or H pile with an oversize shoe (50 mm or 1.97 in. oversize); as the pile is driven, mortar is injected in the annulus.
 * Probably conservative, but the friction cannot be increased without a verification by loadtesting.

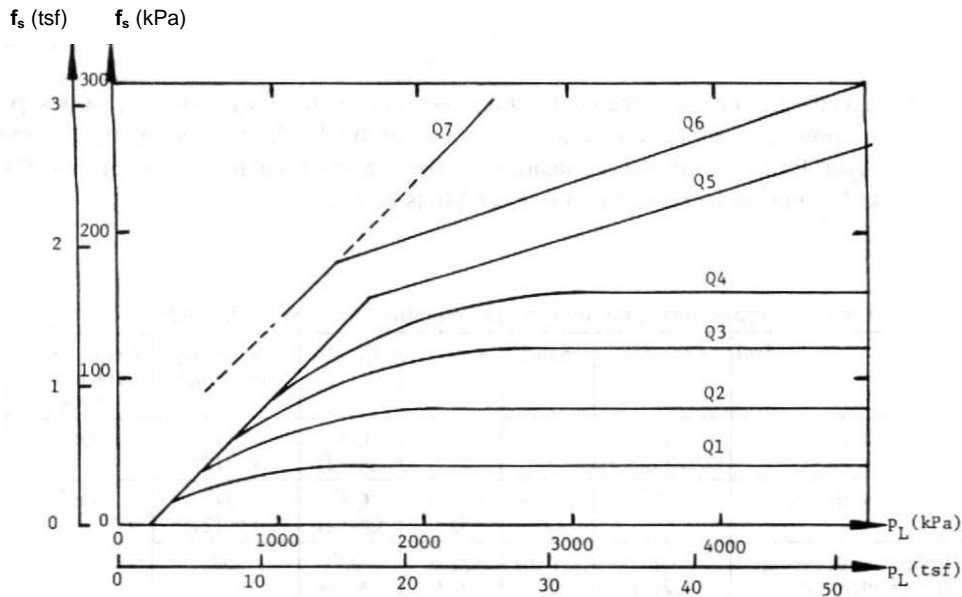


Figure 2.17 Unit Side Shear Correlation Chart for Pressuremeter
(Briaud, 1992)

2.3.4 Proposed Side Shear Method

The main goal of this research is to use the pressuremeter to facilitate the design of side shear resistance for drilled shafts in Florida limestone. Using the relatively reliable strength parameter method described above, the PMT test could provide the q_u and q_t values needed for design. By replacing the two-step process of coring and lab testing with the more immediate pressuremeter test results, the designer may obtain more tests for the same investigation cost. The testing of rock cores incurs two major expenses: a drilling crew to core the rock, and a lab to perform two different tests on the samples. Laboratory strength tests are typically performed on no more than 8 to 10 samples per corehole versus 6 to 8 PMT tests per hole. However, the volume of rock tested by the PMT is much greater. Because only the best portions of the rock are tested, some engineers conservatively multiply the unit side shear by the core recovery percentage to account for potential voids and weak zones. By contrast, core recovery does not affect the pressuremeter as it tests the voids, cracks, fissures, soft zones, and hard zones in an unbiased manner. Lab tests also typically require 2 to 3 weeks to perform, while the PMT provides immediate test results. In summary, using more pressuremeter tests should better define the standard deviation and mean of the q_u and q_t distribution, reducing the sampling error, and increasing confidence in the design parameters. This results in a lower safety factor, and decreased foundation costs. We investigate two alternative methods of obtaining q_u and q_t from the PMT herein:

- Using the PMT cracking pressure to estimate the tensile strength, and either the yield pressure or limit pressure to estimate the compressive strength.
- Using the PMT modulus to estimate the rock modulus. Then use the rock modulus to estimate the unconfined compressive strength, and the unconfined compressive strength to estimate the tensile strength.

The first method is more direct, and it could provide a more reliable correlation.

2.4 Survey of State Drilling Practice

The FDOT currently performs core borings to assess rock competency and obtain core samples for strength tests. They require at least an HW (2.4") size core sample, and recommend a 4" diameter core for better recovery and sample quality. A survey of state drilling practice undertaken during the initial phase of this project provided basic constraints for the size of the insitu device investigated in this research. Six FDOT district offices and two consultant firms responded to the survey questions as follows:

1. What type of drill rigs do you have in your office?
*CME-75, CME-45, CME-550, CME-55, Diedrich D-50, Mobile B-30.
 FDOT State Materials Office and District 5 Materials Office do not have drill rigs, but both have a CPT rig.*
2. In general, how many persons work in one drill crew?
2 to 4 persons, 3 persons common
3. What type of drill bits and sizes do you have in your office?
*Drag bits, size 3 1/8" to 4 1/8", Roller Cone Bits, size 2 1/4" to 14",
 Tri-Cone Roller Bit, size 3 7/8" (Districts 1, 3, 4, 6, 7),
 Tri-Cone Roller Bit 5 7/8" (District 3)*
4. What type of core barrels and sizes do you have in your office?
Acker 4"x5 1/2", Christensen HWD4, Christensen 8WD4
5. What type of casing and sizes do you have in your office?
NW, HW, AW, BW, SW in 5' lengths
6. What type of drill rods and sizes do you have in your office?
AWJ, NWJ in 5' lengths
7. Do you use Hollow-Stem Auger in soil exploration? What size?
seldom used, sizes 2 1/4" to 6 1/4"
8. Based on your local experience, what is the average rock recovery and RQD using different core barrels in different rock condition?
Highly dependent on driller:

Size of Core Barrel	SPT-N <50		SPT-N >50	
	Recovery	RQD	Recovery	RQD
HW 2.4"	50-80%	20-50%	15-90%	15-80%
4"	60%	20%	90%	80%

Final Report Contract #BC354 RPWO #13

9. Do you always perform rock coring when rock is encountered in a boring? If not, what are the criteria for performing rock coring?

Only on projects that drilled shaft design is expected.

10. What type of tests, including in-situ testing and laboratory testing do you perform on rocks?

unconfined compressive and split tensile tests

11. If rock coring and/or strength testing were not performed on rocks, how do you select the unit skin friction and unit end bearing in drilled shaft design?

correlation between SPT-N and skin friction

12. If insitu rock strength testing will be performed in borehole, which approach do you prefer: 1) perform testing between each core run, 2) perform testing after the boring reaches the required depth.

majority prefer performing tests after boring reaches the required depth.

Based on the above results, an insitu test performed within a 3"-6" diameter borehole can utilize a variety of rod sizes and strength tests can be obtained for comparison.

3. LABORATORY TESTS OF FLORIDA LIMESTONE

Laboratory tests performed at UF on limestone samples during this project included compressive strength, elastic modulus, and tensile strength. These samples came from three different sources. First, Cepero (2002) and Jacobs (2003) performed tests on numerous trial mix and core samples of "Gatorock", a synthetic limestone product used to prepare large samples for pressuremeter tests in the UF laboratory. Second, Jacobs (2003) tested several boxes of 4-inch-diameter core samples obtained by the FDOT State Materials Office from two Florida bridge sites, the SR10 Choctawhatchee Bridge and a bridge in Hallandale Beach. Third, Jacobs (2003) obtained N-size (1.75 in diameter) core samples during pressuremeter tests at the SR20 Blountstown Bridge. The State Materials Office also provided lab test results with deflection measurements from tests that they performed on field cores, which we analyzed and included in the Chapter 6 correlation plots. The Appendix contains detailed results from the UF lab tests. The Appendix also contains a summary of all the strength and modulus data used for correlation purposes in Chapter 6.

3.1 Sample Preparation

Other than extrusion from their form and removal of any surface imperfections, samples obtained from the Gatorock trial mix cylinders required little preparation before testing. Core samples were first logged and then cut to length using a concrete masonry saw and cutting template as required in ASTM D 2938. Generally, the prepared samples had length to diameter ratio of 2:1, with a minimum of 1.5:1 accepted for core samples with lower RQD. Most tensile strength samples followed ASTM recommendation of a length to diameter ratio of $L/D = 0.2-0.75$. All samples tested were intact, and zones in the cores with obvious defects due to coring or handling were avoided during sample preparation.

Compressive tests performed during the Gatorock trial mix tests used rubber end caps, the compression of which affected deflection measurements but not the ultimate strength. The remaining test specimens used a lubricant applied to the sample ends to reduce friction between the load platen and the sample. Friction at the sample ends will

produce undesired lateral stresses in contradiction to the intended uniaxial state of stress. Labuz and Bridell (1993) investigated possible lubricants to lessen the frictional constraint during moderate to extreme load and very small displacements. Among other lubricants, they tested stearic acid, a fatty acid with a long molecular chain length. It displayed the lowest coefficient of friction (0.022) out of the six lubricants tested. Prepared by heating a mixture of equal parts (by weight) of stearic acid flakes and petroleum jelly to 70°C, the result wax-like substance solid leaves a thin film when applied to the steel load platens. We used this relatively inert lubricant for all compressive tests that did not have rubber end caps.

3.2 Lab Tests

The following ASTM Specifications provided guidance followed during the tests on the limestone core samples performed at the UF for this research:

- ASTM D 4543-85 Preparing Rock Core Specimens and Determining Dimensional and Shape Tolerances
- ASTM C 469-96 Static Modulus of Elasticity and Poisson's Ratio of Concrete in Compression
- ASTM D 2938-95 Unconfined Compressive Strength of Intact Rock Core Specimens
- ASTM D 3148-96 Elastic Moduli of Intact Rock Core Specimens in Uniaxial Compression
- ASTM D 3967-95a Splitting Tensile Strength of Intact Rock Core Specimens

We used calibrated load cells to obtain accurate force readings for all tests, and linear variable displacement transducers (LVDT) to measure deflection when needed. The LabVIEW 6.0, by National Instruments (a measurement and automation computer program), digitized and stored analog output from the LVDT and load cell every ½ second, providing data for a nearly continuous plot of the stress-strain data. The following sections describe the tests performed in general, followed by any variations in test procedure for each group of samples.

3.3 Compressive Strength

The unconfined (uniaxial) compression tests performed during this research provided a definitive means of assessing the compressive strength of the rock (for at least the intact portion of each core). ASTM D2938 specifies that the loading rate for the unconfined compressive test achieve failure within 2 to 15 minutes, the same load rate used for elastic modulus testing. We chose a time of 8 minutes as the target to achieve failure. When performing modulus tests before compressive strength tests, the sample must first be fully unloaded to remove the compressometer before proceeding to a compressive failure. Tests that measured deflection between the load platens did not require this step (but provided less accurate modulus results). The peak load attained, divided by the sample cross-sectional area, provided the ultimate unconfined compressive strength, q_u , of the specimen.

3.3.1 Compressive Modulus

Measurement of the axial strain that occurs during a compressive strength test provides a modulus to characterize the rock stiffness. Quality stiffness results require a sample compression measurement made directly on the test sample, usually with a compressometer. For the core tests performed for this research, we obtained a compressometer specifically designed for a 4 in core diameter. Measurement of the deflection between the load platens usually includes some seating of the sample, and a deflection measurement of a platen with respect to the machine base will include seating of the load head, platen compression, and any stretch of the loading apparatus. This research included measurements made in all three ways, the latter methods necessitated by the lack of an appropriate size compressometer. For modulus tests conducted without a compressometer, we first calibrated the test system using an appropriately sized cylinder of steel to determine the amount of deflection exceeding that expected for the steel cylinder. We then subtracted this excess deflection from any subsequent test measurements to estimate the true sample deflection. The Gatorock trial mix, SR20 PMT cores, and stress-strain data obtained from the State Materials Office all required such calibration corrections.

ASTM C469 provides better guidance for compressibility testing, and although specific to concrete, generally does not conflict with ASTM D3148 except that it allows a higher rate of loading. For rock testing, D3148 requires a loading rate that would cause failure within 2 and 15 minutes, from which we chose a target of 8 minutes. Varied by anticipated sample strength, this load rate never exceeded 2,500 lbs/min. To maintain an elastic response and protect the compressometer, ASTM C469 also specifies that samples be loaded to only 40% of the ultimate compressive strength for three unload/reload cycles. The specimen stress, the measured force divided by cross-sectional area, divided by its strain, the measured deflection divided by gage length, provides the initial tangent modulus, E_i . When using the compressometer, the user must multiply the LVDT measurement by one half to get the sample deflection and then divide by the gage length. The strain for a platen measurement, after correction for system error, comes from the measured deflection divided by the sample height. The specifications disregard the first load cycle, which contains seating error. The two remaining stress-strain measurements, averaged together, provide the modulus of elasticity for the material. This test process requires an estimate of the sample's ultimate strength prior to the actual test, somewhat difficult to guess for core samples. Therefore, rather than sacrificing a specimen, lower load levels were chosen to avoid damaging the compressometer, and the loading was carefully monitored during the tests.

3.3.2 Splitting Tensile Strength

Loaded on the diameter, the splitting tensile strength tests followed ASTM D3967, with specimen length to diameter ratios of $L/D = 0.20-0.75$. The FDOT core specimens had a 4 in diameter and a 2 in thickness, and the SR20 core specimens had a 1.74 in diameter and a 1 in thickness. The Gatorock cores from the lab PMT tests had a 2.55 in diameter and a 1.5 in thickness. The Gatorock trial mix samples were tested full size with a 4 in diameter and 8 in length, as done for concrete specimens.

Plywood bearing strips, 0.25 in thick, at the top and bottom of the specimen reduced the high point loading stress at the load platen as recommended by ASTM. ASTM specifies that failure occur within 1 to 10 minutes of loading. These tests did not require a lubricant at the platen surface. The compressive force, P , applied on the side of the specimen imparts tensile forces within the specimen causing it to break in half along a vertical plane between the loading points. Eqn. 3.1, from D3967, calculates the splitting tensile strength, q_t , of the limestone samples:

$$q_t = \frac{2P}{\pi LD} \dots\dots\dots(3.1)$$

The above equation divides the splitting force by the area of the material resisting the lateral splitting of the specimen, or the length multiplied by the diameter. The $(2/\pi)$ term adjusts for the shape of the stress distribution across the sample, ranging from compression at the loading points to reasonably uniform tension across the remainder of the split section.

3.3.3 Gatorock Trial Mix Samples

The Gatorock trial mix specimens were tested using the UF Tinius Olsen hydraulic load frame shown in **Figure 3.1**. The load frame included a large hemispherical bearing to insure axial loading. The bottom platen applied the load, and a digital electronic indicator, manufactured by Humboldt (± 0.0001 in precision) measured the deflection of the bottom platen. The tests were run at a nearly constant rate of loading that would achieve failure between 5 and 15 minutes. Readings of the applied load were recorded every 0.005 inches.

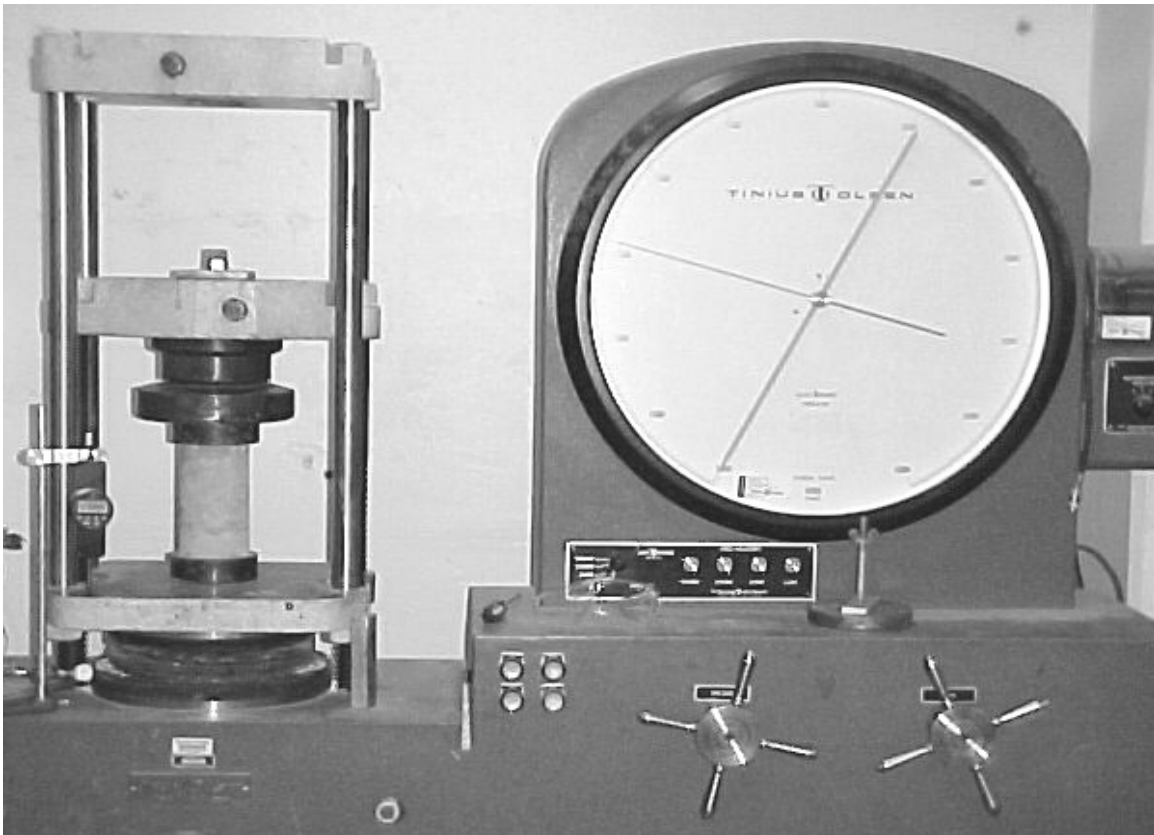


Figure 3.1 Tinius Olsen Load Machine, Gatorock Sample and Digital Dial Indicator

3.3.4 FDOT and Gatorock Cores

To better simulate field conditions and offset the effects of long-term storage the FDOT cores from SR10 and Hallandale Beach were kept submerged for several weeks before testing. **Figure 3.2** shows the UF Tinius Olsen load frame used to perform these tests. For better accuracy, we performed the modulus tests using a compressometer designed for a 4 in core diameter as shown in **Figure 3.3**. A linear variable differential transformer (LVDT) from Schaevitz Engineering measured the sample compression over the 4 in compressometer gage length. The data acquisition A/D card used with the LVDT provided a resolution of 0.000015" for this measurement. Although there were some equipment delays in testing the cores, the effect appear minor and difficult to quantify.



Figure 3.2 Gatorock Sample with Compressometer and LVDT for Deformation



Figure 3.3 Automated Tinius Olsen Load Frame used for Tests of Gatorock Cores

3.3.5 SR20 PMT Cores

The smaller 1.74-in-diameter SR20 cores obtained during pressuremeter testing did not have adequate gage length to obtain accurate sample compression measurements using a compressometer. Therefore, we used the modified triaxial test machine shown in **Figure 3.4**, and measured the sample deflection across the platens. Manufactured by Humboldt (model: HM-2605, Triscan-50), it has a capacity of 11,000 lbs and with the use of a 10,000 lb load cell, provided enough force to adequately test the samples. The triaxial machine allowed the strain rate to be specified for both the loading and unloading of the specimens, which provided complete control of the test.

A ball bearing load platen on the top minimized the potential for non-uniform loading due to non-parallel sample ends. Using the average of two LVDTs also eliminated any bending effects. The difference of the side to side measurements did not exceed 0.005 in during testing.

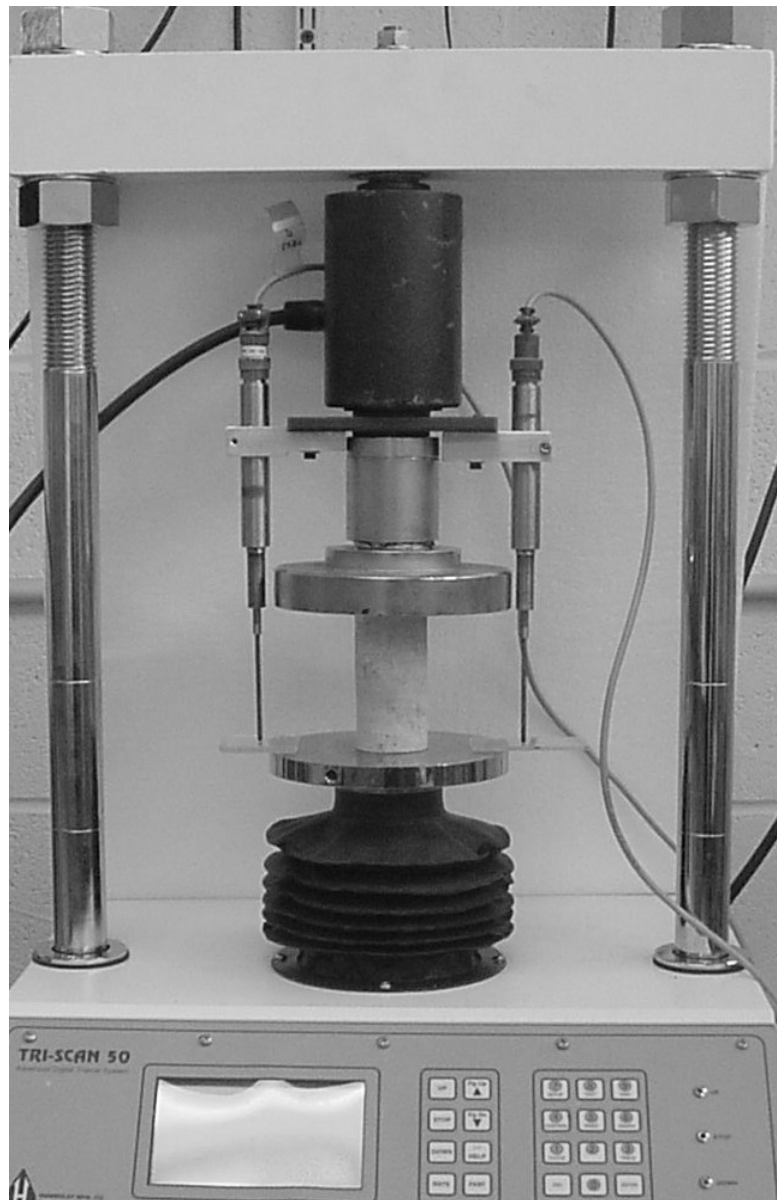


Figure 3.4 Triaxial Machine Used for SR20 Cores

4. PRESSUREMETER DESIGN

The University of Florida owns a Texam pressuremeter, and we chose this device for initial trial tests in limestone. Modifications to the membrane were explored for testing in soft rock, including improving the membrane's resistance to puncture and reducing the hysteresis of its calibrations. Because Florida limestone has a relatively high modulus, any error in volume or pressure measurement may lead to erroneous test results. The manufacturer, Roctest, provides only a rubber membrane and lantern sheath. The other pressuremeters investigated were similar in nature and did not appear to provide stronger membranes (including Cambridge Insitu). Kevlar fiber was investigated as a sheath material because of its strength. Although Kevlar thread is very stiff, a knitted sheath woven from Kevlar might provide flexibility and puncture resistance. We tabled this idea until after evaluation of the Texam during actual tests. Subsequently, four lab tests performed with the Texam during the laboratory trials did not provide the desired results and modifications were required. We rejected additional membrane stiffness because the Texam system did not have adequate pressure reserve and was below the yield pressure in lab trials at its capacity of 1,500 psi with existing membrane. Also, its system compliance (volume loss) was too great for a reliable and accurate modulus measurement in rock.

In searching for a more robust membrane, we identified a system specifically designed for testing soft rock, the Probex-1, also made by Roctest. It had three times the pressure capacity of the Texam, seemed well-designed, had digital data storage, and promised to provide the correlation data required. It did not have a reliable means of controlling the pressure during unloading, but this could be easily fixed by adding a flow control valve to the retract hose. Although the price of this pressuremeter exceeded the dollar amount allotted in this research to develop a new system, we were able to rent it for evaluation in the field and laboratory. We then purchased a triple-tube core barrel with a special bottom discharge bit to form the hole required and provide a core for correlation between PMT field tests and laboratory strength tests. As shown later, lab tests with the Probex-1 were successful, but field tests proved less so.

5. LABORATORY AND FIELD PMT TRIALS

Cepero (2002) and Jacobs (2003), both graduate students at UF, report the details of lab and field trials performed with the Texam and Probex-1 PMT probes. This chapter discusses their tests and results.

5.1 Pressuremeter Lab Tests

Cepero (2002) performed pressuremeter tests at the UF Civil and Coastal Engineering laboratory in eight large samples of “Gatorock”, a synthetic limestone developed specifically for this research. Gatorock is essentially a reconstituted limestone product, mixed from crushed limestone, cement, and water. It has relatively homogeneous, isotropic properties, and changing the water or cement content of the mix affects the strength and stiffness in a predictable manner. Natural limestone samples of the size needed for pressuremeter testing would have been difficult and expensive, both to obtain and to handle. Thus, Gatorock provides a more cost effective means of conducting tests under controlled lab conditions

The major constituent of Gatorock is crushed limestone, sifted through a No. 10 standard sieve to achieve a nearly well-graded distribution (uniformity coefficient ≈ 4) with a maximum particle diameter of 0.08 in (2 mm). The other components are Portland cement (also a limestone product) and water. Before casting the large PMT samples, Cepero (2002) completed a series of mix design tests on smaller test cylinders with a 4 in diameter and 8 in height. Quarries in Newberry and Citra, FL provided the limestone used in the initial mix design tests. Limestone Products, Inc. of Newberry, FL donated $\approx 16 \text{ yd}^3$ of crusher-run limestone used for the larger PMT samples, which the State Materials Office transported this material to the UF lab. All of these quarries excavate rock from the Ocala formation.

5.1.1 Gatorock Sample Preparation

The laboratory pressuremeter tests were performed inside of a hole cored in the center of large, cylindrical Gatorock samples. A steel pipe, 24 in diameter and 36 in long, provided a permanent form to cast these large samples. Cepero (2002) chose

these dimensions to reduce the sample volume while also minimizing boundary effects and simulating the behavior of an infinite rock mass. A parametric study using the Plaxis finite element software indicated that a 24 in diameter pipe would allow the radial stress at the cylinder wall to dissipate to less than 10% of the applied pressuremeter stress, with minimal strain at the boundary. The interior of the steel pipe was also greased with vegetable oil and covered with plastic sheeting to minimize friction at the interface between the Gatorock sample and the inside wall of the steel cylinder.

Based on trial mix design results from 4 in x 8 in cylinders, a workable Gatorock mix with 20% cement and 20% water (by dry limestone weight) was chosen for the PMT samples. After a 14-day cure, the test samples prepared with these constituents obtained an unconfined compressive strength of 1,400-1,600 psi, just within the 1,500 psi limit of the Texam pressuremeter. Each of the large samples required three batches of Gatorock mixed in a 3.5 ft³ drum mixer to obtain the 8.8 ft³ sample volume needed. Graduate students Cepero and Jacobs mixed the limestone and cement dry for approximately 8 to 10 minutes, adding the water incrementally, and then mixing for an additional 8 to 10 minutes, for a total mix time of 25 to 30 minutes. They placed the wet Gatorock mix in 6 in lifts, compacted each lift with a vibratory probe. Cepero compacted the trial mix samples by rodding, but this procedure proved impractical for the larger PMT samples with a volume 150 times the mix design cylinders. Six points of insertion for a period of 4 to 5 seconds each, proved adequate to compact each lift without segregation, with one vibration point in the center and five around the perimeter approximately 6 in from the form wall.

After a 14-day-curing period, the PMT samples were cored along the central axis, over the full 36 in height, using a Hilti drill press with a 37-in-long, custom-manufactured, Hilti core barrel (**Figure 5.1**). The core barrel's outer diameter of 2-7/8 in provided a corehole with a 3.0 in diameter for the pressuremeter probe. The core samples had a diameter of approximately 2.5 in with 100% recovery. Tests on the core samples provided measurements of stiffness and strength for correlation with the pressuremeter tests. Unfortunately, unconfined compressive tests on the cores

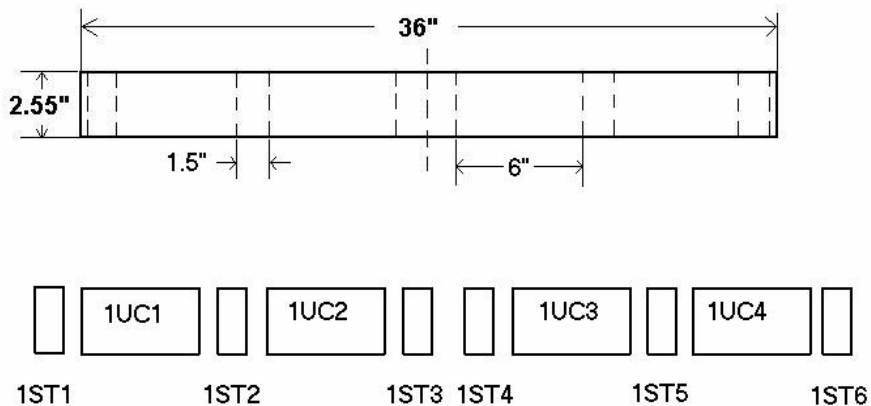
measured a greater strength, 1,949-3,213 psi, than anticipated from the mix design. This was probably due to the vibratory compaction. Therefore, the final two PMT samples were prepared with less cement, 17.5%, which reduced the strength to 1,630-1,660 psi (see Appendix).

5.1.2 Gatorock Core Tests

Gatorock cores, taken from the pressuremeter coreholes were cut to length with a masonry table saw and then tested to determine unconfined compressive strength, q_u , the splitting tensile strength, q_t , and initial tangent modulus, E_i . **Figure 5.2** shows the typical sample dimensions and the layout within each core. The Appendix presents the q_u and E_i values obtained from the compressive tests, and the results of the splitting tensile strength tests.



Figure 5.1 C. Kohlhof and C. Cepero Using Hilti Rig to Core Gatorock Sample



UC = Unconfined Compressive Test, ST = Splitting Tensile Test

Figure 5.2 Gatorock Core Layout

5.1.3 PMT Lab Setup

After coring the PMT samples and calibrating the PMT, the pressuremeter probe was placed in the center of the sample and testing begun. To assess the effects of overburden stress, some of the samples were loaded with axial pressures of 40 or 80 psi, representing 50' or 100' of soil/rock at a unit weight of 115 pcf. These samples were loaded in a large 400 kip frame (Riehle), the top load platen of which includes a central hole for access to insert the PMT probe.

Figure 5.3 shows a sketch of the sample setup for loading and **Figure 5.4** shows a picture of a sample in front of the load frame. The sample top was leveled with a paste composed of 20% water and a 50-50 mix of crushed limestone and quick set cement. (The sample bottom had a smooth and level form finish.) Plywood and steel plates were used top and bottom of the sample to apply the axial load evenly.

Figure 5.4 Gatorock PMT Sample in Front of Riehle Load Frame

After applying the desired axial confining stress, we performed stress-controlled pressuremeter tests, with constant pressure

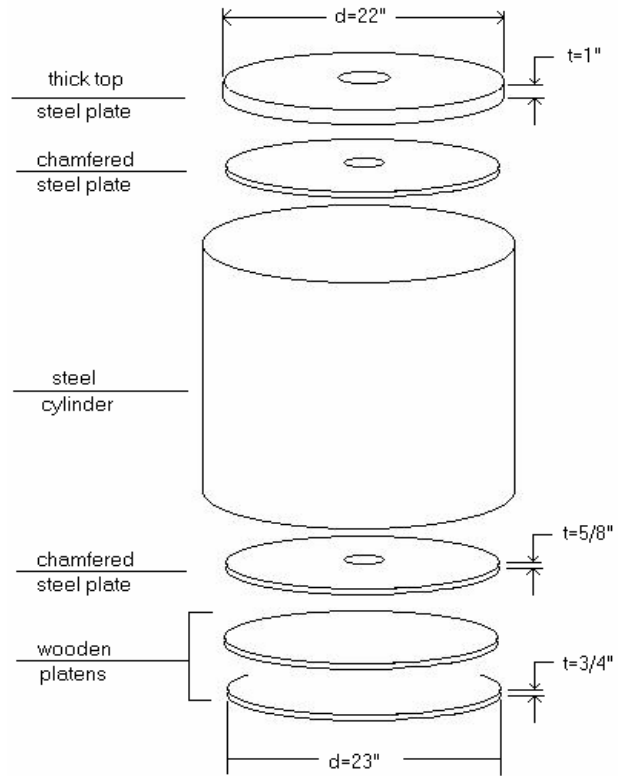
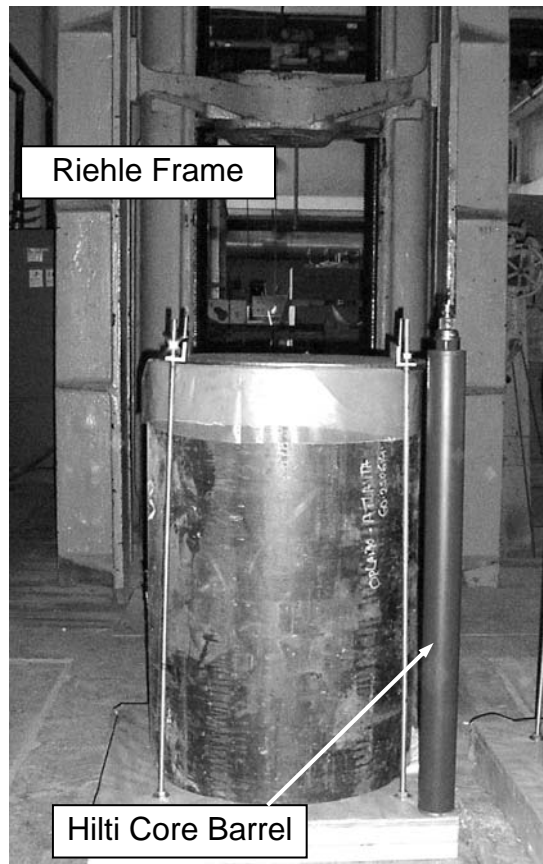


Figure 5.3 Layout Under Loading Frame



intervals and volume readings at 30 and 60 second elapsed times. The first four PMT samples were tested using the Texam probe, designated as "TT#", and the last four were tested using the Probex-1, designated "PT#." **Figures 5.5 and 5.6** show typical test curves from each probe. The larger volume correction associated with the Texam PMT added significant uncertainty to the modulus results, which are based on the slope of the curve. The higher pressure rating of the Probex-1 also provided yield and limit pressures, not attained during the Texam tests. All of the Gatorock samples cracked during the pressuremeter tests, essentially splitting the sample into two halves lengthwise, with the steel pipe preventing the halves from separating. **Table 5.1** includes the cracking pressure, readily evident in **Figures 5.5 and 5.6**.

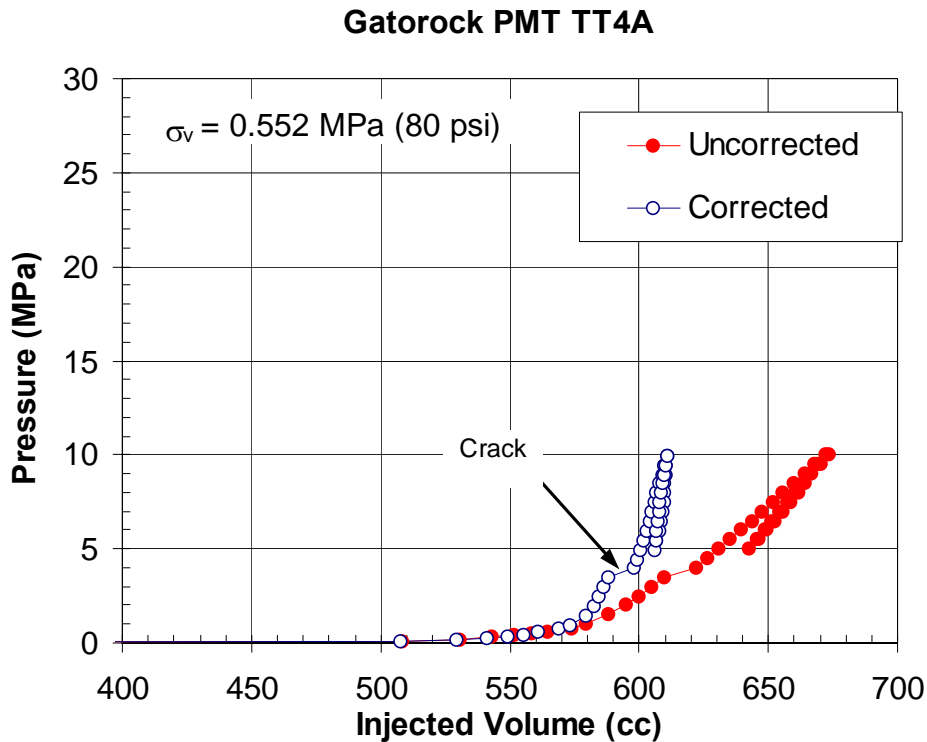


Figure 5.5 Typical Texam PMT Test

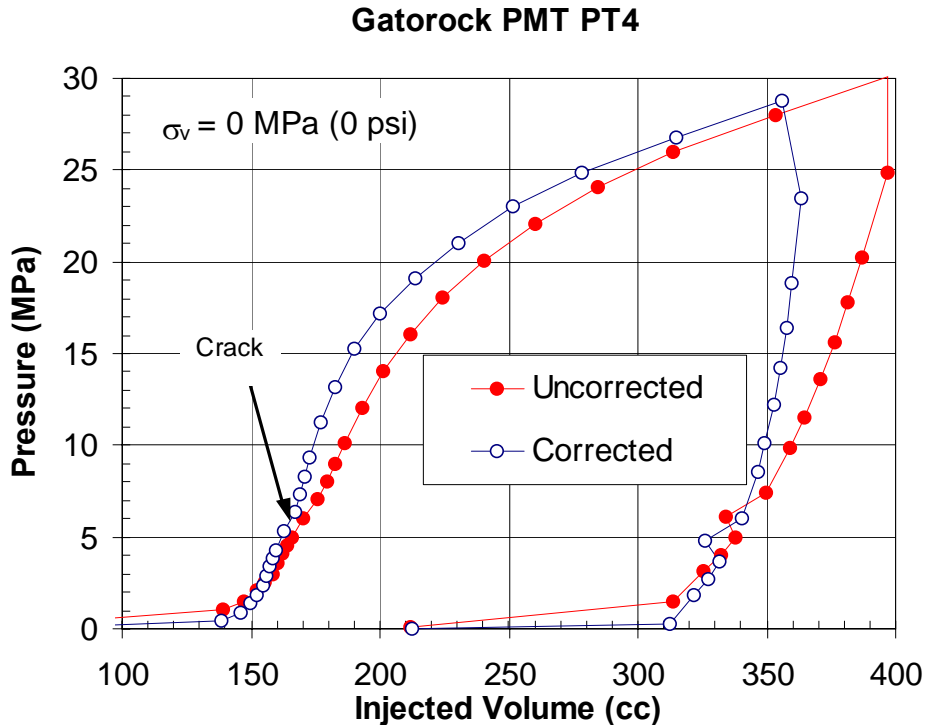


Figure 5.6 Typical Probex PMT Test

5.1.4 PMT Lab Results

Table 5.1 presents the modulus results for the lab PMT tests, calculated over linear portions of the volume-pressure curve using the classic equation (2.1).

Tables 5.4 and 5.5 compare the PMT results with the strength and modulus measurements from the core tests. In **Table 5.1**, E_{bc} refers to the modulus calculated just before the sample cracked. E_{ac} refers to the modulus calculated over the linear curve after the sample cracked, and E_{ur} refers to the modulus calculated during an unload-reload cycle after the sample cracked. The post-cracking behavior probably does not reflect the design load conditions on a drilled shaft and this report focuses correlation efforts on the modulus before cracking, referred to herein as E_{PMT} .

Figure 5.7 shows the effect of vertical stresses on the modulus (E_{bc}). The slight negative trend shown is unreasonable and indicates that, at least for the eight tests performed with Gatorrock, changes in effective stress over the expected range had a negligible effect on PMT stiffness.

Table 5.1 Lab PMT Gatorock Results

Test	PMT	Cast Date	Test Date	Elapsed Time (days)	Vertical Stress (psi)	Modulus (psi)		
						Before Crack, E_{bc}	After Crack, E_{ac}	Unload-Reload, E_{ur}
TT1	Texam	08/31/01	10/23/01	53	0	207,200	340,500	465,600
TT2	Texam	09/01/01	10/24/01	53	0	428,200	584,900	673,700
TT3	Texam	10/30/01	11/13/01	14	40	234,300	520,400	1,019,000
TT4	Texam	11/06/01	11/20/01	14	80	227,800	386,300	921,700
PT1	Probex	12/13/01	12/28/01	15	40	277,600	522,100	N/A
PT2	Probex	12/14/01	12/29/01	15	80	284,300	436,200	N/A
PT3	Probex	01/14/02	01/29/02	15	80	227,900	271,000	N/A
PT4	Probex	01/25/02	02/13/02	19	0	298,700	374,000	N/A

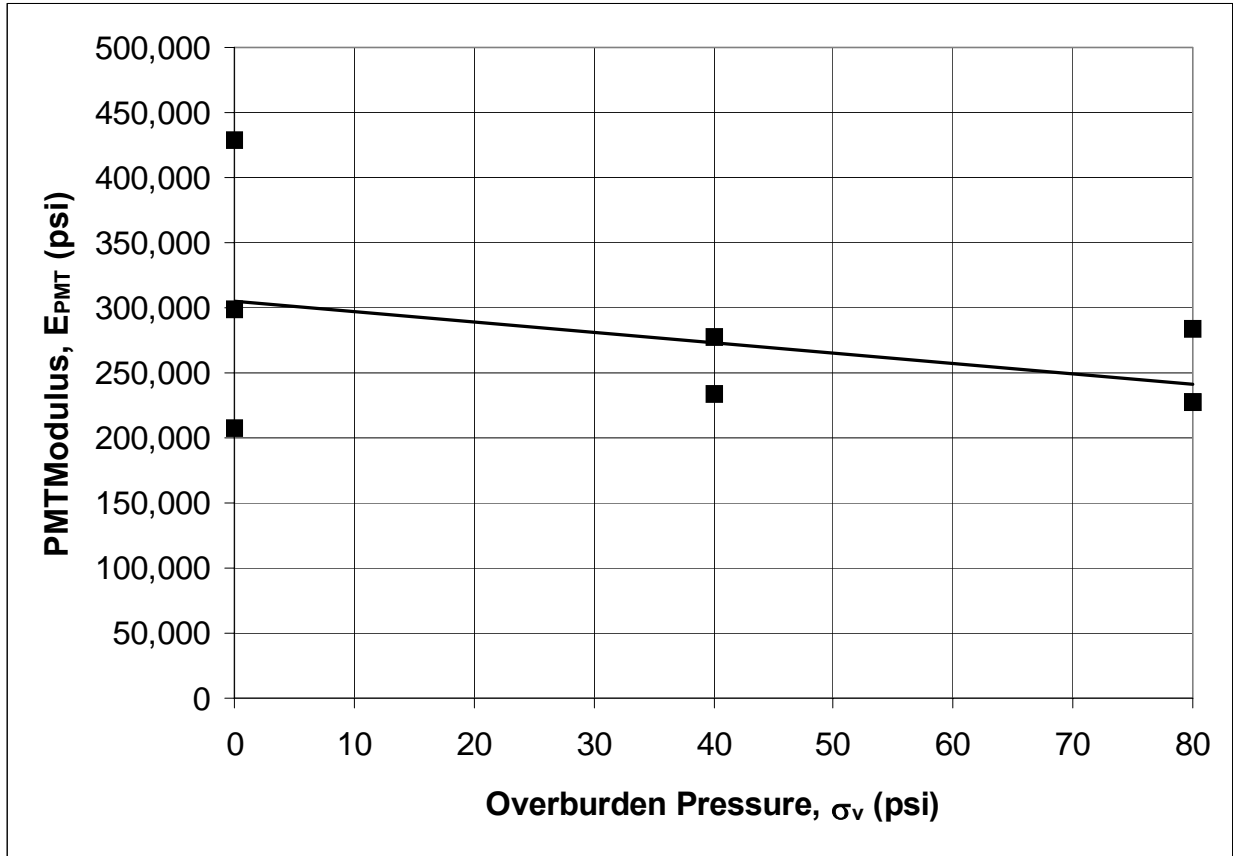


Figure 5.7 Effect of Overburden Stress on PMT Modulus in Lab Samples

5.1.5 Comparison of Lab PMT and Core Tests

Table 5.2 compares the PMT modulus (before cracking, E_{bc}) with the compressometer modulus values from the core tests. The pressuremeter modulus is generally at least 2-3 times less than the actual field modulus for a variety of reasons, among them:

- The PMT measurement occurs in the horizontal direction, which generally has lower confining stress than the vertical direction and may be affected by anisotropic properties.
- PMT measurement involves a combination of compression in radial direction and tension in circumferential direction. The tension modulus may be lower.
- The PMT modulus reflects behavior at a relatively high strain. During these PMT tests the net cavity strain at yield (ignoring end effects) is 0.5-1.0% while the compressometer strain is more than order of magnitude lower at 0.02-0.04%.

Table 5.2 indicates an average bias of 8.25, higher than expected but with a reasonably low coefficient of variation, COV = 21%. Of course, this research presents only eight tests in an artificial rock, and the correlation will require further confirmation.

Table 5.2 Lab PMT Comparison with Core Modulus

Test	PMT	Vertical Stress (psi)	E_{PMT} (psi)	E_{Core} (psi)	E_{Core}/E_{PMT} bias (psi)
TT1	Texam	0	207,200	2,226,465	10.75
TT2	Texam	0	428,200	3,517,500	8.21
TT3	Texam	40	234,300	2,395,838	10.23
TT4	Texam	80	227,800	2,041,564	8.96
PT1	Probex	40	277,600	2,079,708	7.49
PT2	Probex	80	284,300	2,042,554	7.18
PT3	Probex	80	227,900	1,764,000	7.74
PT4	Probex	0	298,700	1,625,000	5.44
Average Bias					8.25
Std. Dev. Bias					1.71
COV					20.7%

Table 5.3 tabulates the cracking pressures, yield pressures, and limit pressures obtained from the PMT tests with the core strength tests.

Table 5.3 Lab PMT Comparison with Core Tensile Strength

Test No.	σ_v (psi)	σ_h est. (psi)	K_0	Crack Press. σ_{cr} (psi)	Est. $q_t = (\sigma_{cr} - 2\sigma_h)$ (psi)	Msd. q_t (psi)	q_t bias msd/est
TT1	0	36	N/A	609	537	545.1	1.016
TT2	0	36	N/A	681	608	451.6	0.742
TT3	40	17	0.42	538	505	384.1	0.761
TT4	80	17	0.21	538	505	217.4	0.430
PT1	40	36	0.91	458	386	224.7	0.582
PT2	80	44	0.54	724	637	146.0	0.229
PT3	80	36	0.45	541	468	163.6	0.349
PT4	0	51	N/A	772	670	191.2	0.285
Average Bias						0.549	
Std. Dev. Bias						0.274	
COV						49.9%	

As discussed in Chapter 2 (see eqn. 2.8), calculation of the tensile strength from the cracking pressure requires an estimate of the insitu lateral stress. Per Briaud (1992), this relatively crude estimate was taken at the point of maximum curvature near the bottom of the transition to the linear portion of the PMT cavity strain curve. The coefficient of lateral stress, K_0 , calculated from these values is somewhat variable, possibly due to either a poor estimate of σ_h , or lateral stresses induced by expansion and contraction of the cementitious Gatorock mix as it set. **Figure 5.8** plots the estimated and measured tensile strengths.

The cracking pressure estimate of tensile strength has an average bias of 0.55, with a relatively high coefficient of variation, COV = 50%. It also appears that the Probex-1 tests overestimated the tensile strength by a greater degree than Texam tests. This may be due to the greater end restraint of the stiffer Probex membrane, which

confinement may load less of the probe length and thereby require a greater pressure to induce cracking.

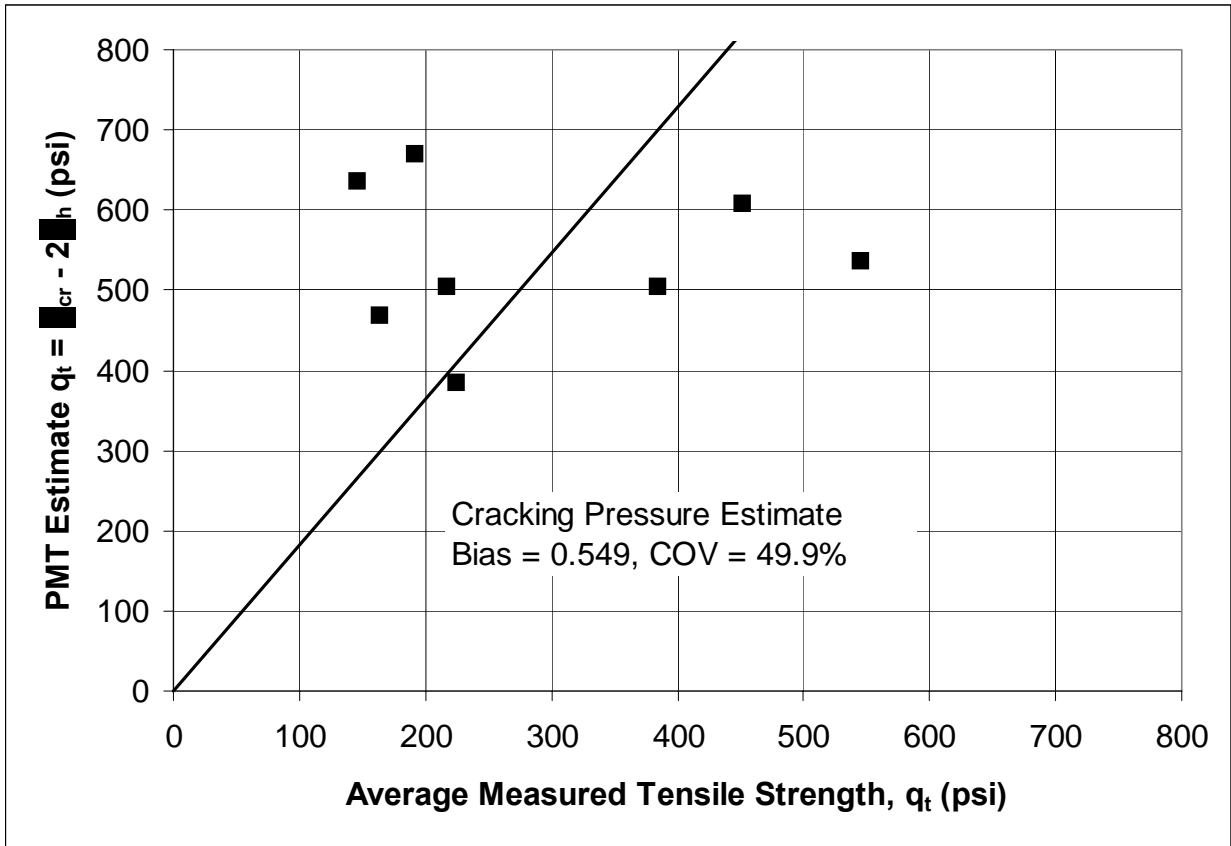


Figure 5.8 PMT Estimate of Tensile Strength

Table 5.4 shows unconfined compressive strength estimates based on correlation with yield and limit pressures. Because the Gatorock sample cracks during the PMT test at a pressure less than the yield pressure, the circumferential stress near the wall of the PMT cavity should approach zero, which results in boundary conditions analogous to the unconfined compressive test at the cavity wall. Although only the Probex-1 tests reached a yield pressure, the four values obtained correlate well with the compressive strength (bias = 0.92, COV = 13%). This strength estimate applies to both undrained and drained test conditions.

Assuming undrained behavior for the PMT above the yield pressure (i.e. zero volume change), then the limit pressure can also provide a compressive strength estimate by combining eqn. 2.7 and eqn. 2.14:

$$q_u = 2c_u = 2\left(\frac{p_L - \sigma_h}{\beta}\right) = 2\left(\frac{p_L^*}{\beta}\right) \dots\dots\dots (5.1)$$

$\beta = 5$ to 8 with higher values for stiffer material

Using $\beta = 6.5$ gives excellent agreement between the limit pressure and q_u (bias = 1.04, COV = 5%). The assumption of undrained conditions is reasonable at the cavity wall but ignores possible cracking effects. As **Figure 5.9** shows, both the yield pressure and limit pressure provide reasonable estimates of compressive strength over the limited range of material strength in these tests.

Table 5.4 Lab PMT Comparison with Core Compressive Strength

Test No.	σ_v (psi)	σ_h est. (psi)	k_0	Yield Press. σ_y (psi)	Limit Press. p_L (psi)	Msd. q_u (psi)	Est. q_u from σ_y (psi)	Est. q_u from p_L^* $\beta = 6.5$ (psi)	Bias Est. q_u from σ_y (psi)	Bias Est. q_u from p_L (psi)
TT1	0	36	N/A	N/A	N/A	N/A	N/A	N/A	N/A	N/A
TT2	0	36	N/A							
TT3	40	17	0.42							
TT4	80	17	0.21							
PT1	40	36	0.91	2757	7008	2091	2757	2145	0.759	0.975
PT2	80	44	0.54	2180	6005	1949	2180	1834	0.894	1.062
PT3	80	36	0.45	1617	5252	1660	1617	1605	1.026	1.034
PT4	0	51	N/A	1637	4900	1630	1637	1492	0.995	1.092
								Average Bias	0.919	1.041
								Std. Dev. Bias	0.121	0.050
								COV	13.1%	4.8%

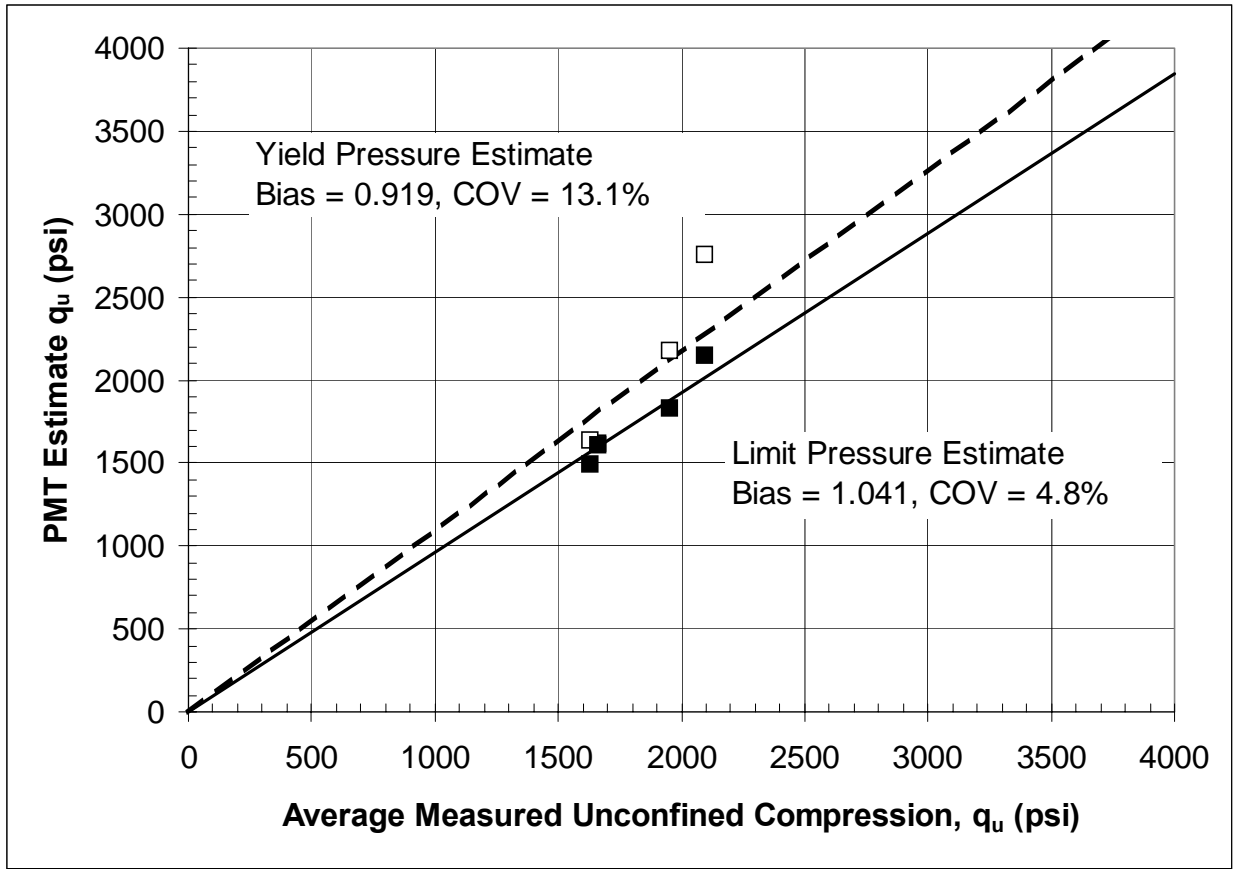


Figure 5.9 PMT Estimates of Compressive Strength

Several factors may affect the strength correlations in **Table 5.4**:

1. Limited quantity and range of experimental data - possibly important
2. Core sample material and testing variability – probably secondary effect
3. Greater age of core samples at time of test – probably secondary effect
4. Effect of crack progression on compressive strength – probably important

Confirmation of the proposed relationships is needed for design use and can be best obtained by direct correlation with drilled shaft load test data.

5.2 Pressuremeter Field Tests

During November and December of 2002, Jacobs (2003) performed field pressuremeter tests using the Probex-1 at the SR20

Apalachicola River Bridge in Blountstown, Florida

(Figure 5.10). In all, he performed thirty-one pressuremeter tests in four separate coreholes (about 8 tests per test hole) adjacent to two test shafts used previously complete the foundation shaft design for the new bridge. FDOT

District 3 provided a drill rig and crew to perform the rock coring and assist with the pressuremeter testing. Chapter 6 will compare the rock strength parameters estimated from the pressuremeter tests with shear strength from the drilled shaft load tests performed during the construction of the new SR20 Bridge. This chapter presents the results of the pressuremeter tests and the corresponding rock core tests.

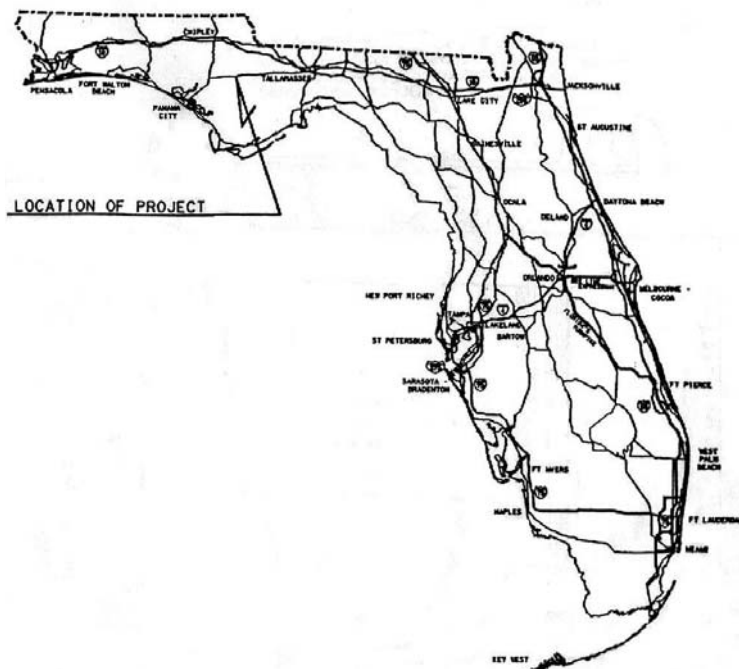


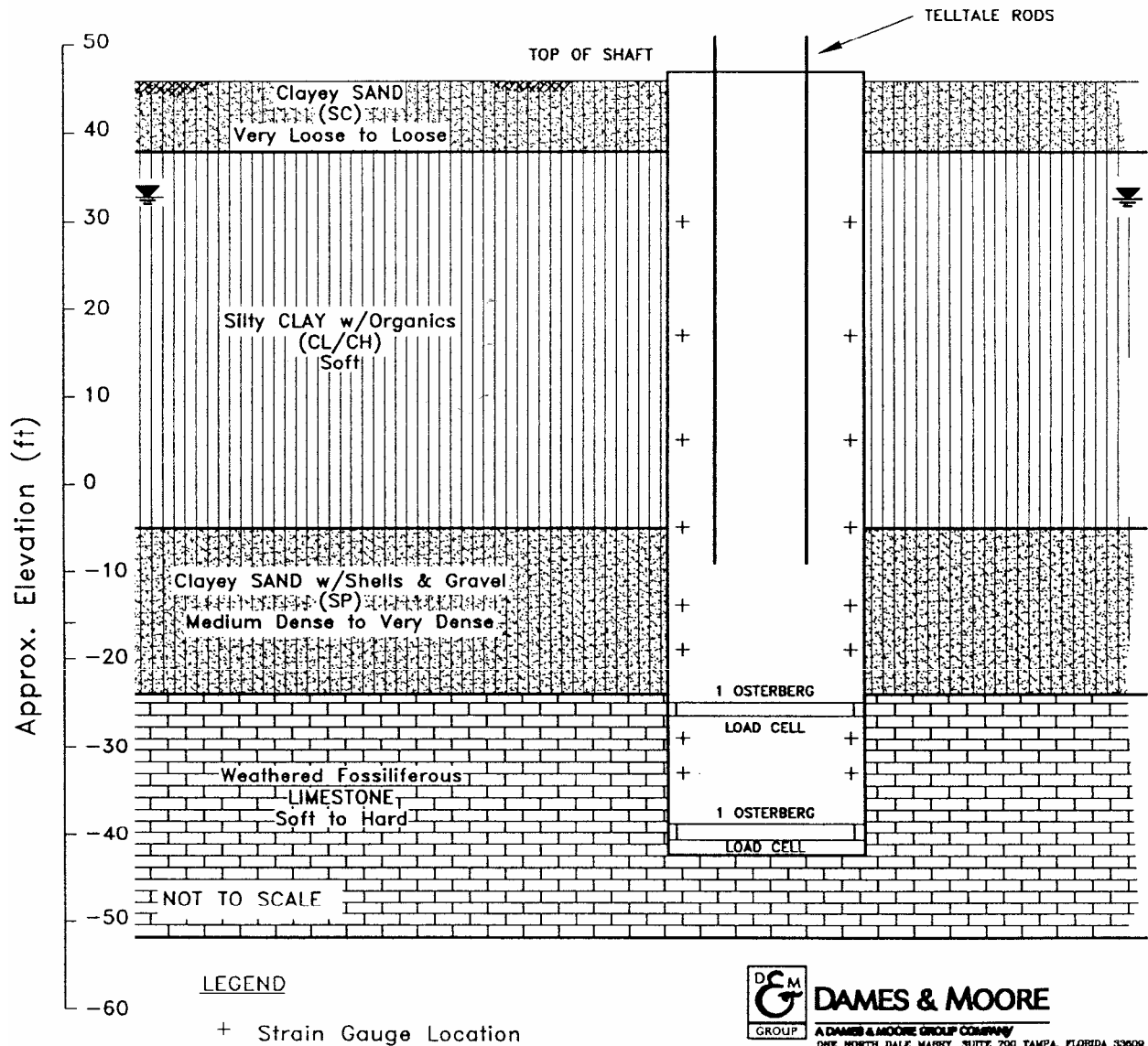
Figure 5.10 Site Location Map (Sharpe, 1998)

5.2.1 SR20 Stratigraphy

The SR20 test shafts are located approximately 750 ft apart within the alluvial flood plain of the Apalachicola River. The Woodruff Dam upstream controls the river level, which floods the site regularly during spring and summer rains. Figures 5.11 and 5.12, from the test shaft report by Sharpe (1998), show the general stratigraphy at each test site. Figures 5.13-5.15 show FDOT borings for each test site from the project plans. The ground surface around the shafts is relatively level with an elevation of +45 to +47 ft. The overburden soils and depth to rock are similar across the site, with the rock surface dipping downward toward the east. Both sides of the river have a 10 to 20 ft thick surface layer of clayey sand. The soil beneath this layer on the West side consists predominantly of sand, while the East side contains a thick layer of soft clay with some

Final Report Contract #BC354 RPWO #13

organic content. Limestone lies beneath the overburden soil starting at an elevation of -14 ft to about -25 ft. The limestone is less competent near its surface but improves in hardness, consistency, and strength with depth. The four PMT coreholes showed significant variability, but in general, the quality and strength of the limestone improved approximately 20 ft below the rock surface. The higher quality rock there did not erode as easily during coring and the PMT results improved.



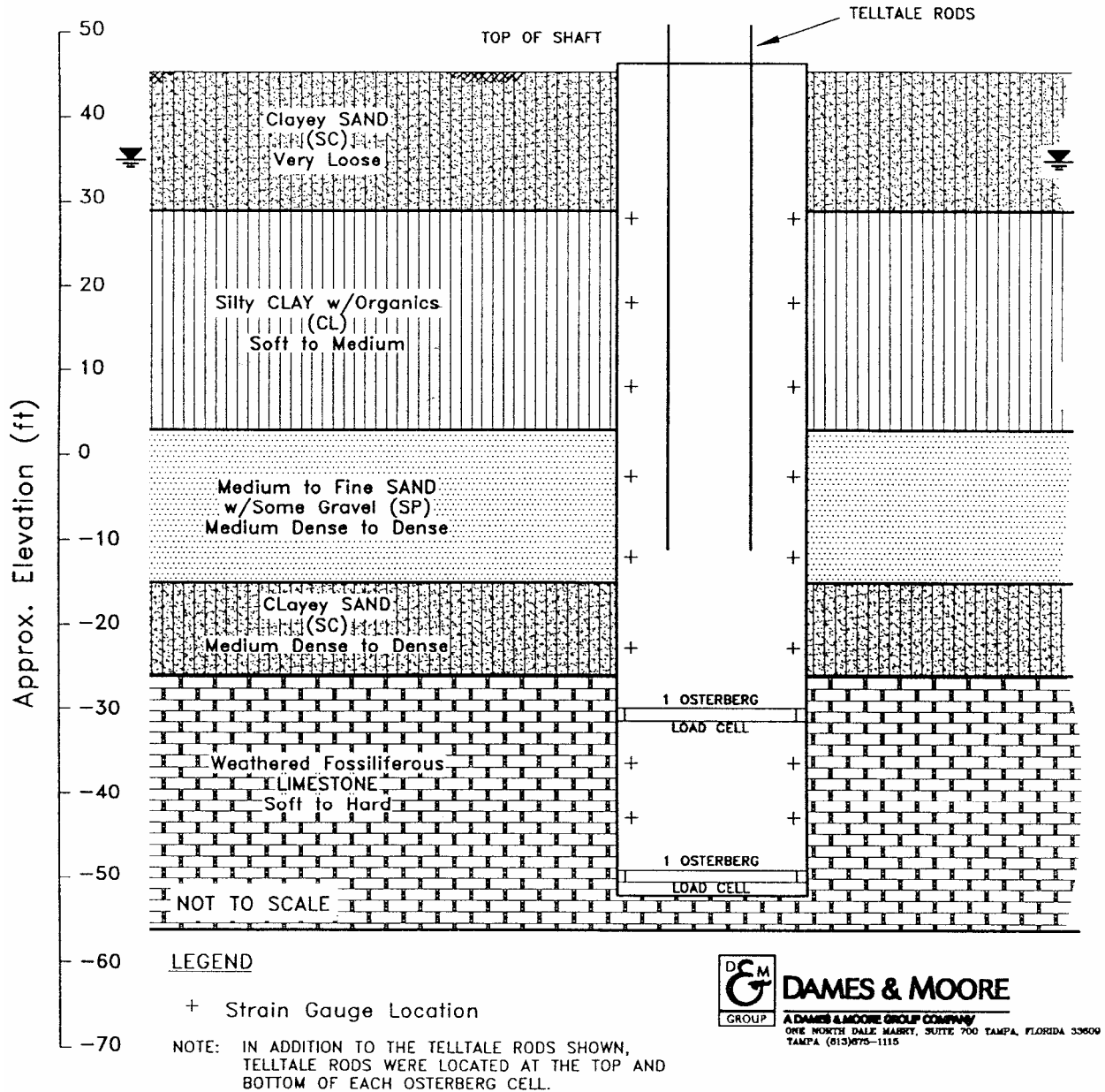


Figure 5.12 Shaft 7 Soil Stratigraphy (Sharpe, 1998)

Final Report Contract #BC354 RPWO #13

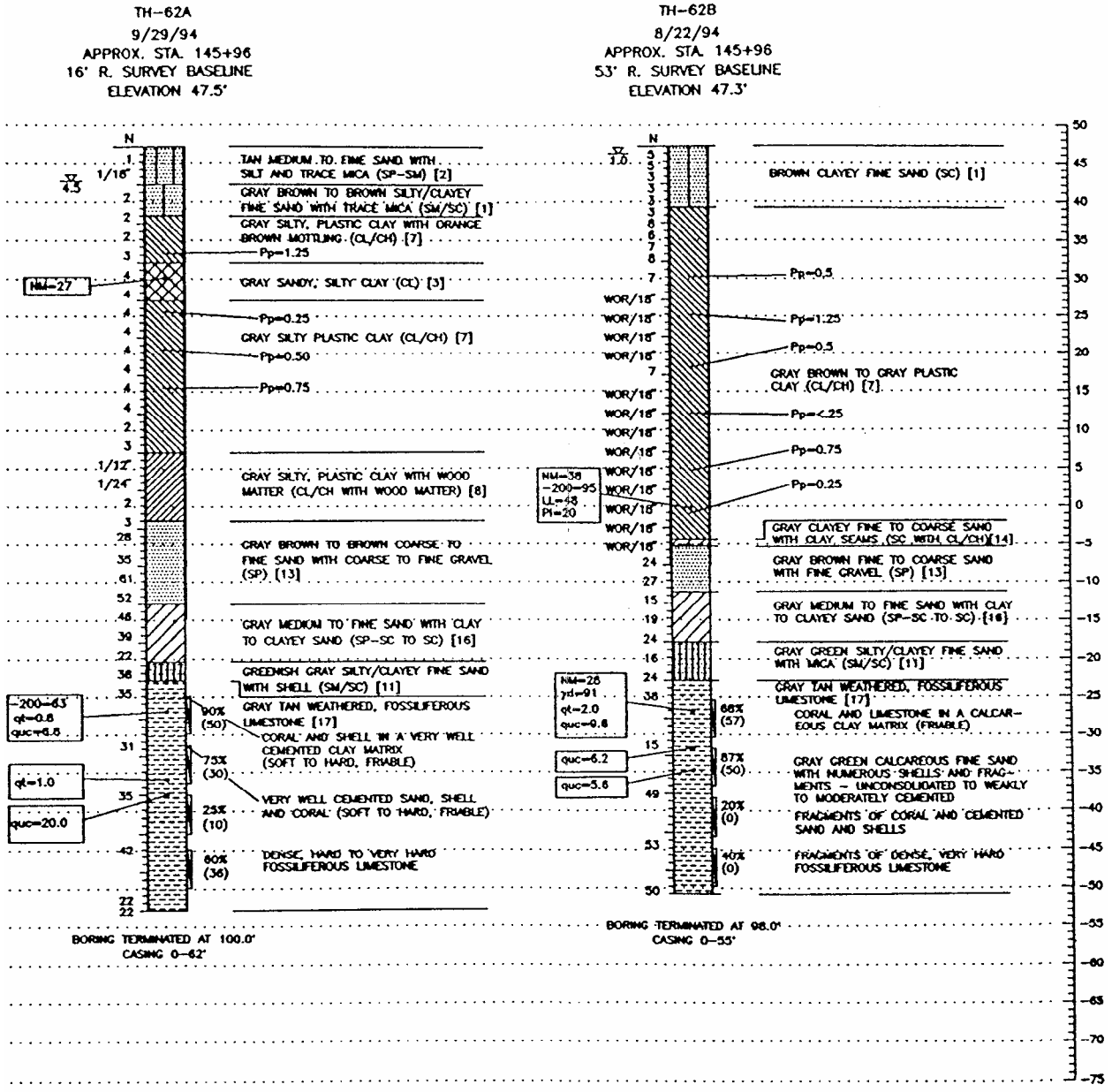


Figure 5.13 Shaft 5 Boring Logs (TH-62A and TH-62B)

Final Report Contract #BC354 RPWO #13

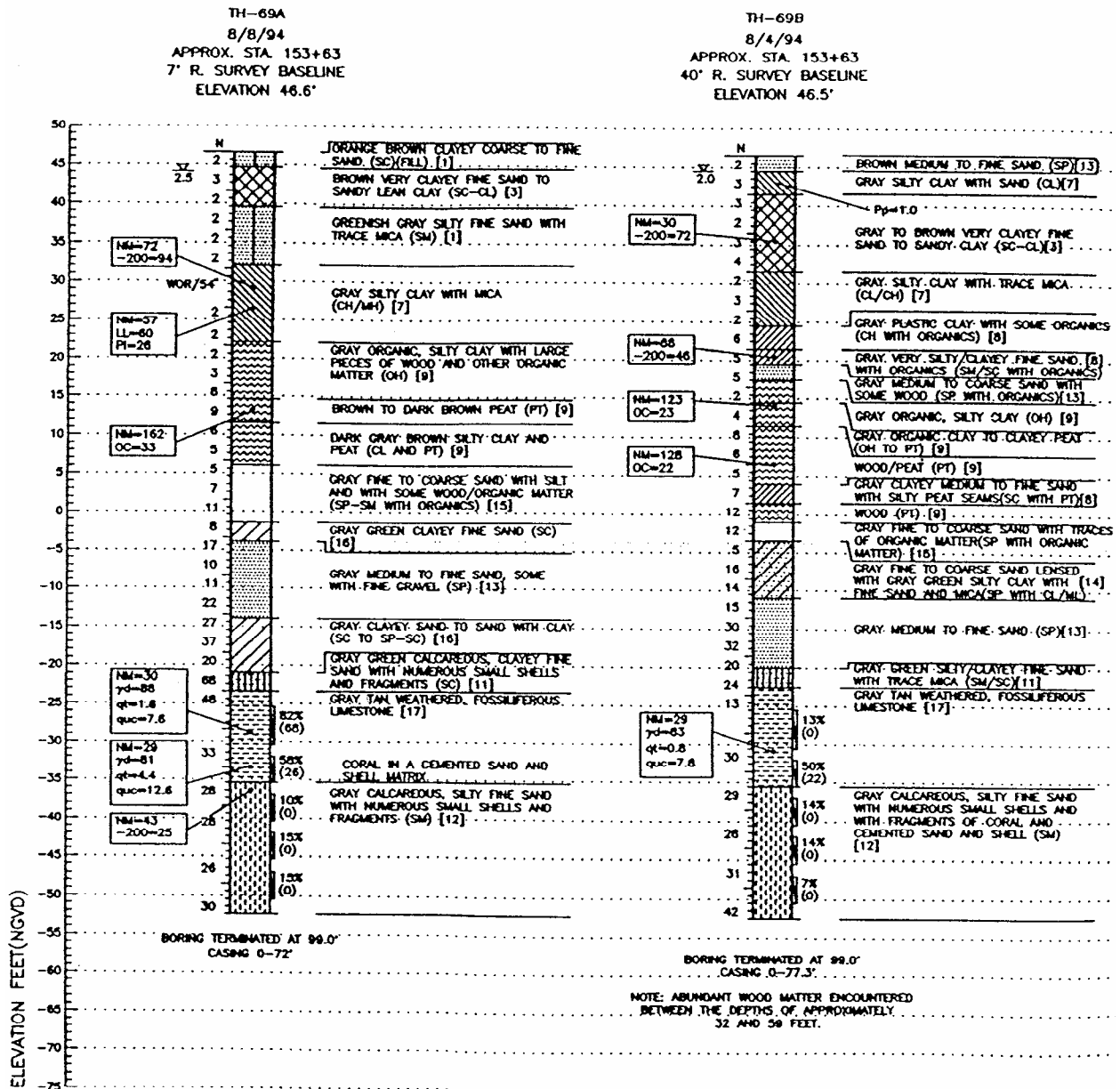


Figure 5.14 Shaft 7 Boring Logs (TH-69A and TH-69B)


Final Report Contract #BC354 RPWO #13

LEGEND INFORMATION

- TH STANDARD PENETRATION TEST (SPT) BORING LOCATION
- N STANDARD PENETRATION RESISTANCE IN BLOWS PER FOOT
- 50/3^o 50 BLOWS FOR 3-INCH PENETRATION INTO SOIL
- 13/50/5 13 BLOWS FOR 6-INCH, 50 BLOWS FOR 5-INCH PENETRATION INTO SOIL
- $\frac{US-1}{(100\%)}$ UNDISTURBED SAMPLE
% RECOVERY
- 5% \Rightarrow ESTIMATED % WATER LOSS
- \sphericalangle GROUNDWATER LEVEL MEASURED ON DATE DRILLED
- NM NATURAL MOISTURE CONTENT IN PERCENT (ASTM D-2216)
- 200 PERCENT PASSING No. 200 SIEVE SIZE (PERCENT FINES)(ASTM D-1140)
- γ_d DRY UNIT WEIGHT, POUNDS PER CUBIC FOOT
- quc CORRECTED UNCONFINED COMPRESSIVE STRENGTH (ksf)
- qt SPLITTING TENSILE STRENGTH (ksf)
- Pp UNCONFINED COMPRESSIVE STRENGTH (ksf) USING POCKET PENETROMETER
- LL LIQUID LIMIT (ASTM D-424)
- PI PLASTICITY INDEX (ASTM D-424)
- SP,SP-SM UNIFIED SOIL CLASSIFICATION SYSTEM
- SM,SC,CH

| | CASING

ROCK CORING DATA

 % RECOVERY (ROD)

CORE SIZE -- HW4 AND HW-WIRE LINE

STANDARD PENETRATION TEST DATA:

SPOON I.D. = 1.5" HAMMER DROP = 30"
SPOON O.D. = 2.0" HAMMER WEIGHT = 140 lbs.

DRILL RIG: CME 45, CME 55(2)
AND CME 75

DRILLERS: F. SMITH, K. McDOUGAL, G. SHIELDS, P. BONEY
AND G. LEDBETTER (TALLAHASSEE)
R. PRATHER AND T. BUCHAN (ORLANDO)
S. PARKER AND J. BOSWELL (BARTOW)

- NOTES: 1) UPON COMPLETION OF EACH BORING, THE BOREHOLE WAS GROUTED WITH A CEMENT-BENTONITE SLURRY.
- 2) SOIL LEGEND AND SOIL SYMBOLS DEVELOPED FROM ARDAMAN & ASSOCIATES, INC. PHASE I PRELIMINARY GEOTECHNICAL REPORT FOR THE PROPOSED ALIGNMENT C ADDITION TO THE CALHOUN BRIDGE OVER THE APALACHICOLA RIVER BASIN ALONG STATE ROAD 20 IN LIBERTY AND CALHOUN COUNTIES, FLORIDA DATED DECEMBER 17, 1992.
- SUBSURFACE INFORMATION IS ALSO PRESENTED IN THE ABOVE REFERENCED REPORT.
- 3) NUMBER IN BRACKETS ([7]) FOLLOWING SOIL/ROCK DESCRIPTIONS ON THE FOLLOWING SHEETS REFERENCES THE SOIL/ROCK STRATA NUMBERS SHOWN WITH THE SOIL LEGEND ON THIS SHEET.

Figure 5.15 Boring Log Legend

5.2.2 PMT Corehole Preparation

The primary concern during the coring operation performed for the pressuremeter tests was the resulting quality of the corehole, with core recovery secondary. The Probex-1 has maximum expanded diameter of 3.36 in (85.3 mm), only about 0.46 in (11.6 mm) greater than its initial diameter of 2.90 in (73.7 mm), leaving little size tolerance when drilling the test hole. Several factors affect the preparation of a corehole satisfactory for the PMT:

- Wobbling of the core bit may produce both a core sample and a corehole with a corkscrew shape, leading to erroneous lab test results and undesirable stress concentrations during the pressuremeter test. Inadequate down-pressure prevents the core barrel from advancing, but too much down-pressure can cause the core bit to “walk” around the inside of the hole because it cannot cut the material fast enough. The correct down-pressure advances the core bit at a steady, constant rate. At the SR20 site the driller typically applied down-pressure of less than 100 psi, relying mostly on the weight of the drill rods.
- Rotational rates too slow or too fast may generate excess heat and damage the bit. Too slow a rate may also gouge the sidewalls and clog the bit. We used an average rate of 90 -100 rpm.
- Coring reduces the insitu stress at the corehole wall down to the pressure exerted by the head of drill fluid. The rock may relax inward, reducing the corehole diameter, loosening the rock, and reducing its strength and stiffness. This disturbance lengthens the initial phase of the PMT, affects the overall shape and magnitude of the test curve, and may truncate the test before obtaining any useful parameters. Mineral slurry drill mud (Bentonite or Attapulgate) has a greater unit weight than the groundwater, and its fluid pressure helps replace the sidewall stresses. Mineral slurry also coats the sidewall, inhibiting the flow of water into or out of the surrounding rock, and reducing swelling effects due to water content changes.
- The driller must supply drill fluid at the proper velocity, pressure, and viscosity to obtain a quality corehole. Too much pressure or velocity may erode the sidewall excessively, while too little may cause the core bit to clog, overheat, or lock up. A thick mud may clog the bit and raise the circulation pressure, which causes excessive erosion. A thin mix will not suspend the cuttings or support the sidewall. At SR20 we used a relatively slow rate of circulation at low pressure (<25 psi) and medium viscosity.
- Double-tube and triple-tube core barrels provide internal protection for the core and an internal conduit for the downward flowing drill fluid, thus reducing erosion of the core.

All of the above considerations require constant adjustment because the rock penetrated varies in strength and competence. Driller experience and technique control the success of the coring process. A larger core size helps compensate for poor technique, and the FDOT now typically requires 4" diameter cores obtained using a double tube core barrel.

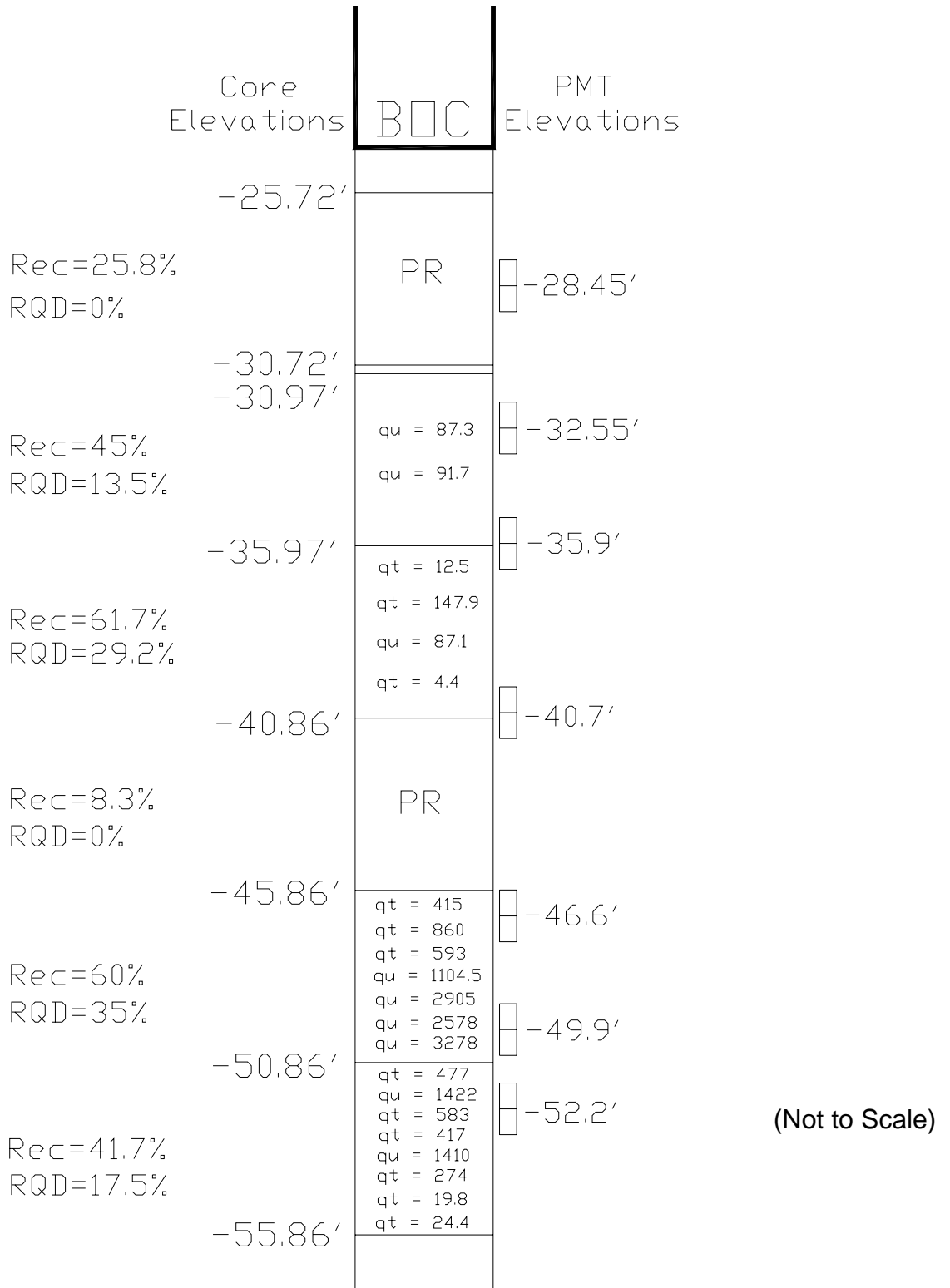
PMT test depths at the SR20 site corresponded to the strain gage elevation in the adjacent test shafts. By coring 2 to 3 feet beyond the test depth, we could position the membrane centerline at the desired depth and provide room for any cuttings that might settle out. For better drilling and testing efficiency, when feasible, we planned the core run elevations to allow two pressuremeter tests within the open hole. Graduate Student Scott Jacobs recorded the drill fluid pressure, penetration rate, and rotational rate during each core run, and then logged and boxed the core for transport to the UF lab. **Figures 5.16 - 5.19** show the locations of the core runs and pressuremeter tests performed in each of the test holes. These figures include the core recovery, Rec, and the Rock Quality Designation, RQD, calculated as follows:

$$\text{Rec} = (\text{Core Length} / \text{Core Run}) \times 100\% \dots\dots\dots (5.2)$$

$$\text{RQD} = ((\sum \text{Core Length} > 4 \text{ in Pieces}) / \text{Core Run}) \times 100\% \dots\dots\dots (5.3)$$

These parameters provide a relative measure of the quality and soundness of the rock sampled, but poor coring technique can artificially reduce either parameter. For the 24, five-foot-long, core runs performed for the PMT at the SR20 site, the recovery ranged from 0 to 73.3% with an average of 32.9% and a coefficient of variation of 61%, and the RQD ranged from 0 to 53.6% with an average of 10.0% and a coefficient of variation of 139%. The best quality limestone was found in the deepest core runs.

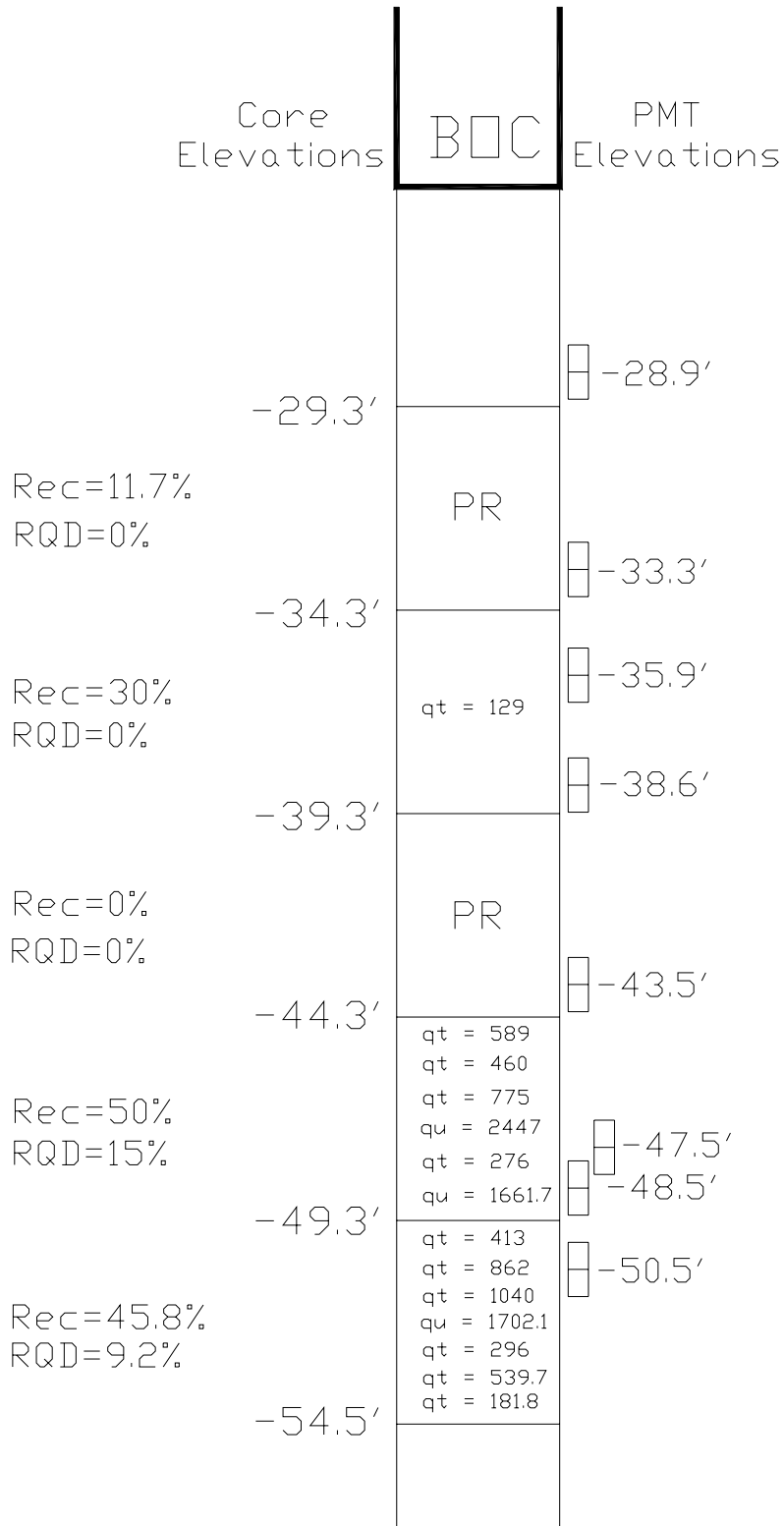
Final Report Contract #BC354 RPWO #13



Notes: q_u and q_t in psi, BOC = Bottom of casing, PR = Poor Recovery

Figure 5.16 Test Hole 1 Core and PMT Locations

Final Report Contract #BC354 RPWO #13

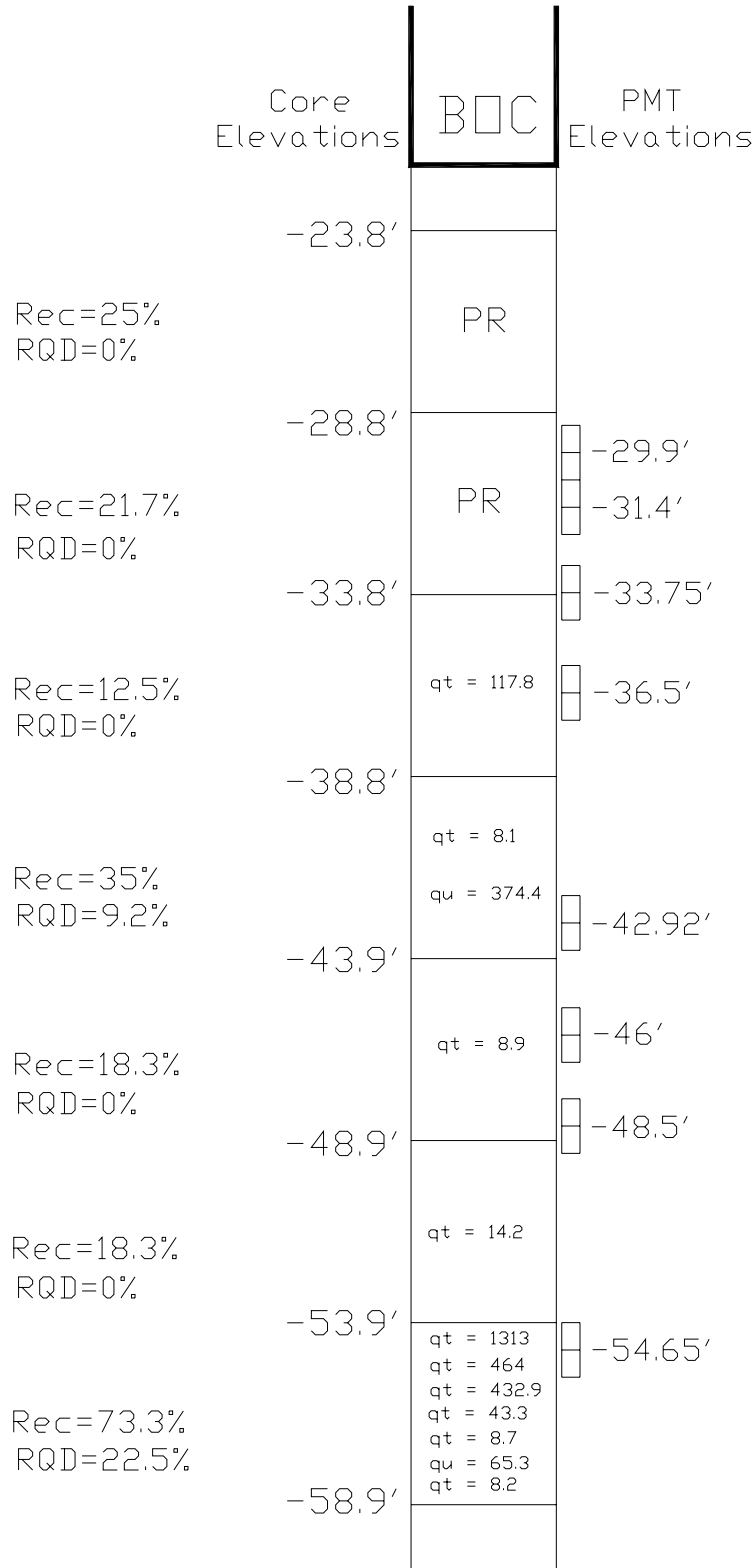


(Not to Scale)

Notes: q_u and q_t in psi, BOC = Bottom of casing, PR = Poor Recovery

Figure 5.17 Test Hole 2 Core and PMT Locations

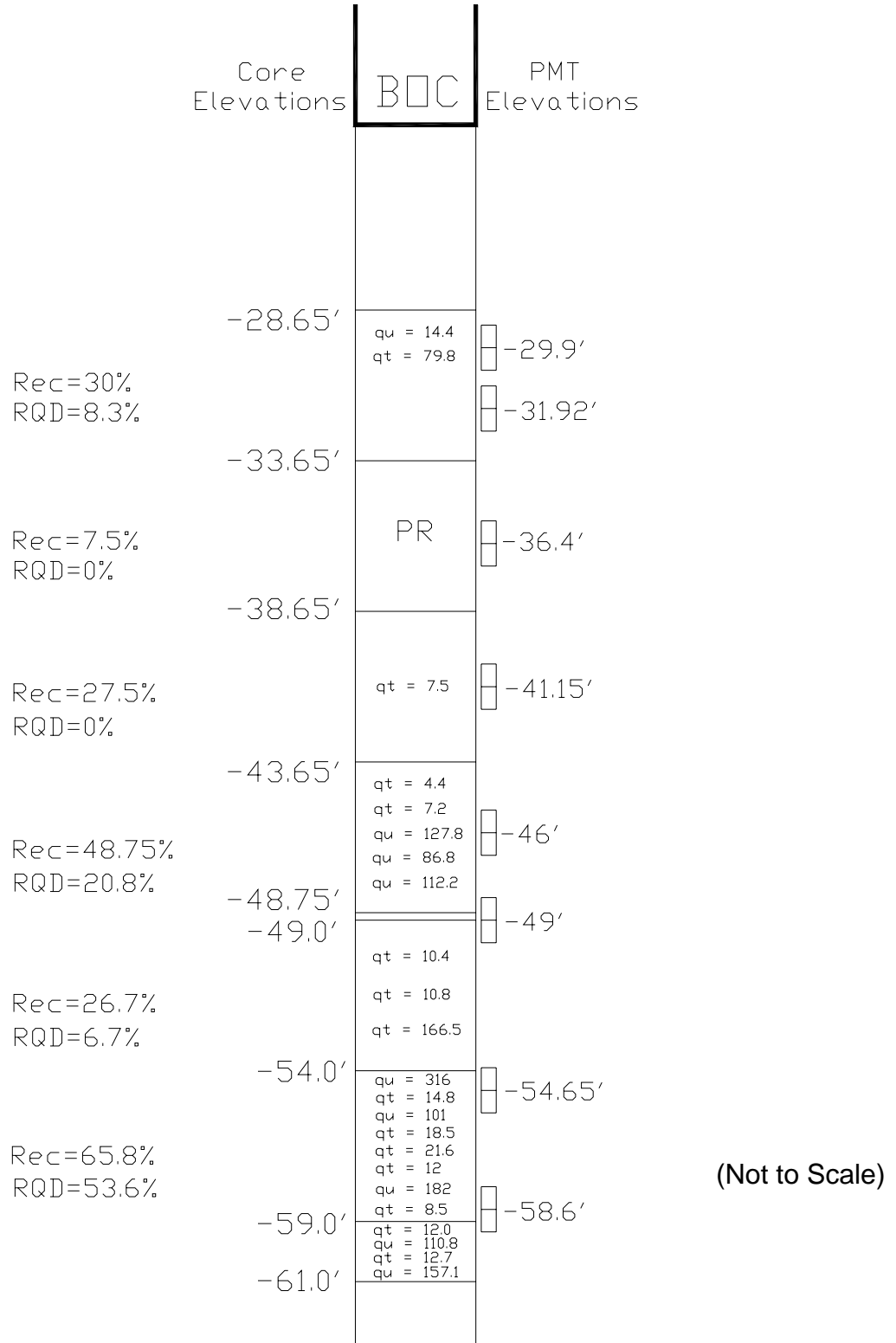
Final Report Contract #BC354 RPWO #13



Notes: q_u and q_t in psi, BOC = Bottom of casing, PR = Poor Recovery

Figure 5.18 Test Hole 3 Core and PMT Locations

Final Report Contract #BC354 RPWO #13



Notes: q_u and q_t in psi, BOC = Bottom of casing, PR = Poor Recovery

Figure 5.19 Test Hole 4 Core and PMT Locations

5.2.3 PMT Results

Jacobs (2003) used the Probex-1 exclusively at the SR20 site, expecting yield and limit pressures that would exceed the capacity of Texam and desiring a less compliant system to achieve more accurate stiffness estimates. He inflated and deflated the Probex-1 three times to exercise it before performing any calibrations. He then performed both pressure and volume calibrations before each test. Depending on the variation observed, he obtained 2 to 3 volume calibrations. Ignoring the expansion of the probe to contact the calibration pipe, he extrapolated the remaining linear portion of the calibration curve back to zero pressure. Because the calibrations did not vary much, Jacobs (2003) averaged the volume calibrations for each day's testing. The pressure calibration, performed to remove the resistance of the membrane from the test pressure, inflates the membrane in air and records the pressure at fixed volume increments. Jacobs (2003) used least squares regression to fit a second-order polynomial through all the pressure calibration data taken each test day and shifted the resulting curve to the origin to accommodate the electronic offsets of the pressure and volume readings. He also added a pressure correction for the hydrostatic head of oil in the hydraulic line of the Probex-1 between the pump and probe elevations.

The SR20 PMT tests were performed as stress-controlled tests to better define the linear elastic region and better define the insitu horizontal stress and yield limit. The tests were performed with 0.5MPa pressure increments with volume readings recorded at elapsed times of 30 seconds and 60 seconds. A plot of the results prepared during each test helped to monitor its progress and adjust pressure increments if required. If the test pressure exceeded the yield limit an unload-reload cycle was performed for comparison of the modulus value with the elastic phase of the PMT test. Jacobs (2003) provides plots of both uncorrected and corrected pressure corrected volume, as well as the corrected pressure versus the relative increase of the probe radius ($\Delta R/R_0$). Chapter 2 describes the methods used to analyze these curves. When possible, the use of multiple analysis methods provided additional confidence in the estimated test parameters. **Table 5.5** shows the results available from analysis of the 31 tests performed by Jacobs (2003). The following sections discuss these results.

Table 5.5 SR20 PMT and Lab Core Results

PMT Test Hole	Elev.		PMT P vs. $\Delta R/R_0$ Curve			PMT Creep Plot		Eqn 2.5	G&A	G&A	(p_L /6.5)	Modulus	Lab Tests on Cores		
	msl	ft	P_0	P_{cr}	P_y	P_0	P_y	P_L	P_L	C_u	C_u	E_m	Avg. qt	Avg. q_{lu}	Avg. E_i
		psi	psi	psi	psi	psi	psi	psi	psi	psi	psi	psi	psi	psi	psi
1	-28.45	179.8	315.9	352.4	226.3	340.8	592.7	776.1	133.0	84.6	11,111				
1	-32.55	7.7	271.9	271.9	151.6	311.8	642.0	810.4	165.7	101.4	11,944			89.5	17,984
1	-35.90	13.5	270.3	364.5	279.2	404.4	925.4	1213.5	287.9	143.7	10,405	54.9		88.7	19,671
1	-40.70														
1	-46.60	121.8	187.6	258.2	232.1	292.8	681.5	729.7	167.3	80.5	6,455	622.7	2466.4	2466.4	1,144,151
1	-49.90	169.7	328.0	329.2	166.8	402.5	539.2	755.3	133.8	122.6	10,625	407.0	2116.3	2116.3	991,443
1	-52.20	94.3	180.1	407.5	257.4	349.9	770.9	963.9	182.4	92.4	15,062	309.2	1416.0	1416.0	686,025
2	-28.90				112.4	333.6	514.3	858.2	185.1	111.9	10,108	129.0		129.0	
2	-33.30	123.3	290.6	324.9	257.4	349.9	514.3	858.2	185.1	92.4	10,108	129.0		129.0	
2	-35.90	89.9		340.8	112.4	333.6	568.4	840.0	170.6		12,098	129.0		129.0	
2	-38.60														
2	-43.50														
2	-47.50	43.5	210.1	232.1	192.2	246.6	383.2	559.4	115.7	60.0	8,434	525.0	2054.4	2054.4	1,314,737
2	-48.50	87.0	221.2	221.2	155.9	212.2	602.0	541.7	128.6	50.7	4,138	543.3	1936.9	1936.9	1,278,004
2	-50.50	49.3	224.8	224.8	219.4	286.4	382.1	485.4	84.8		8,404	555.4	1702.1	1702.1	1,204,536
3	-29.90	142.1	261.1	261.1			470.2	609.4	118.2		5,533				
3	-31.40														
3	-33.75														
3	-36.50														
3	-42.92	130.5		275.6	195.8	259.3	450.8	580.1	109.9	59.1	5,173	8.1	374.4	374.4	466,372
3	-46.00	103.4	157.4	263.2	181.3	285.6	480.2	695.6	145.2	79.1	9,020	8.9			
3	-48.50	81.2	147.9	297.3	210.3	279.2	797.2	760.7	205.0	84.7	5,233	11.6			
3	-54.65	49.3	162.8	297.3	126.9	279.2	797.2	890.9	199.2	117.5	14,201	326.3	65.3	65.3	57,178
4	-29.90	158.1	255.6	261.1	261.1	375.3	523.9	903.4	213.9	98.8	6,487	79.8	14.4	14.4	3,876
4	-31.92	216.1	308.9	308.9	253.8	326.6	648.1	773.5	149.6	79.9	6,108	79.8	14.4	14.4	3,876
4	-36.40	159.5	265.4	377.1	257.4	375.3	523.9	880.5	181.0	95.9	8,641				
4	-41.15	72.5	192.0	313.7	108.8	362.6	648.1	870.2	164.5	117.1	16,707	7.5			
4	-46.00	74.0	308.2	308.2	175.9	293.7	527.7	683.7	115.6	78.1	12,886	5.8	108.9	108.9	66,509
4	-49.00	213.2	362.6	362.6	228.4	340.8	534.0	738.8	114.2	78.5	9,550	39.9	108.9	108.9	66,509
4	-54.65	179.8	216.7	340.8	228.4	340.8	444.5	580.1	111.2	72.0	3,735	15.1	199.7	199.7	75,209
4	-58.60	52.2	257.4	257.4	126.9	262.9	484.6	595.1	95.2		20,272	14.3	173.4	173.4	87,698

Two methods provided an estimate of the insitu horizontal stress, p_0 : the intersection of the initial and elastic straight-line portions of the pressure versus $\Delta R/R_0$ curve and the creep plot of pressure versus $(V_{60} - V_{30})$.

Figure 5.20 compares the results from the two methods. The creep method, based on material behavior rather than curve interpretation, provides a more definitive estimate of p_0 , but also significantly over predicts the visually interpreted value.

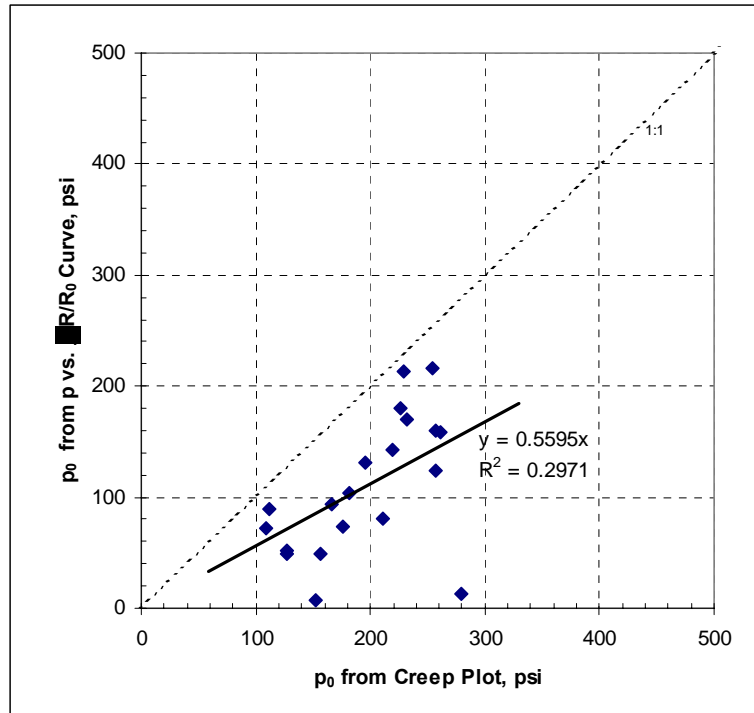


Figure 5.20 SR20 Insitu Horizontal Stress Estimates

We also used two different methods to estimate the yield pressure, p_y : the end of the linear elastic portion of the pressure versus $\Delta R/R_0$ plot, and the creep plot. **Figure 5.21** compares the results of these two methods, which agree well. Because of the consistency of these results, we used average values for later analyses.

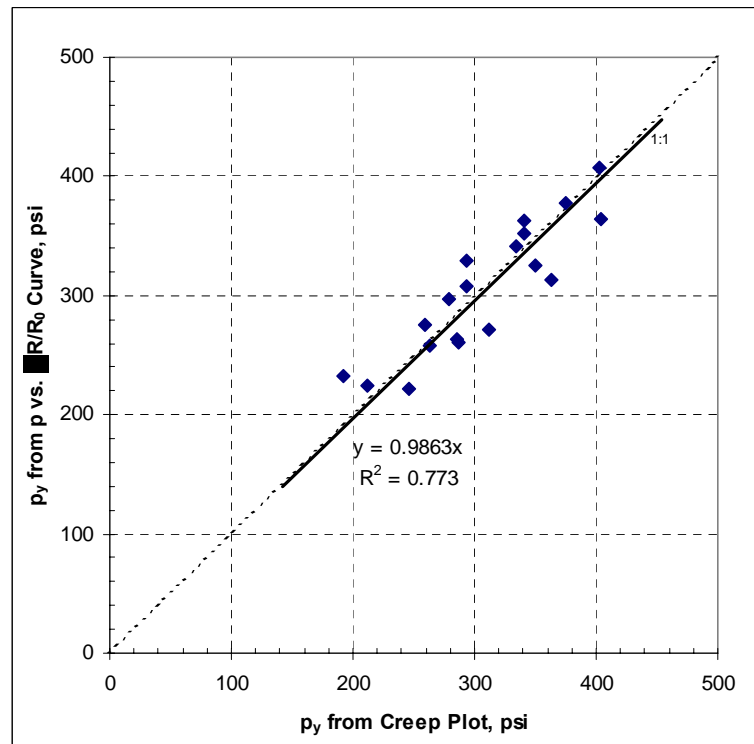


Figure 5.21 SR20 Yield Pressure Estimates

Relatively straightforward extrapolation of the test curve provided estimates of the limit pressure, p_L . A least-squares curve fit using eqn. 2.5 in the software program GraphPad provided the first estimate of p_L at $\Delta R/R_0=0.5$ (see eqn. 2.4). As **Figure 5.22** shows, the Gibson and Anderson Method gave slightly higher values. We chose the Gibson and Anderson estimates because its extrapolation to $\Delta V_0/V_0=1.0$ depends less on the form of the non-linear equation and probably provides a more accurate estimate of p_L .

Undrained shear strength was determined by two different methods. Both assume undrained conditions and plastic behavior. Eqn. 2.14, using the horizontal stress from the creep plot with $\beta = 6.5$, provides the first estimate. The second, the Gibson and Anderson Method, obtains c_u as the slope of the pressure versus $\ln(\Delta V_0/V_0)$ plot.

Figure 5.23 shows a

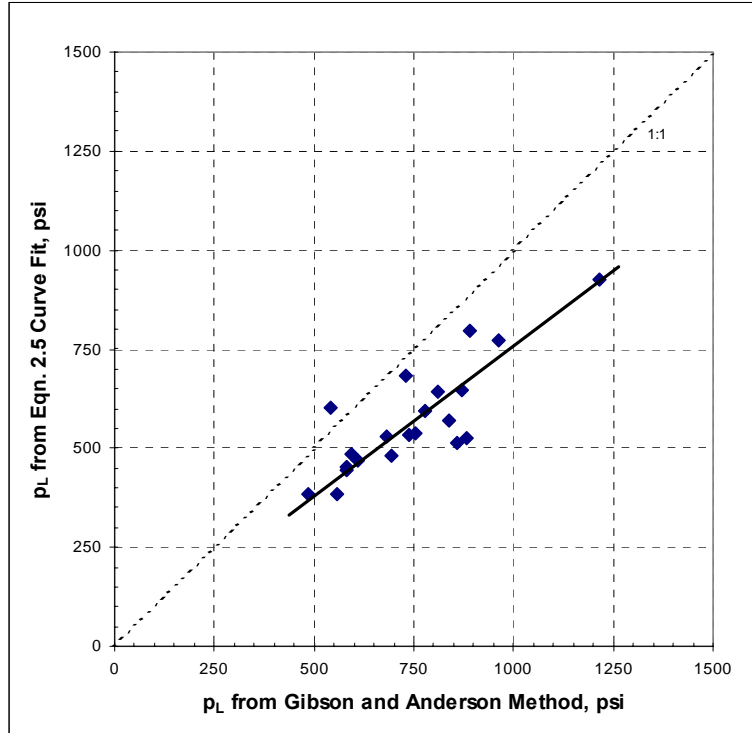


Figure 5.22 SR20 Limit Pressure Estimates

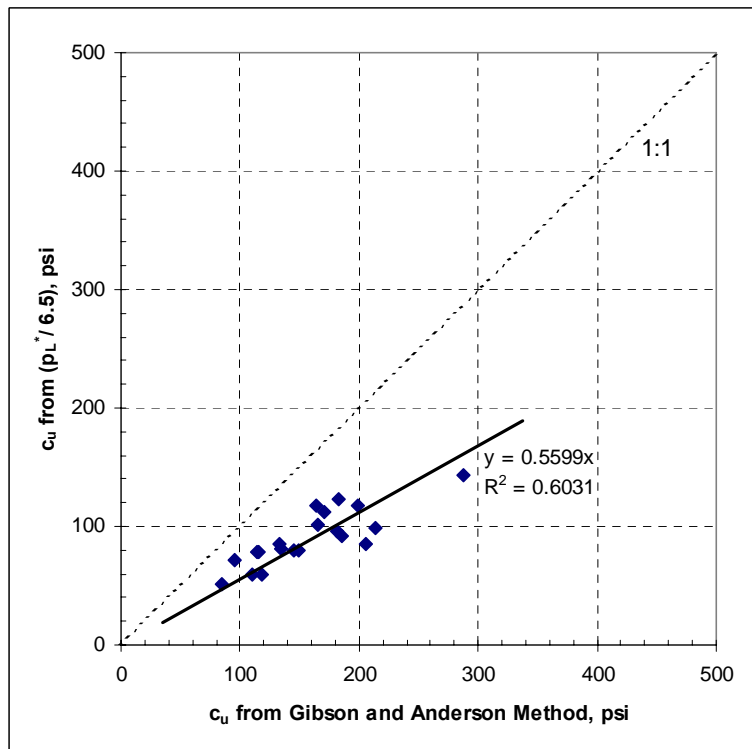


Figure 5.23 SR20 Undrained Shear Strength

comparison of the two methods for the SR20 tests. The comparison shows that using $\beta = 6.5$ consistently under-predicts the Gibson and Anderson Method, which appears more theoretically sound and less reliant on empiricism. The β factor depends on G/c_u , which changes with material composition and stress history. Using a lower $\beta = 3.6$ for the Florida Limestone at SR20 would lead to almost exact agreement between the two methods.

5.2.4 PMT - Core Correlation

The section investigates the correlation of PMT results (σ_{cr} , p_y , p_L^* , and E_m) with parameters measured during lab tests on the corresponding core samples, and in Chapter 6, with the measured shear strength of the test shaft. This step requires matching the individual strength tests on the recovered rock core with the individual PMTs, including unavoidable variability due to material mismatch. **Figures 5.16-5.19** showed the core and PMT depths, along with the strength test results, recovery, and RQD obtained from the recovered core sample. With core recoveries $< 100\%$ and precise sample elevation necessarily uncertain, we grouped and averaged core test values near each PMT elevation.

Therefore, the correlations discussed in this section will tend to have greater variability than the tests performed in relatively uniform Gatorock.

Eqn. 2.6 proposed a total stress relationship between the tensile strength, σ_t , cracking pressure, σ_{cr} , the insitu horizontal stress, $\sigma_h = p_0$, from the PMT, and the tensile strength. Only about 2/3 (15 of 24 usable tests) of the PMT tests displayed

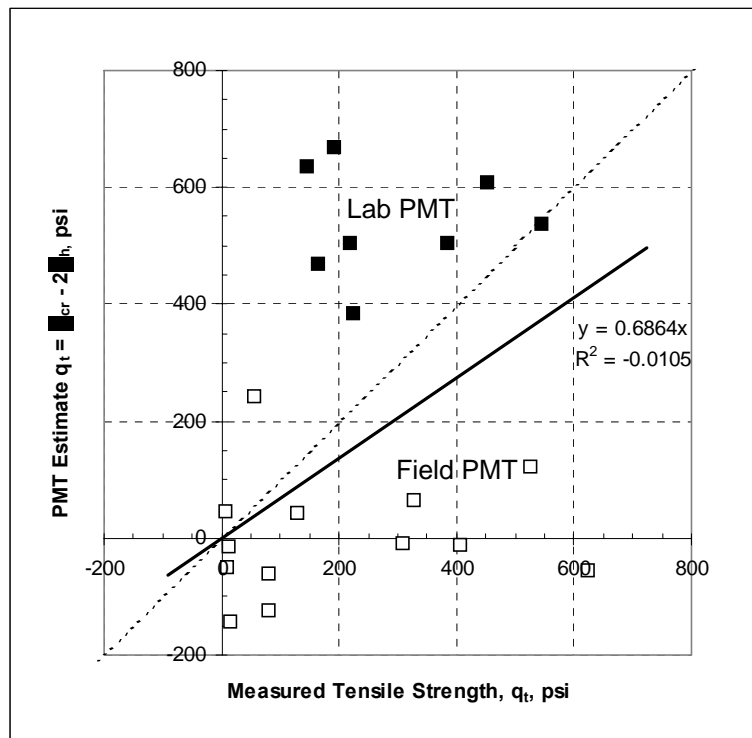


Figure 5.24 PMT Estimate of Tensile Strength

evidence of cracking indicated by a sharp discontinuity or change in the slope of the PMT curve. Horizontal stresses sufficient to prevent cracking may explain the remaining 1/3 of the test results. Only the p_0 estimates based on visual interpretation of $\Delta R/R_0$ curve provided usable tensile strength estimates, and many of them gave a slightly negative $|q_t|$, indicating either too low an estimate of the cracking pressure or too high an estimate of the insitu horizontal stress. **Table 5.6** and **Figure 5.24** compare the PMT estimates with the measured tensile strength of the corresponding core samples. The average bias calculation for this comparison is not useful, but the trend line shown in **Figure 5.24** is reasonable. Additional tests may improve this correlation.

Table 5.6 PMT vs. Core Tensile Strength

Test or Hole	Elev. msl ft	σ_h est. $\Delta R/R_0$ Curve psi	Crack Press., σ_{cr} psi	Est. $q_t = (\sigma_{cr} - 2\sigma_h)$ (psi)	Msd. q_t psi	q_t bias msd / est
TT1	n/a	36.3	609.1	536.6	545.1	1.016
TT2	n/a	36.3	680.8	608.3	451.6	0.742
TT3	n/a	16.7	538.4	505.0	384.1	0.761
TT4	n/a	16.7	538.4	505.0	217.4	0.430
PT1	n/a	36.3	458.3	385.8	224.7	0.582
PT2	n/a	43.5	723.7	636.7	146.0	0.229
PT3	n/a	36.3	541.0	468.5	163.6	0.349
PT4	n/a	50.8	771.6	670.1	191.2	0.285
1	-35.90	13.5	270.3	243.3	54.9	0.226
1	-46.60	121.8	187.6	-56.1	622.7	-11.108
1	-49.90	169.7	328.0	-11.4	407.0	-35.751
1	-52.20	94.3	180.1	-8.5	309.2	-36.443
2	-33.30	123.3	290.6	44.1	129.0	2.926
2	-47.50	43.5	210.1	123.1	525.0	4.266
3	-46.00	103.4	157.4	-49.4	8.9	-0.180
3	-48.50	81.2	147.9	-14.5	11.6	-0.796
3	-54.65	49.3	162.8	64.2	326.3	5.085
4	-29.90	158.1	255.6	-60.6	79.8	-1.318
4	-31.92	216.1	308.9	-123.3	79.8	-0.647
4	-41.15	72.5	192.0	47.0	7.5	0.160
4	-54.65	179.8	216.7	-143.0	15.1	-0.105
Average Bias						-3.300
Std. Dev. Bias						11.312
COV						-342.8%

Final Report Contract #BC354 RPWO #13

The unconfined compressive strength estimated from the field PMTs at SR20 did not provide good correlation with the values obtained from lab tests on the corresponding core samples. **Table 5.7** compares the yield pressures, limit pressures, undrained shear strength values with the corresponding average q_u values available from the core tests, for both the SR20 field tests and the Gatorock test performed in the UF lab. This table also includes the bias and COV for each estimate. **Figure 5.25** shows that the field measurements did not bear out the promising results obtained from lab tests in the Gatorock samples. The SR20 PMT consistently under predicted the lab core tests. The core tests performed for SR20 included only intact core samples and not any weaker material tested by the PMT. Coring disturbance may also have reduced the PMT values. In any case, these correlations require additional field work in better quality limestone for verification.

Table 5.7 PMT Estimate vs. Core Compressive Strength

Test or Test Hole	Elev. msl ft	PMT Estimated q_u				Avg. Msd. q_u psi	q_u bias = (msd / est.)			
		Avg. p_y psi	G&A p_L psi	G&A c_u psi	2 x ($p_L^*/6.5$) psi		Avg. p_y	G&A p_L	2 x G&A c_u	2 x ($p_L^*/6.5$)
PT1	n/a	2757.1	7008.1		2145.2	2091.2	0.759	0.298		0.975
PT2	n/a	2179.8	6005.4		1834.4	1948.8	0.894	0.325		1.062
PT3	n/a	1617.1	5252.1		1604.9	1659.6	1.026	0.316		1.034
PT4	n/a	1637.4	4900.2		1492.1	1629.8	0.995	0.333		1.092
1	-32.55	291.9	810.4	331.3	202.7	89.5	0.307	0.110	0.270	0.441
1	-35.90	384.4	1213.5	575.8	287.5	88.7	0.231	0.073	0.154	0.309
1	-46.60	258.2	729.7	334.6		2466.4	9.554	3.380	7.371	
1	-49.90	311.0	755.3	267.7	161.0	2116.3	6.804	2.802	7.905	13.144
1	-52.20	405.0	963.9	364.8	245.3	1416.0	3.496	1.469	3.881	5.773
2	-47.50	212.1	559.4	231.4		2054.4	9.685	3.672	8.877	
2	-48.50	233.9	541.7	257.1		1936.9	8.282	3.576	7.533	
2	-50.50	218.5	485.4	169.7	101.4	1702.1	7.790	3.506	10.031	16.788
3	-42.92	267.4	580.1	219.8	118.3	374.4	1.400	0.645	1.703	3.166
3	-54.65	288.3	890.9	398.5	235.1	65.3	0.227	0.073	0.164	0.278
4	-46.00	300.9	683.7	231.3	156.2	108.9	0.362	0.159	0.471	0.697
4	-49.00	351.7	738.8	228.4	157.0	108.9	0.310	0.147	0.477	0.694
4	-54.65	340.8	580.1	222.3		199.7	0.586	0.344	0.898	
4	-58.60	260.2	595.1	190.3	144.1	173.4	0.666	0.291	0.911	1.204
Average Bias							2.965	1.196	3.618	3.333
Std. Dev. Bias							3.607	1.442	3.823	5.186
COV							121.7%	120.6%	105.7%	155.6%

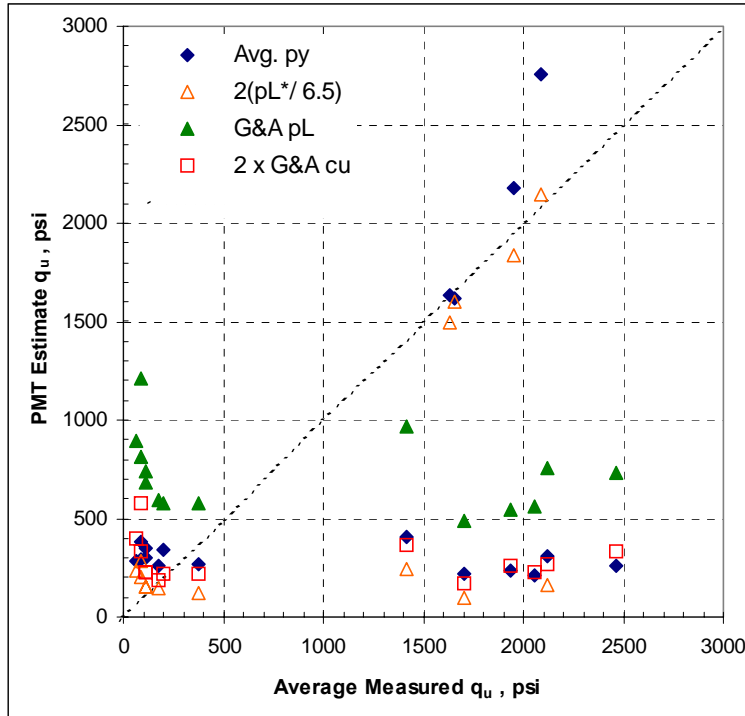


Figure 5.25 PMT Estimate of Compressive Strength

Table 5.8 compares the values of the PMT modulus, E_m , calculated before cracking using Eqn. 2.1, with the average initial tangent modulus values from tests of the corresponding core samples. The modulus comparison shown in Figure 5.26 would seem to indicate that the PMT grossly under predicts the material stiffness. The Gatorock samples show some correlation, but the SR20 cores show little correlation. Chapter 2 provides reasoning for a low

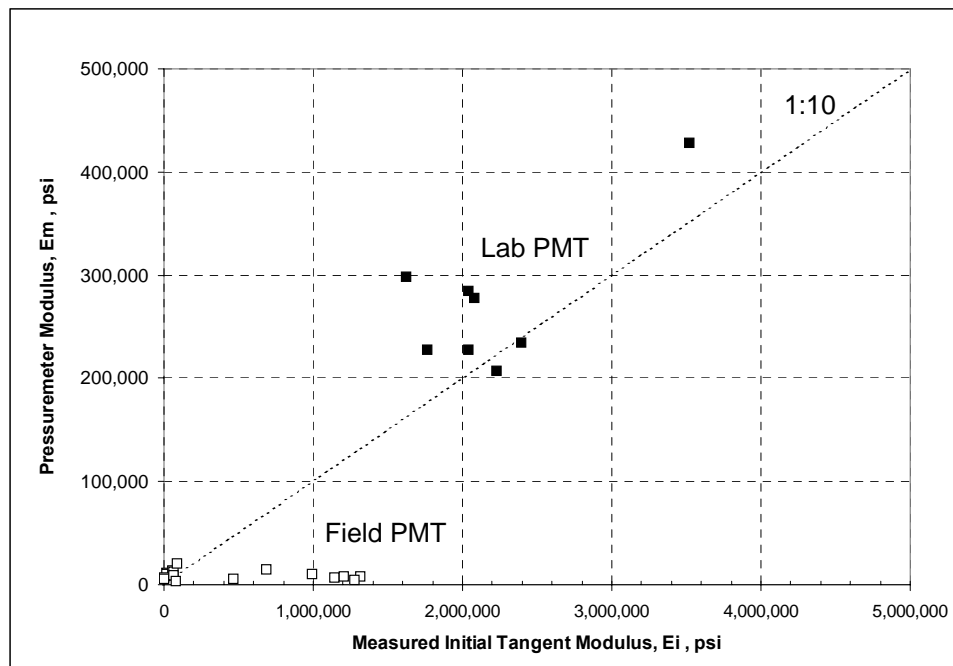


Figure 5.26 PMT Modulus Estimate

PMT prediction. The poor recovery and loss of the weakest portion of the core appear to render this comparison useless.

Overall, the SR20 test results shown above, though poorly correlated to the core tests, do not definitively deny the capability of the PMT to provide accurate insitu test results of Florida limestone. A disparity between tests in the rock mass made with an 18 in long probe and tests on much smaller, intact cores representing the best portion of the rock mass was expected, and part of the reason for using the PMT. The lab results in Gatorock samples offer encouragement and indicate that more definitive tests in sound rock of various strengths should help to better develop confidence in the PMT. Chapter 7 will compare the SR20 PMT results with the shear strength measured on the full-size test shafts.

Table 5.8 PMT Estimate vs. Core Modulus

Test or Hole	Elev. msl ft	PMT E_m psi	Core Avg. E_i psi	E_i bias msd / est
TT1	n/a	207,200	2,226,465	10.745
TT2	n/a	428,200	3,517,500	8.215
TT3	n/a	234,300	2,395,838	10.226
TT4	n/a	227,800	2,041,564	8.962
PT1	n/a	277,600	2,079,708	7.492
PT2	n/a	284,300	2,042,554	7.185
PT3	n/a	227,900	1,764,000	7.740
PT4	n/a	298,700	1,625,000	5.440
1	-32.55	11,944	17,984	1.506
1	-35.90	10,405	19,671	1.891
1	-46.60	6,455	1,144,151	177.260
1	-49.90	10,625	991,443	93.315
1	-52.20	15,062	686,025	45.548
2	-47.50	8,434	1,314,737	155.893
2	-48.50	4,138	1,278,004	308.871
2	-50.50	8,404	1,204,536	143.329
3	-42.92	5,173	466,372	90.153
3	-54.65	14,201	57,178	4.026
4	-29.90	6,487	3,876	0.597
4	-31.92	6,108	3,876	0.634
4	-46.00	12,886	66,509	5.161
4	-49.00	9,550	66,509	6.964
4	-54.65	3,735	75,209	20.139
4	-58.60	20,272	87,698	4.326
Average Bias				46.90
Std. Dev. Bias				77.70
COV				165.7%

6. CORRELATION OF FLORIDA LIMESTONE PROPERTIES

This chapter presents a database of strength and modulus tests assembled for Florida limestone and Gatorock. This database includes rock core tests performed by FDOT consultants during bridge design, tests performed on rock cores at the FDOT State Materials Office (SMO), and tests performed at UF on Gatorock samples, rock cores obtained from the State Materials Office, and rock cores from the SR20 Blountstown Bridge obtained during pressuremeter tests. The data come from six different bridge sites around Florida and should represent the variability expected. Gatorock is included in the database primarily to confirm that it is comparable to Florida limestone. Modulus tests performed without a compressometer were corrected by calibration of the test apparatus as described in Chapter 4. Correlations between modulus and compressive strength, and between compressive and tensile strength are developed herein for future reference. The Appendix tabulates the data used to prepare the correlation plots presented herein.

6.1 Compressive Strength vs. Modulus

The SMO provided unconfined compression stress-strain data for rock cores from three different drilled shaft projects, including the SR20 Blountstown Bridge, the US90 Victory Bridge near Chattahoochee, and the US92 Broadway Bridge in Daytona Beach. Modulus tests at the UF included Gatorock trial mix samples, Gatorock cores, cores from the SR10 Choctawhatchee Bridge, cores from a Hallandale Beach Bridge, and cores from the SR20 Blountstown Bridge. Most of the limestone from these sites was visually similar in appearance, except for the notable presence of a crystalline structure (probably calcite) in the Hallandale and Victory core samples. **Figure 6.1** shows the modulus data vs. unconfined compression strength with each site denoted by symbol. Trend lines through the data were fit by non-linear least squares regression (not by less accurate regression of linearized data). There is considerable scatter in this plot data, but by removing the crystalline samples from Victory and Hallandale the correlation coefficient improves to 0.62 (but not the bias).

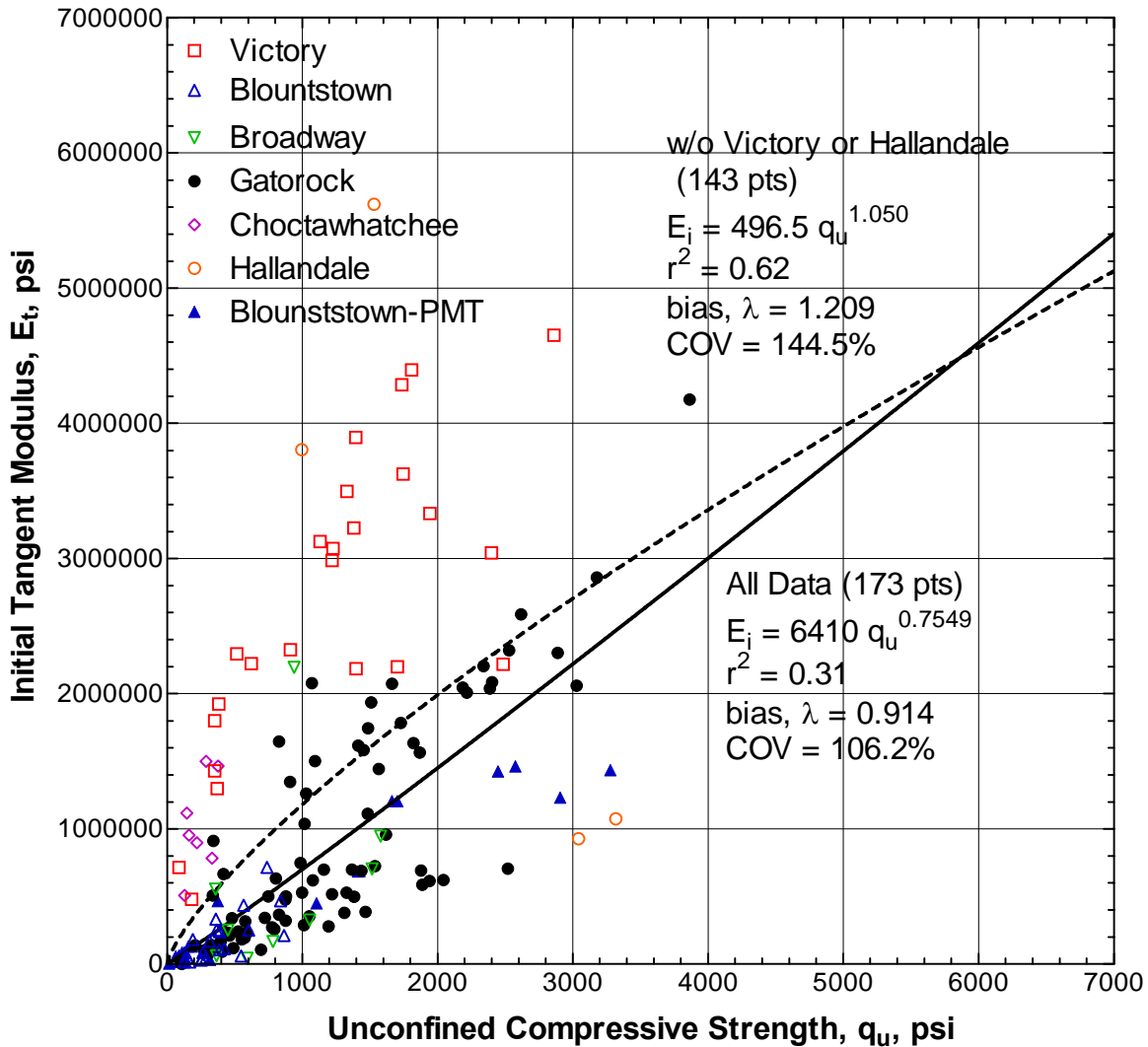


Figure 6.1 Unconfined Compressive Strength versus Initial Tangent Modulus

For concrete, a material similar to limestone, structural engineers often use the formula $E_i = 57,000 q_u^{0.5}$ to relate strength and modulus (both in psi). Forcing a fit to the square root of q_u , we found a numerically similar formula with less correlation: $E_i = 41,396 q_u^{0.5}$ with $R^2 = 0.28$ for all data or $E_i = 28,227 q_u^{0.5}$ with $R^2 = 0.48$ excluding the crystalline data. Site-specific consideration, such as shown in Figure 6.2 for the SR20 data, may significantly improve the correlation coefficient, but this approach requires a sizeable sample of data.

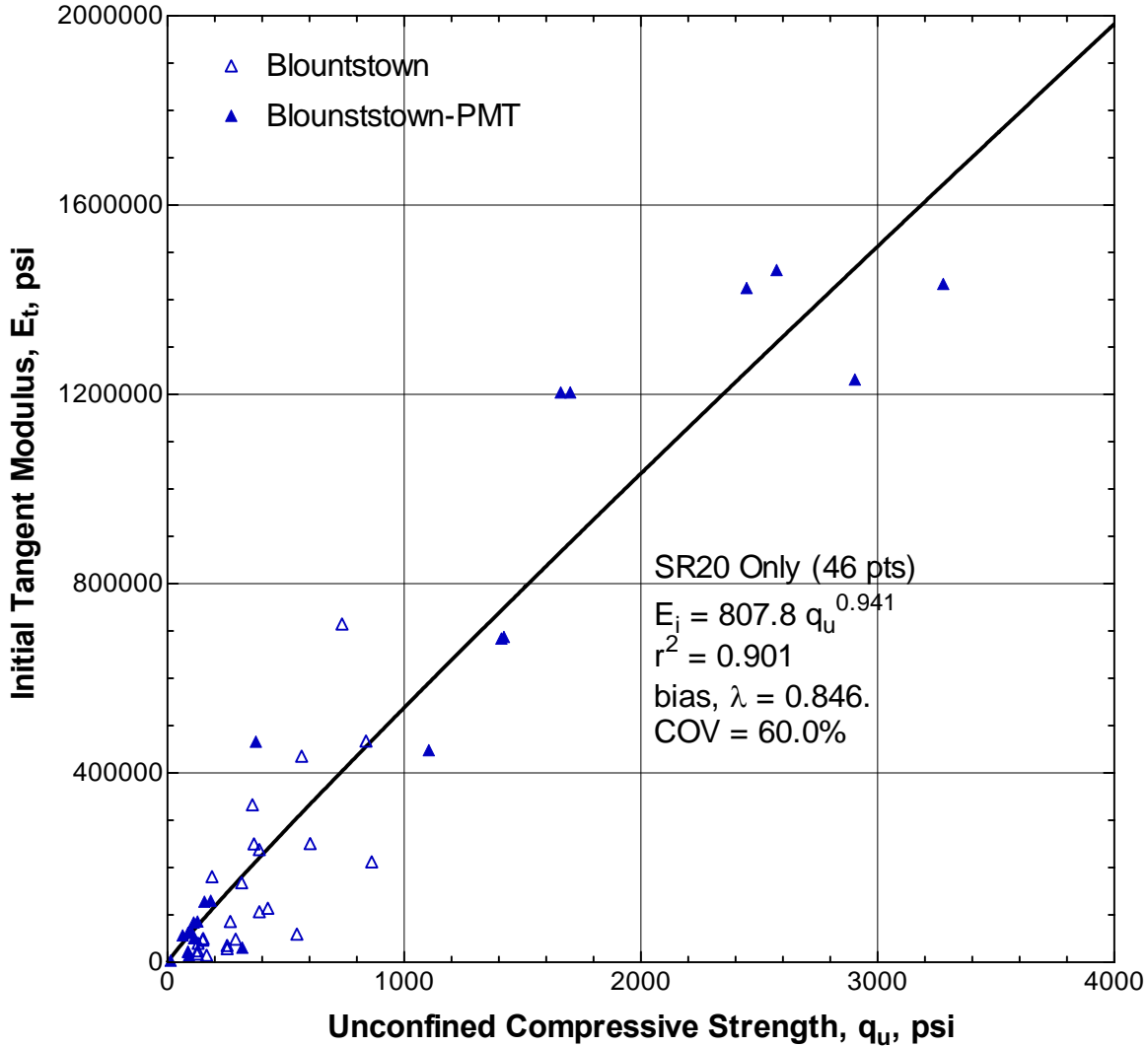


Figure 6.2 SR20 Unconfined Compressive Strength vs. Initial Tangent Modulus

6.2 Compressive Strength vs. Tensile Strength

In addition to stress-strain data, the SMO also provided strength test results (without strain) for the US92 Broadway Bridge, SR10 Choctawhatchee River Bridge, and the SR30 St. Marks River Bridge. Coupled with core boring results from the SR20 Blountstown Bridge and strength tests performed at UF during this project, they formed a sizable database of 419 comparisons between compressive and tensile strength. Unlike the modulus tests performed on the same sample as the compressive strength test, compressive and tensile tests require separate samples from the same core. Splitting tensile tests also use smaller samples, increasing the effects of discontinuities

in the rock, test sample preparation, and test support conditions. **Figure 6.3** shows the correlation between tensile and compressive strength tests, and as expected, greater scatter.

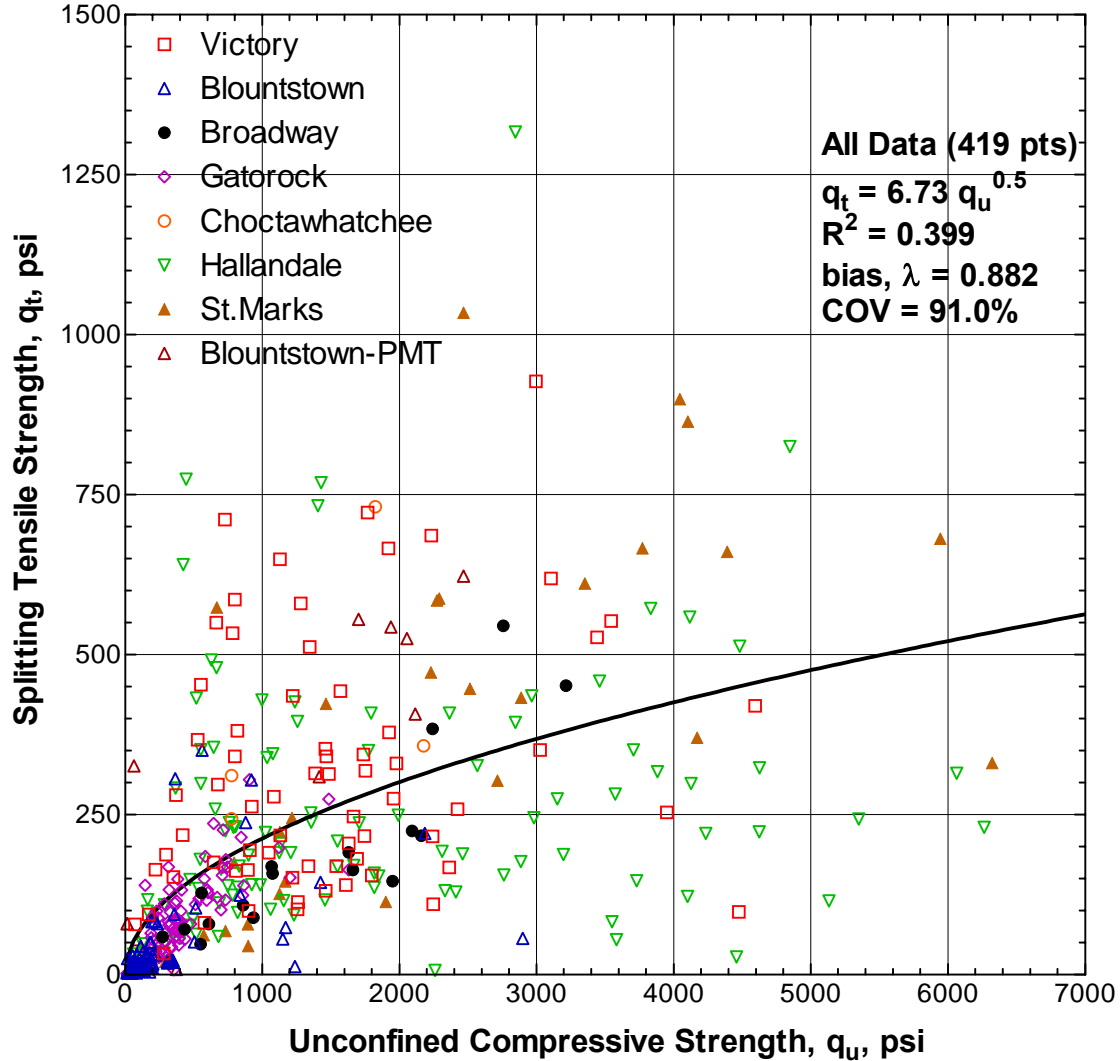


Figure 6.3 Unconfined Compressive Strength vs. Splitting Tensile Strength

Figure 6.3 shows a non-linear least squares regression using the square root of compressive strength, similar to the ACI Building Code formula of $q_t = 6.7 q_u^{0.5}$. The best-fit curve of $q_t = 69.4 q_u^{0.262}$ with $R^2 = 0.413$ only improves the correlation by a small amount. **Figure 6.4** plots the average q_u and q_t values from each group of core tests. While the averaging process does not affect the correlation, it visually removes the

scatter. **Figure 6.5** shows a site-specific correlation between tensile and compressive strength for the SR20 Blountstown site, which as expected, increases the correlation.

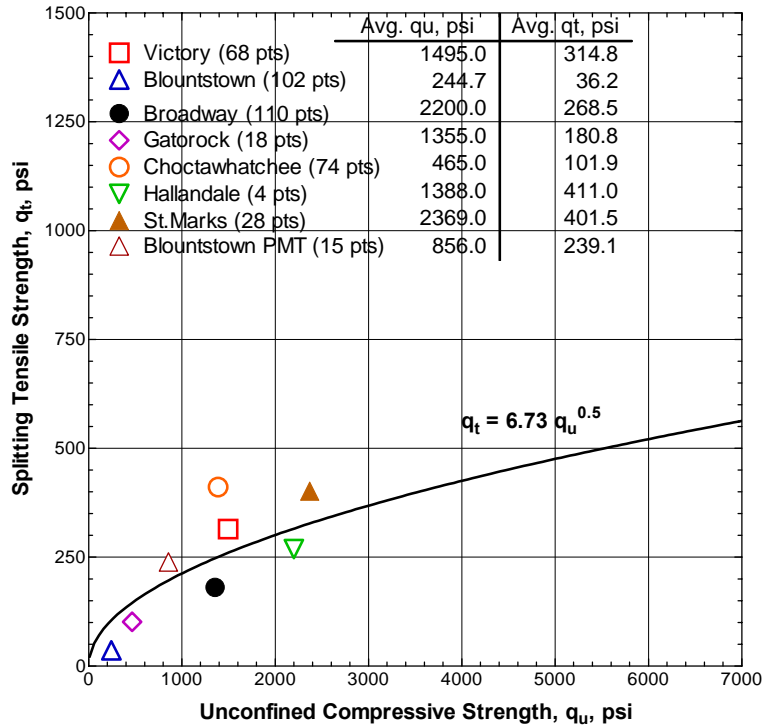


Figure 6.4 Average q_u vs. Average q_t

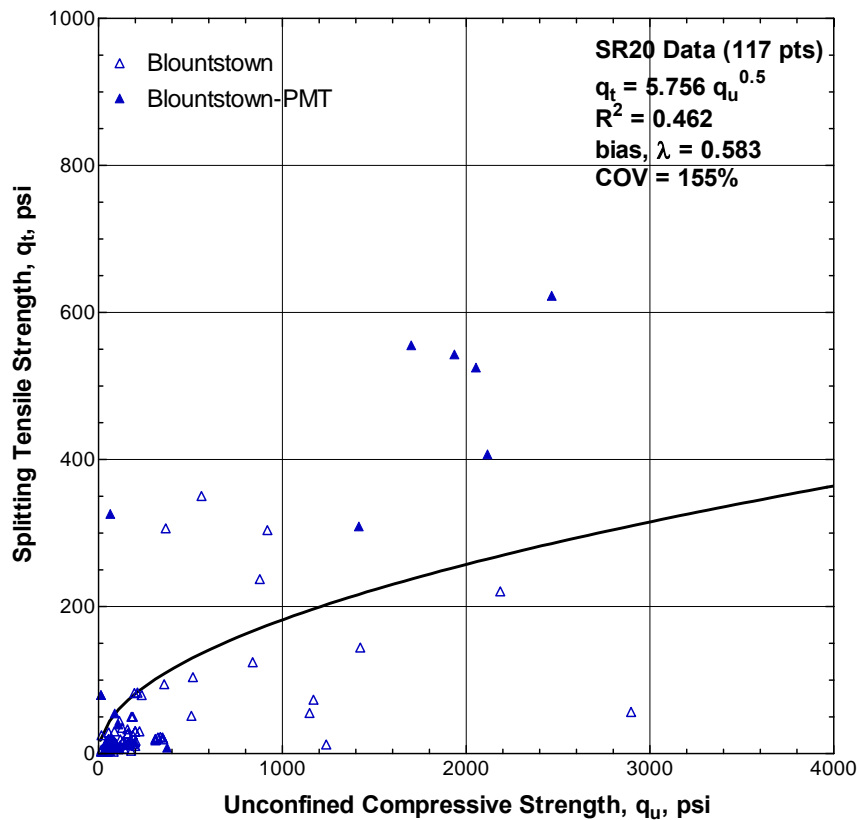


Figure 6.5 SR20 Unconfined Compressive vs. Splitting Tensile Strength

6.3 Validity of Correlations

The data correlations in **Figures 6.1-6.5** contain considerable scatter, much of it unavoidable. Possible reasons for this scatter include:

- Variability of the limestone samples, especially within the samples matched for each q_u - q_t comparison.
- Testing uncertainty, especially in correcting the modulus values for tests performed without a compressometer.
- Site to site variation in the property correlations. Engineers generally consider stiffness and strength as independent variables, affected by the crystalline structure of the material.

While both the q_u - E and q_u - q_t correlations have a precedent in the previously documented properties of concrete and seem reasonable, they also have too much variability for reliable use in design. As shown, the designer can develop better correlation on a site-specific basis, but this will require a statistically significant sample of tests from the site. In addition, the plots above also show that the behavior of Gatorock falls within the range of data collected at the FDOT bridge sites for real limestone. This verification validates the use of Gatorock in lab samples for further study of the pressuremeter and other insitu tests.

7. DRILLED SHAFT SIDE SHEAR FROM SR20 PMT

Chapter 5 focused on correlating the SR20 PMT test results to strength and stiffness parameters from lab tests of rock cores. This chapter compares the same PMT results with the measured unit side shear from the adjacent Test Shafts 5 and 7.

7.1 LPC Method

The LPC method uses the empirical correlations between limit pressure and side shear presented in **Table 2.1** and **Figure 2.17**. The "Q6" curve in **Figure 2.17** best describes the SR20 shafts constructed using drilling mud in weak limestone. The LPC estimate shown in **Table 7.1** uses the following empirical equations to represent the "Q6" curve and estimate the unit side shear, f_{su} , from the PMT limit pressure, p_L , both in kPa:

$$f_{su} = 129.2 + (p_L / 29.27) \quad \text{for } p_L \geq 1400 \text{ kPa} \dots\dots\dots (7.1)$$

$$f_{su} = 33 + (p_L / 9.72) \quad \text{for } p_L < 1400 \text{ kPa} \dots\dots\dots (7.2)$$

7.2 Strength Parameter Estimates

The strength parameter method uses eqn. 2.19 from McVay et al. (1992) and repeated here, to estimate the shaft's unit side shear capacity, f_{su} , based on the compressive strength, q_u , and the tensile strength, q_t , from rock core tests (using consistent units):

$$f_{su} = \frac{1}{2} \sqrt{q_u} \sqrt{q_t} \dots\dots\dots (7.3)$$

Table 5.7 presented measurements of these parameters made on rock cores retrieved during the pressuremeter tests, as well as estimates from the PMT results. **Table 7.1** shows the unit side shear calculated from eqn. 7.3 using the core measurements multiplied by the core recovery. However, the pressuremeter probe tests a larger volume of the rock insitu, and it does not exclude the soft rock normally lost during the coring process. Therefore, we did not apply this reduction to the side shear calculated from the PMT results. While the cracking pressure provided estimates of q_t for the pressuremeter tests, the relative inaccuracy of the horizontal stress estimate

generally provided inconsistent and poor results. Therefore, to predict the unit side shear, we used the q_u - q_t correlation developed for the limestone property database to calculate q_t as shown in **Figure 6.3**:

$$q_t = 6.73\sqrt{q_u} \dots\dots\dots(7.4)$$

7.3 Comparison of f_{su} Results

Table 7.1 lists the results of the predicted f_{su} values and the values calculated by Sharp (1998) from strain gage measurements made during the load test. Note that the test measurements represent the average unit side shear over the distance between shaft strain gage levels, typically about 10 ft, while the pressuremeter estimates represent a measurement made over a depth interval of approximately 1.5 ft. Furthermore, some of the PMT results did not provide usable test curves, possibly as a result of corehole disturbance or very weak rock. The PMT soundings extend deeper than the test shafts, so **Table 7.1** does not provide measured values for comparison with all of the estimates.

Figures 7.1 and 7.2 compare the PMT measured unit side shear from load tests (solid line) with estimates from the LPC Method and estimates from the strength parameter method based on the core tests and the PMT estimates of q_u . The LPC Method matched best with the measured unit side shear of the shaft. This empirical method had the best bias of 0.68 and a COV 81%. Eqn. 2.14, using $\beta = 6.5$, produced the best PMT estimate of unit side shear, with a bias of = 0.61, and a COV of 67%.

Except for the core measurements, all of the side shear estimates over predict the measured shaft side shear. Construction techniques may partially explain this consistent lack of agreement. Significant construction delays may have reduced the side shear capacity of both test shafts. The shaft contractor kept Test Shaft 5 open for 3 days and Test Shaft 7 for 8 days. The contractor overreamed both shafts before concrete placement, but depending on the condition of the overreaming tool, it may not have removed all of the rock softened by exposure to the drill fluid during the delay..

Final Report Contract #BC354 RPWO #13

Therefore, the measured unit side shear may represent a lower bound for the potential side shear at the SR20 Site. Site variability may also explain some of the disagreement

Table 7.1 Summary of Test Shaft Unit Side Shear Estimates

Test Shaft	Test Hole	Elevation msl ft	Test Shaft f_{su} tsf	Estimates of Unit Side Shear, f_{su} , tsf					LPC Method
				Strength Method					
				Lab q_u q_t	from PMT q_u Estimate				
					Avg. p_y	G&A p_L	2 x G&A c_u	$2(p^*_L / 6.5)$	
5	1	-28.45	0.90		7.42	13.75	6.16	4.39	3.26
5	1	-32.55	0.90		6.94	14.20	7.26	5.02	3.34
5	1	-35.90	3.80	1.34	8.43	19.22	10.99	6.53	4.33
5	1	-46.60		26.77		13.13	7.31		3.14
5	1	-49.90		20.05	6.62	13.47	6.19	4.23	3.21
5	1	-52.20		9.93	8.40	16.17	7.80	5.79	3.72
5	2	-33.30	3.80		7.56	14.82	7.89	4.69	3.46
5	2	-35.90	3.80		7.30	14.59	7.42	5.41	3.42
5	2	-47.50		18.69	4.83	10.75	5.55		2.73
5	2	-48.50		18.46	5.82	10.50	6.00		2.68
5	2	-50.50		16.03	5.20	9.67	4.40	2.99	2.54
7	3	-29.90	5.30		6.51	11.47	5.64	3.39	2.85
7	3	-42.92	1.70	0.69	6.04	11.05	5.34	3.35	2.78
7	3	-46.00	1.70		6.49	12.66	6.58	4.17	3.06
7	3	-48.50	1.70			13.54	8.52	4.39	3.22
7	3	-54.65		3.85	6.39	15.25	8.34	5.61	3.54
7	4	-29.90	5.30	0.37		15.41	8.79	4.93	3.57
7	4	-31.92	5.30	0.37		13.71	6.73	4.20	3.25
7	4	-36.40	1.60		7.97	15.11	7.76	4.82	3.52
7	4	-41.15	1.60		7.77	14.98	7.22	5.60	3.49
7	4	-46.00	1.70	0.44	6.63	12.50	5.54	4.13	3.03
7	4	-49.00	1.70	0.63	7.42	13.25	5.49	4.15	3.17
7	4	-54.65		1.30		11.05	5.38		2.78
7	4	-58.60		1.18	6.10	11.26	4.79	3.89	2.81
Mean (tsf)			2.81	8.01	6.83	13.40	6.80	4.58	3.20
Std.Dev.(tsf)				9.35	1.00	2.18	1.51	0.90	0.40
Avg. Bias				6.80	0.33	0.20	0.38	0.61	0.68
Std.Dev. of Bias				5.97	0.20	0.12	0.24	0.41	0.56
COV of Bias (%)				87.8	61.3	62.2	62.1	66.8	81.1

Table 7.1 also shows the mean unit side shear of 2.81 tsf calculated over the sum of the rock socket length for the two shafts. The LPC method with a mean

prediction of 3.20 tsf came closest to the mean of the test shafts, while the other methods were significantly greater.

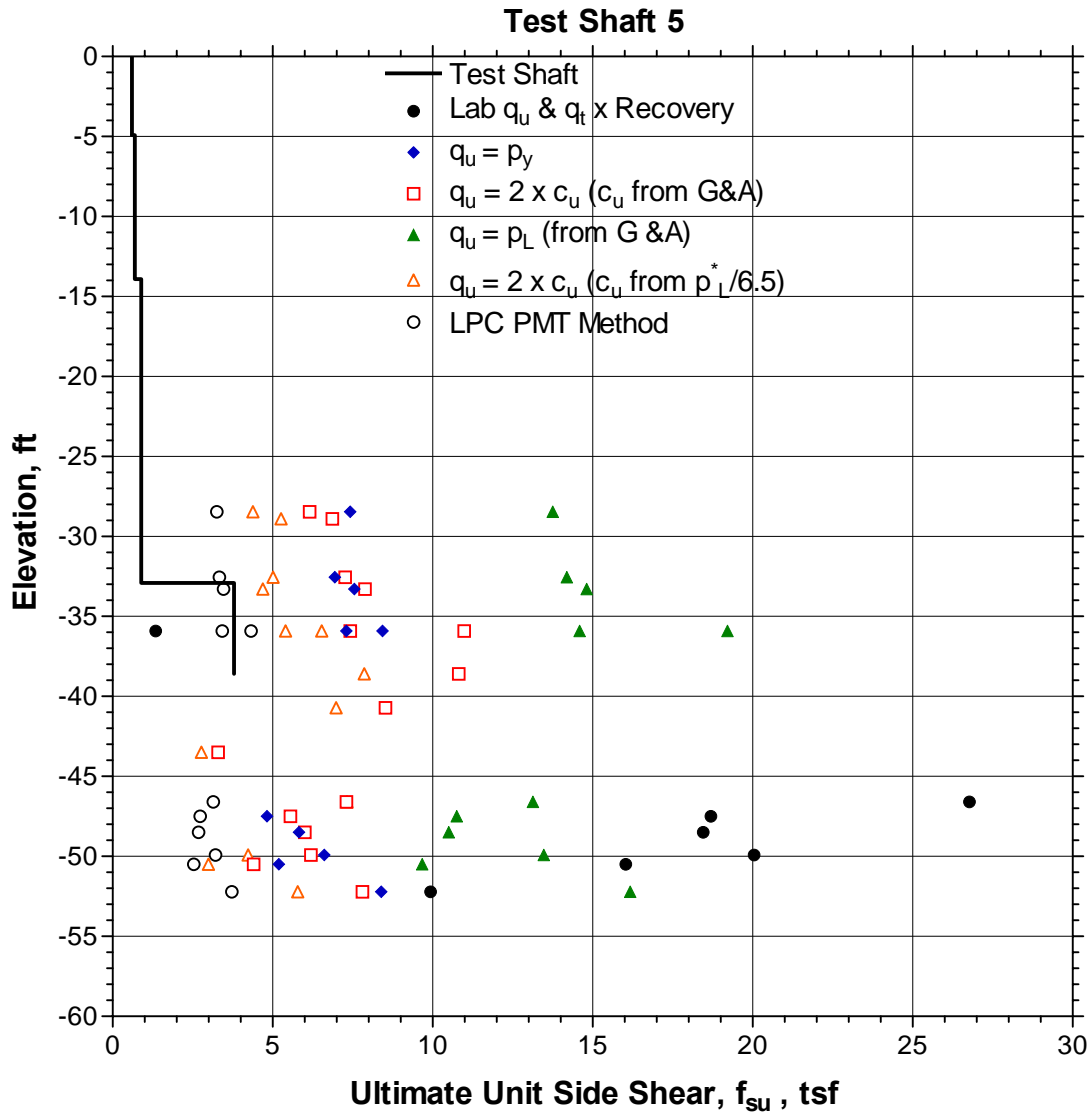


Figure 7.1 SR20 Unit Side Shear Distribution Estimates, Test Shaft 5

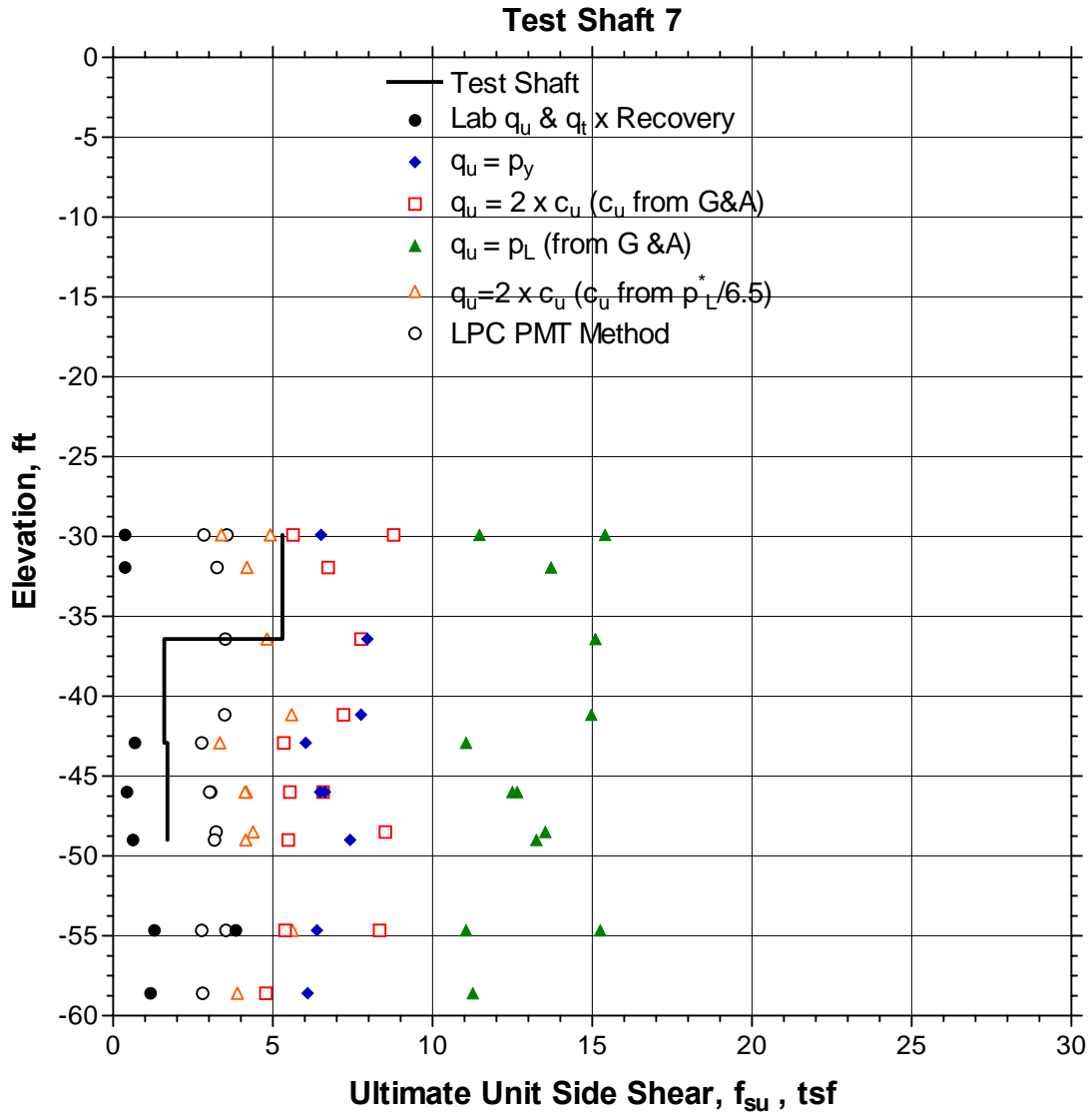


Figure 7.2 SR20 Unit Side Shear Distribution Estimates, Test Shaft 7

7.4 Site Variability at SR20

The variability of strength parameters within the SR20 rock formation may help explain the generally poor prediction of side shear based on the strength method, including the under prediction based on the measured core strengths. If random site variability across the site affects the values of q_u and q_t , then a large sample of test results is needed to adequately characterize the design properties. **Figure 7.3** shows the frequency distribution of q_u from the entire site along with the distributions of q_u estimates from the PMT and the PMT cores adjacent to Test Shafts 5 and 7. This figure shows a frequency distribution for the site with a mode, or peak frequency, significantly lower than the PMT estimates of q_u . However, the mode of the PMT field cores q_u appears to nearly match the mode of the entire site distribution.

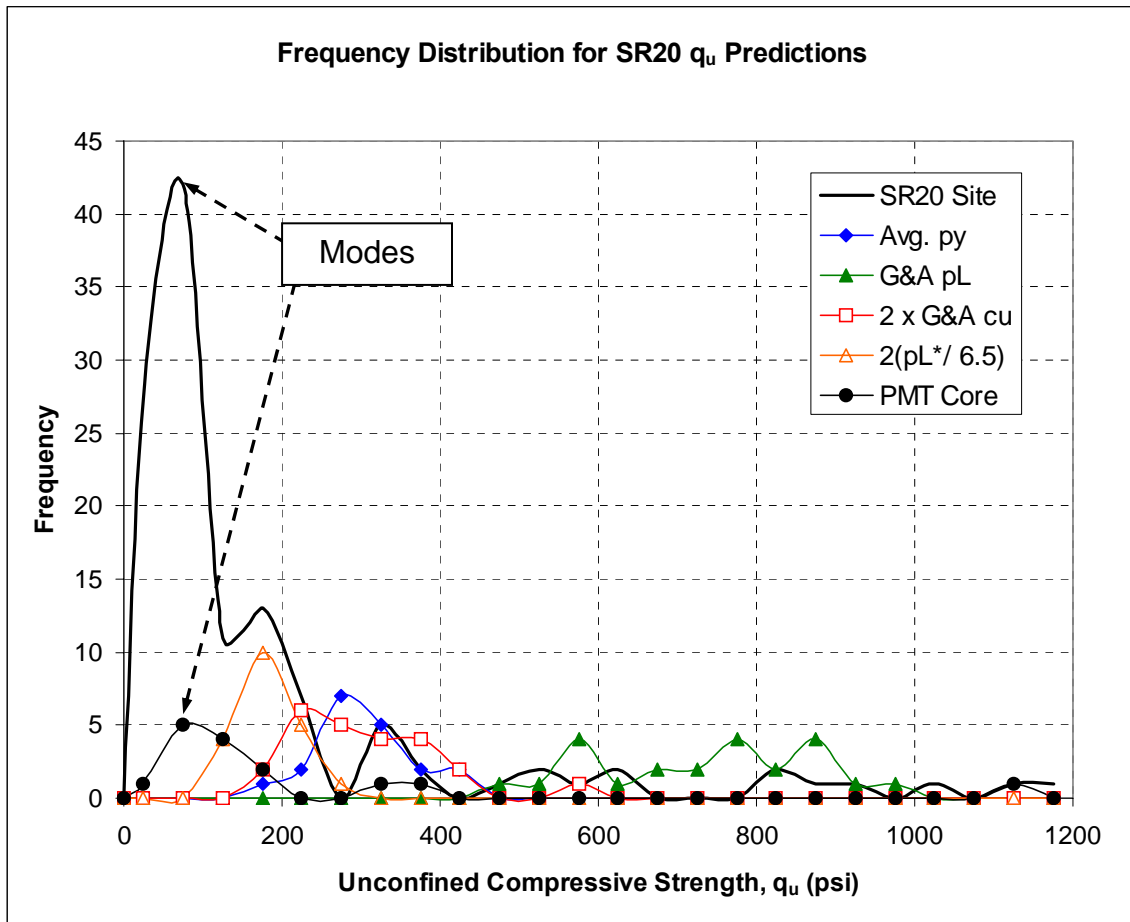


Figure 7.3 Frequency Distribution for SR20 Blountstown q_u Values

Figure 7.4 shows the frequency distribution of q_t from the entire site along with the distributions of q_t estimates from the PMT cracking pressure and the PMT cores adjacent to Test Shafts 5 and 7. This plot cuts off some of the frequency distribution of the PMT predicted q_t that falls below zero, but clearly its mode does not coincide with that of the measurements from the site or the PMT cores, which do have nearly the same mode.

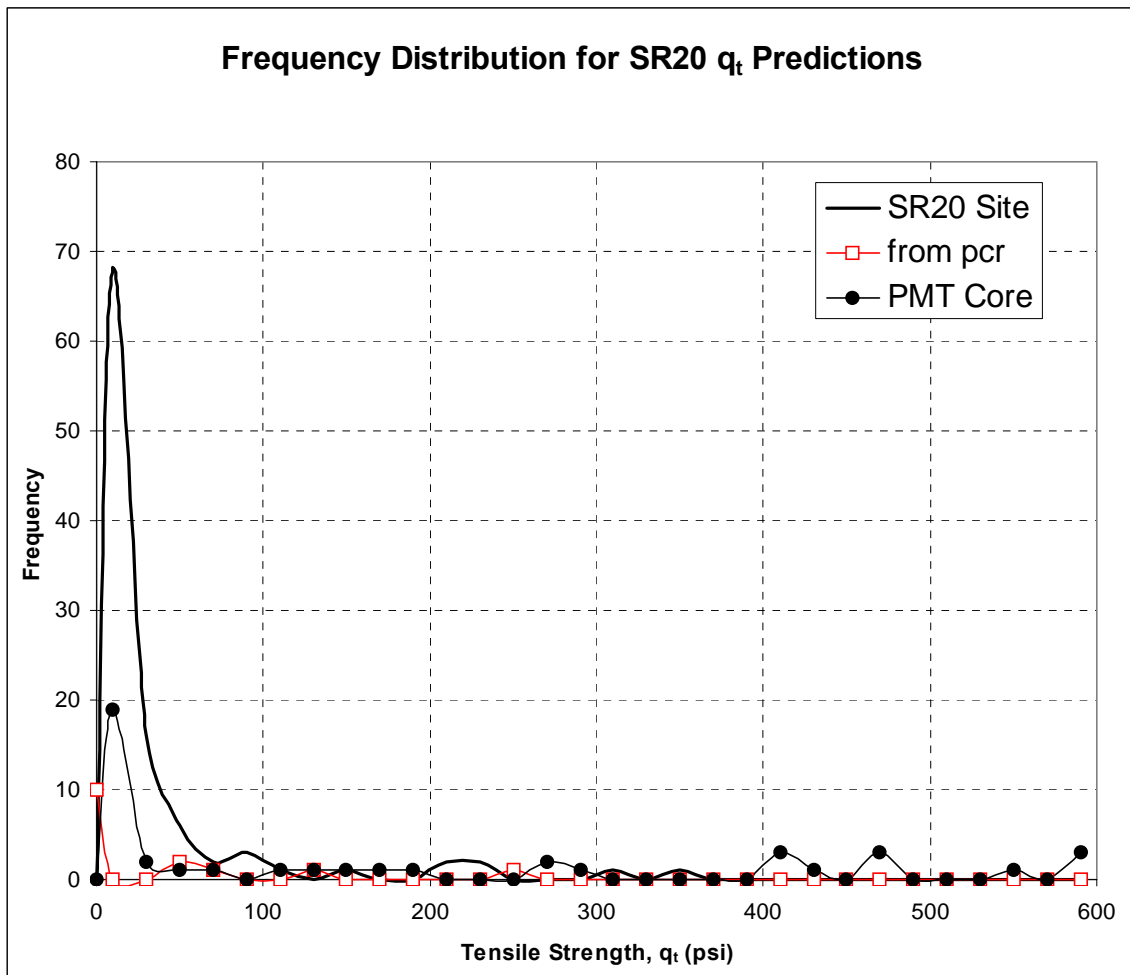


Figure 7.4 Frequency Distribution for SR20 Blountstown q_t Values

Using the correlation shown in **Figure 6.2** to calculate the limestone modulus from the q_u values of the SR20 site, **Figure 7.5** shows the frequency distribution for the core modulus, E_i , plotted along with the distribution of the pressuremeter modulus, E_m . As found for the q_u distributions, the mode of the site E_i disagrees with the PMT E_m , with

the site value about seven times greater than the PMT modulus. However, many authors, including Briaud (1992), have documented this limitation of the PMT modulus, thought due chiefly to the horizontal orientation of the test and the effects of disturbance. This result is more encouraging than the point to point comparison shown in **Figure 5.26**.

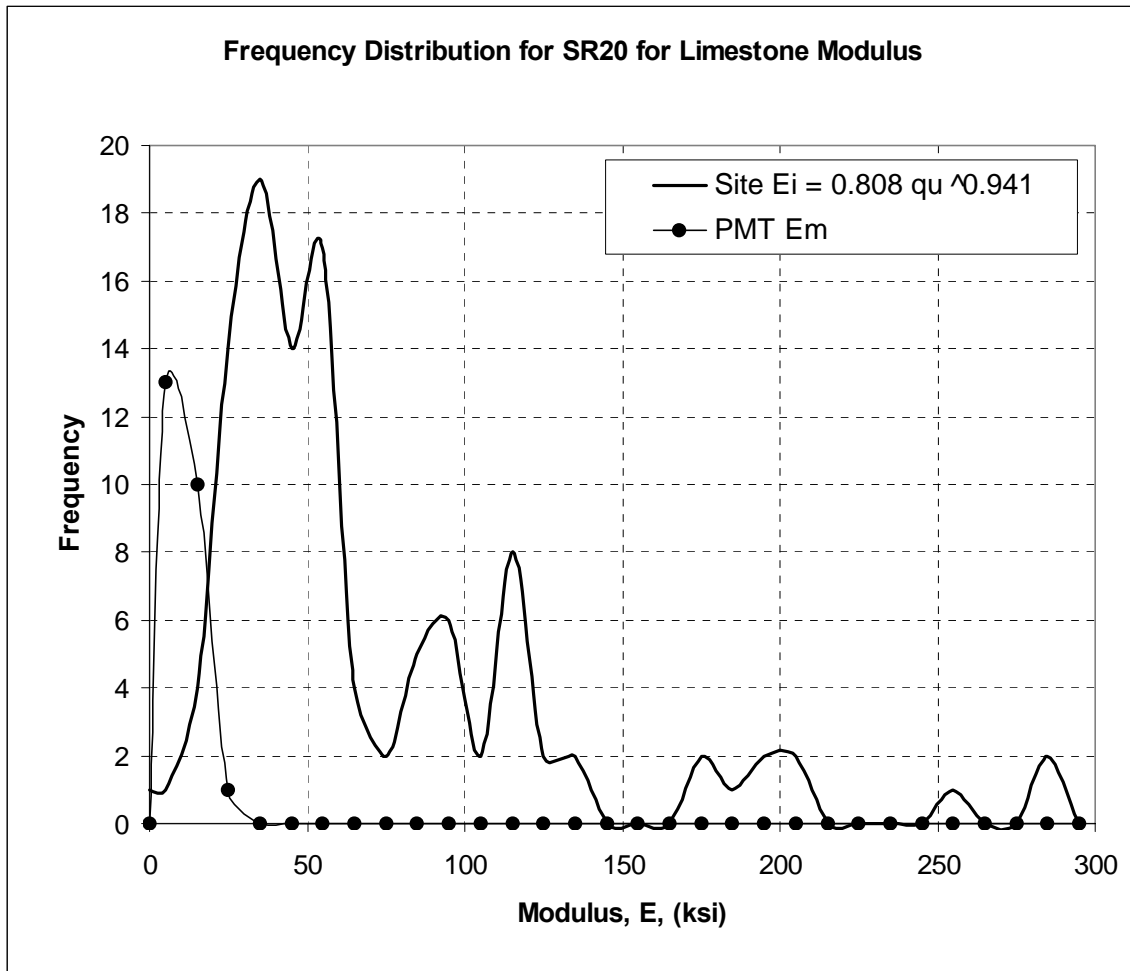


Figure 7.5 Frequency Distribution for SR20 Blountstown Modulus

In summary, the frequency distributions of the PMT results do not match those of the site core data or the field core data. The tests on the rock cores from the site and from the PMT coreholes have similar modes for q_u and q_t . But, as shown in **Table 7.2**, the q_u and q_t distributions have much higher mean values than modes. The skewed distributions of q_u and q_t may help explain the failure of the point to point PMT

correlations attempted for q_u , q_t , E_i , and f_{su} . Much more PMT data will be required to statistically compare the design predictions from the PMT with field core data or shaft test results.

Table 7.2 Comparison of Distribution of q_u and q_t Results from Core Tests at SR20

Distribution Parameter	Site q_u psi	PMT q_u psi	Site q_t psi	PMT q_t psi
Mode	75	75	10	10
Mean	274	888	36	260
No. of Points	127	23	103	47

The mean-mode discrepancy described above for the SR20 data also verifies the need to use a statistical approach for drilled shaft design based on q_u and q_t data, especially with limited core tests. **Table 7.2** selects the mode of the site q_u distribution at the peak frequency, but this distribution has a secondary peak at about 175 psi, which will provide a greater f_{su} value in statistical design approach such as the Monte Carlo Method. **Table 7.3** shows the affect of using the mean value versus the mode of the q_u and q_t distributions in eqn. 7.4 (without correction for recovery that will reduce all cases). The limited number of samples available for the PMT cores combined with the use of the mean values instead of the mode provides a dramatic over prediction of the unit side shear.

Table 7.3 Comparison of f_{su} Predictions based on Source of Core Tests and Distribution Parameter at SR20

Distribution Parameter	Core Tests	q_u psi	q_t psi	Predicted f_{su} tsf	Measured f_{su} tsf
Mode	Entire Site	75	10	0.99	2.81
Mean	Site	274	36	3.58	
Mode	PMT Coreholes	75	10	0.99	
Mean	Coreholes	888	260	17.30	

8. CONCLUSIONS AND RECOMMENDATIONS

The large number of field and lab tests performed for this project, and the subsequent analyses presented herein, lead to the following conclusions and recommendations:

8.1 Conclusions

The main goal of this research, to verify and develop the use of a pressuremeter for the design of drilled shaft side shear, was only partially successful. Additional correlation tests with the Probex-1 will be required to develop confidence in the test. Lab tests seem promising, but field test results at the SR20 site did not confirm them, possibly because of variable, weak rock and/or poor test shaft construction. The Probex-1 meets most of the requirements for a usable pressuremeter test in Florida limestone, with the exception that it requires a good quality test hole (a generic drawback to preboring pressuremeters). Because the Probex-1 is commercially available and supported, its usage is more likely to be successful in practice. Specific conclusions about the lab and field test program follow.

8.1.1 Limestone Property Measurements in the Laboratory

1. The database correlations show that the synthetic Gatorock, used to prepare large limestone samples for lab testing, exhibited behavior similar to tests on actual limestone cores. This material should provide a basis for future lab work using other test methods.
2. The database of 419 comparisons of q_u vs. q_t and 173 comparisons of q_u vs. E_i for the limestone cores obtained from six bridge sites indicates that both E and q_t may be correlated with the square root of q_u , a form similar to that commonly used for concrete. However, the precision needed for design use will require site-specific correlations, which may make better use of a power curve.
3. The early lab tests underscored the importance of using a compressometer to measure sample deflection on the sample, rather than depending on deflection measurements across the platens or the load apparatus.

8.1.2 Pressuremeter Tests in the Laboratory

1. Gatorock lab samples, with a 24 in diameter and 36 in length, were prepared with relatively consist properties. The resulting sample was stronger than trial mix

samples with the same cement and water content, probably because of the vibratory compaction used in place of rodding.

2. Vertical stress, up to 80 psi, applied to the PMT samples in a load frame had little apparent effect on the PMT results.
3. All of the samples cracked diametrically along the full sample length during the pressuremeter test. The test curve plainly showed the point of cracking, also visually observed during the test.
4. The yield pressure correlated well (bias = 0.92) directly with the unconfined compressive strength, q_u , of the sample cores.
5. The net limit pressure divided by $\beta = 6.5$ correlated well (bias = 1.04) with the unconfined compressive strength of the sample cores. The relatively small horizontal stress had little effect on this correlation.
6. The pressuremeter modulus, E_m , correlated well directly with the initial tangent modulus, E_i , of the sample cores (bias = 8.25, COV = 21%).
7. The cracking pressure estimate of splitting tensile strength, q_t , correlated poorly with the sample core measurements. The horizontal stress estimate had a significant effect on these relatively low values.
8. The Texam PMT did not provide adequate capacity to obtain the yield pressure in the lab tests. Excessive system compliance caused undesired variability in the pressure and volume calibrations.
9. The Probex-1 PMT provided adequate capacity to obtain both the yield and limit pressures in the lab tests. The Probex-1 needs a micrometer release valve to control the pressure release during the unload-reload cycle, but otherwise performed very well. Because all of the samples cracked, the unload-reload modulus did not prove useful.

8.1.3 Pressuremeter Tests in the Field

1. We performed 31 Probex-1 stress-controlled tests in four test holes in limestone at the SR20 Blountstown Bridge. Of these tests, 24 provided usable test curves. Either improper coring techniques or poor quality limestone may have caused the failed tests. The Probex-1 performed well.
2. The SR20 test holes were cored using a NQ triple tube core barrel. For 24 core runs 5 ft long, the recovery averaged 32.9% and the RQD averaged 10.0%. The low recovery and RQD probably indicate poor quality limestone.
3. We emphasized the preparation of quality hole for the PMT, using a bottom discharge bit with only enough fluid pressure, down pressure on the rods, and rotational speed to advance the core run at steady pace.

4. Core tests at the SR20 site indicate relatively weak limestone, with average values of $q_u = 274$ psi and $q_t = 36$ psi for the entire site. Tests of the PMT cores provided average values of $q_u = 888$ psi and $q_t = 260$ psi for the PMT coreholes.
5. The horizontal stress determined from the PMT curves and from the creep plot did not agree well with each other.
6. Of the 24 usable PMT curves, 13 showed a cracking pressure, but the magnitude of the cracking pressure was relatively low and the method proposed for q_t based on the cracking pressure and the horizontal stress did not provide good correlation with the core tests.
7. The PMT yield pressure calculated from the creep plot agreed very well with that observed on the test curve.
8. PMT estimates of the initial tangent modulus and unconfined compressive strength of the core tests, based on the same correlations used in the lab, were poor.
9. Direct comparison of PMT test measurements with adjacent core tests was generally poor. However, their frequency distributions compare better, an indication of random variability. Frequency distributions of q_u , q_t , and E_i indicate significant variability of these limestone parameters at the SR20 site. No significant depth trend was identified.
10. The mode of the q_t and q_u frequency distributions for the PMT core tests is similar to that of the entire site obtained from 4 inch cores. The modes of the PMT q_u estimates are higher.
11. The mode of the core test modulus, based on the site q_u values, was approximately seven times the mode of the PMT modulus, in good agreement with the ratio of 8.25 observed during the lab PMTs.

8.1.4 Unit Side Shear Predictions

1. The strength parameter method using point estimates did not accurately predict the unit side shear from the Test Shafts. This is probably due to the lack of a fully populated distribution from which to draw q_u and q_y values that account for the site variability.
2. The empirical LPC PMT Method based on limit pressure and construction methods gave the best estimate of unit side shear. The LPC method is an empirical design method that has benefited from 5 updates to the load test database over 25 years.
3. The PMT lab correlations with Gatorock, though limited, seemed to promise good field correlations. Variability and weak rock at the SR20 did not confirm the lab correlations.

8.2 Recommendations

1. The pressuremeter test applies a unique stress field to the material tested, combining axisymmetric and plane strain conditions. Its results may prove amenable to inverse finite element modeling not within the scope of the research.
2. Additional field work or lab work with the Probex-1 can confirm (or deny) the viability of this test for drilled shaft design.
3. A more direct approach to measuring unit side shear insitu may prove useful for drilled shaft design. Previous attempts include pullout tests of cast-in-place concrete plugs and the Iowa Borehole Shear Test (IBST), both used successfully on FDOT bridge projects in the past. Alternatively, a shear device similar to the IBST with a flexible membrane, such as used for the pressuremeter, should conform better to the irregular and variable corehole dimensions often encountered in Florida Limestone. Unfortunately, existing PMT membranes are designed to withstand internal normal pressure, not axial shear. The membrane envisioned must be flexible to obtain good sidewall contact, but also strong so that the shear failure occurs in the rock interface rather than in the membrane material.

REFERENCES

- Bacciarelli, Robert E. (1986). "The calibration and use of a high capacity pressuremeter to determine rock stiffness." *The Pressuremeter and Its Marine Applications: Second International Symposium*. J.L. Briaud and J.M.E. Audibert, (eds.), ASTM, Philadelphia, PA, STP 950.
- Baguelin, F., Jezequel, J.F., Lemee, E. and Le Mehaute, A. (1978). "Expansion of cylindrical probes in cohesive soils." *ASCE J. Soil Mech.* ASCE, Reston, VA, Vol. 98, No. SM11, pp. 1129-1142.
- Baguelin, F., Jezequel, J. F., and Shields, D. H. (1978). *The Pressuremeter and Foundation Engineering*. Trans Tech Publications. Clausthal-Zellerfeld, Germany.
- Beer, F.P. and Johnston, E.R. Jr. (1992). *Mechanics of Materials*. 2nd edition, McGraw Hill, New York, NY.
- Bjerrum, L. & Andersen, K.H. (1972). "In-situ measurement of lateral earth pressures in clay." *Proceedings of the 5th European Conference on Soil Mechanics & Foundation Engineering*. Balkema, Brookfield, VT, vol.1, pp. 11-20.
- Bjerrum, L. Nash, J.K., Kennard, R.M. and Gibson, R.E. (1974). "Hydraulic fracturing in field permeability testing." *Geotechnique*. Institution of Civil Engineers, London, England, 22: 319-332.
- Bozozuk, L. (1974). "Minor Principal stress measurements in marine clays with hydraulic fracture tests." *Proceedings of ASCE Conference on Subsurface Exploration for Underground Excavation and Heavy Construction*. Henniker, pp: 333-349, NH.
- Briaud, J.L. (1986). "Pressuremeter and foundation design." *Use of In-Situ Tests in Geotechnical Engineering*. ASCE, Reston, VA, GSP 6.
- Briaud, J.-L. (1992). *The Pressuremeter*. Balkema, Brookfield, VT.
- Briaud, J.-L. (1989). "The pressuremeter test for highway applications." FHWA-IP-89-008, Federal Highway Administration, McLean, VA.
- Briaud, J.-L., & Gambin, M. (1984). "Suggested practice for drilling boreholes for pressuremeter testing." *ASTM Geotechnical Testing Journal*. Philadelphia, PA, Vol.7, No.1.
- Cepero, C. (2002). "Insitu rock modulus." *Master's Thesis*. University of Florida, Gainesville, FL.
- Clarke, B.G. (1995). *Pressuremeters in Geotechnical Design*. Blackie Academic and Professional, Glasgow, England.
- Gibson, R.E. and Anderson, W.F. (1961). "Insitu measurement of soil properties with the pressuremeter." *Civil Engineering Public Works*, Rev. 56, No. 658, pp. 615-618.

- Goodman, R. E. (1989). *Rock Mechanics*. John Wiley & Sons, New York, NY.
- Haberfield, C.M. (1987). "The performance of the pressuremeter and socketed piles in weak rock." *Doctor of Philosophy Dissertation*, University of Monash, Australia.
- Haberfield, C.M. (1997). "Pressuremeter testing in weak rock and cemented sand." *Proceedings of the Institution of Civil Engineers Geotechnical Engineering*. Institution of Civil Engineers, London, England, (125)3, 168-178.
- Haberfield, C.M., and Johnston, I.W. (1986). "Concepts for pressuremeter interpretation in soft rock." *Speciality Geomechanics Symposium*. Barton, Australia, (86)8.
- Haberfield, C.M. and Johnston, I.W. (1989). "Model studies of pressuremeter testing in soft rock." *ASTM Geotechnical Testing Journal*. Philadelphia, PA, Vol. 12, No. 2, pp. 150-156.
- Haberfield, C.M. and Johnston, I.W. (1990). "A numerical model for pressuremeter testing in soft rock." *Geotechnique*. Institution of Civil Engineers, London, England, 40 (4): 569-580.
- Hoyt, J.H. (1969). "Late Cenozoic structural movement, northern Florida." *Transactions of the Gulf Coast Association of Geological Societies*. 19:1-9, 1969.
- Ismail, M.A., Joer, H.A. and Randolph, M.F. (2000). "Sample preparation technique for artificially cemented soils." *ASTM Geotechnical Testing Journal*. Philadelphia, PA, Vol. 23, No. 2, pp. 171-177.
- Jacobs, S. (2003). "Insitu measurement of Florida limestone modulus and strength properties." *Master's Thesis*. University of Florida, Gainesville, FL.
- Johnston, I.W. and Choi, S.K. (1986) "A synthetic soft rock for laboratory model studies." *Geotechnique*, Institution of Civil Engineers, London, England, Vol. 36, No. 2, pp. 251-263.
- Johnston, I.W. and Choi, S.K. (1982). "Failure mechanisms of foundations in soft rock." *11th International Conference on Soil Mechanics*. Balkema, Brookfield, VT, Vol. 3, pp.1397-1400, 1982.
- Johnston, I.W. and Choi, S.K. (1986). "A synthetic soft rock for laboratory model studies." *Geotechnique*. Institution of Civil Engineers, London, England, Vol. 36, No. 2, pp. 251-263.
- Johnston, I. W., and Chiu, H.K. (1981). "The consolidation properties of a soft rock." *Proceedings of the 10th International Conference on Soil Mechanics and Foundation Engineering*. Balkema, Brookfield, VT, (1), 661-664.

Johnston, I.W., Williams, A.F., and Chiu, H.K. (1980). "Properties of soft rock relevant to socketed pile design." *Proceedings of the International Conference on Structural Foundations on Rock*. Vol. 1, pp. 55-64, Sydney.

Jones, Douglas, S. (1997). "The marine invertebrate fossil record of Florida." *The Geology of Florida*. Randazzo, A.F. and Jones, D.S. (eds.), University Press of Florida, Gainesville, FL.

Labuz, J. F., and Bridell, J. M. (1993). "Reducing frictional constraint in compression testing through lubrication." *International Journal of Rock Mechanics and Mining Science and Geomechanics Abstracts*. (30)4, 451-455.

Ladanyi, B. (1967). "Expansion of cavities in brittle media." *Int. J Rock Mech. Min. Sci.* Vol. 4, pp. 301-328.

Ladanyi, B. (1976). "Quasi-static expansion of a cylindrical cavity in rock." *Eng. App. of Solid Mech. Proc. 3rd Symp.* Vol. 2, pp. 219-240.

Liu, C. and Evett, J.B. (1998). *Soils and Foundations*. 4th ed. Prentice Hall, Upper Saddle River, NJ.

Lutgens, F.K. and Tarbuck, E.J. (1998). *Essentials of Geology*. 6th ed., Prentice Hall, Upper Saddle River, NJ 1998.

Mair R. J., and Wood D. M. (1987). *Pressuremeter Testing*. Butterworths, England.

McVay, M. C., Townsend, F. C. and Williams, R. C. (1992). "Design of socketed drilled shafts in limestone." *ASCE Journal of Geotechnical Engineering*. ASCE, Reston, VA, 118(10), 1626-1637.

Menard, L. (1975). "The Menard pressuremeter: interpretation and application of the pressuremeter test results to foundation design." *Soils-Soils*, No. 26.

Oluokun, F.A., Burdette, E.G. and Deatherage, J.H. (1991). "Elastic modulus, poisson's ratio, and compressive strength relationships at early ages." *ACI Materials Journal*. Vol. 88, No. 1.

Oluokun, F.A. (1991). "Prediction of concrete tensile strength from its compressive strength: Evaluation of existing relations for normal weight concrete." *ACI Materials Journal*. Vol. 88, No. 3.

Oluokun, F.A., E.G. Burdette, E.G. and Deatherage, J.H. (1991). "Splitting tensile strength and compressive strength relationship at early ages." *ACI Materials Journal*. V. 88, No.2.

Randazzo, Anthony F. (1997). "The sedimentary platform of Florida: Mesozoic to Cenozoic." *The Geology of Florida*. Randazzo, A.F. and Jones, D.S. (eds.), University Press of Florida, Gainesville, FL.

Rocha, M., De Silveira, A., Grossman, N and De Oliveira, E. (1966). "Determination of the deformability of rock masses along boreholes." *Proc. of the 1st Cong. of the ISRM*. pp. 697-704.

Schmidt, W. (1997) "Geomorphology and physiography of Florida," *The Geology of Florida*. Randazzo, A.F. and Jones, D.S. (eds.), University Press of Florida, Gainesville, FL.

Sharpe, M.R. (1998). *Final Geotechnical Report, SR20 Over Apalachicola River, Blountstown Bridge*. Dames and Moore, Inc., Tampa, FL.

Shields, D.H. and Bauer, G.E. (1975). "Determination of the modulus of deformation of a sensitive clay using laboratory and in-situ test." *ASCE Specialty Conference on In-Situ Measurement of Soil Properties*. ASCE, Reston, VA.

Smith, Douglas L. and Kenneth M. Lord. (1997). "Tectonic evolution and geophysics of the Florida basement." *The Geology of Florida*. Randazzo, A.F. and Jones, D.S. (eds.), University Press of Florida, Gainesville, FL.

Takeuchi, T. and Suzuki, T. (1981). "An evaluation of in-situ deformation coefficient, c and ϕ of soft rock by borehole load test." *Proc. of the Int. Symp. On Weak Rock*. Tokyo, pp. 417-422.

Wicander, R. and Monroe, J.S. (1993). *Historical Geology: Evolution of the Earth and Life through Time*. 2nd edition, West Publishing Company, Minneapolis, MN.

9. APPENDIX

SUMMARY OF LIMESTONE LAB TESTS

Final Report Contract #BC354 RPWO #13

Table A.1 Unconfined Compressive and Tensile Strength of Gatorock Trial Mix

Trial Mix	Trial Mix	Compressive Strength Tests				Splitting Tensile Strength Tests				Average	Average
		L / D	γ_t	w	q_u	L / D	γ_t	w	q_t		
Cement	Water	Ratio	pcf	%	psi	Ratio	pcf	%	psi	psi	psi
10.0%	15.0%	2.032	102.0	10.33	302.5	1.844	115.5	12.02	61.3	272.3	59.4
10.0%	15.0%	1.984	102.9	10.13	295.4	1.843	115.9	13.31	63.4		
10.0%	15.0%	2.024	104.7	13.21	273.9	1.992	117.2	13.83	53.5		
10.0%	15.0%	1.992	96.4	12.18	217.5						
10.0%	20.0%	1.984	118.1	15.00	407.4	1.938	121.4	17.63	79.7	432.7	71.2
10.0%	20.0%	2.008	121.1	16.39	395.4	2.000	122.7	16.58	58.4		
10.0%	20.0%	2.016	118.3	15.49	478.5	2.000	124.7	17.97	75.4		
10.0%	20.0%	2.065	122.5	14.77	449.4						
10.0%	25.0%	1.969	117.4	21.31	341.9	1.906	121.1	21.27	18.7	328.2	20.3
10.0%	25.0%	2.000	113.3	20.31	336.2	2.008	121.2	21.21	22.2		
10.0%	25.0%	1.937	119.4	20.91	326.5	1.984	38.2	20.49	20.1		
10.0%	25.0%	1.922	117.0	21.05	308.1						
11.1%	10.0%	1.742	100.2	8.70	120.0						
11.1%	10.0%	2.065	92.3	8.70	103.0						
15.0%	12.8%	1.984	91.4	11.00	108.0						
15.0%	12.8%	1.906	107.8	10.39	699.1						
15.0%	15.0%	2.032	105.9	12.03	427.9	1.683	113.3		156.7	557.2	127.5
15.0%	15.0%	2.024	114.4	13.27	747.3	1.610	72.9		98.3		
15.0%	15.0%	2.016	109.6	11.83	561.0						
15.0%	15.0%	2.008	109.0	12.25	460.8						
15.0%	15.0%	2.000	112.8		588.9						
15.0%	20.0%	1.984	122.6	16.88	997.7	1.875	116.8	15.27	94.6	935.3	89.1
15.0%	20.0%	2.000	120.1	16.04	873.0	1.953	119.4	15.19	79.1		
15.0%	20.0%					1.969	118.6	15.52	93.5		
15.0%	25.0%	1.969	116.1	20.79	524.2	1.891	123.2	16.53	52.7	550.4	47.7
15.0%	25.0%	1.969	116.6	18.74	576.6	1.898	122.8	22.29	41.9		
15.0%	25.0%					1.884	119.5	22.58	48.6		
17.5%	17.5%	2.000	113.1	13.36	573.9	2.000	100.0	12.47	48.7	611.1	79.3
17.5%	17.5%	2.008	116.7	13.34	776.0	2.016	109.3	11.83	52.3		
17.5%	17.5%	2.016	115.2	14.52	483.4	2.000	120.3	13.94	137.0		
17.5%	20.0%	1.992	117.5	13.77	1139.0	2.016	119.2		144.7	1068.4	169.1
17.5%	20.0%	2.000	123.7	14.98	1219.0	1.701	125.6		198.7		
17.5%	20.0%	2.032	123.8	15.58	722.7	2.000	125.5	15.86	189.0		
17.5%	20.0%	2.008	122.5		1192.9	2.000	124.3	17.29	144.0		
17.5%	25.0%	2.008	118.4	17.91	877.9	1.984	123.9	20.10	111.9	859.6	108.8
17.5%	25.0%	1.961	117.6	18.99	825.6	1.984	124.9	19.98	113.5		
17.5%	25.0%	1.984	121.0	18.07	875.4	1.984	123.4	20.96	101.1		

Table A.1 (cont.) Unconfined Compressive and Tensile Strength of Gatorock Trial Mix

Trial Mix	Trial Mix	Compressive Strength Tests				Splitting Tensile Strength Tests				Average q _u psi	Average q _t psi
		L / D Ratio	γ _t pcf	w %	q _u psi	L / D Ratio	γ _t pcf	w %	q _t psi		
17.6%	15.0%	1.984	117.7		791.7						
20.0%	20.8%	1.734	119.9	15.44	1303.4						
20.0%	20.8%	1.977	121.1	16.59	1465.3						
20.0%	20.8%	2.008	120.2	15.30	1488.1						
20.0%	25.0%	2.000	123.9	20.66	1052.0	1.992	122.9		162.2	1075.4	158.1
20.0%	25.0%	1.938	121.0	20.87	1010.7	1.953	123.1		163.0		
20.0%	25.0%	1.992	108.4	20.12	1309.2	2.000	124.2	20.10	149.2		
20.0%	25.0%	1.984	109.4		1380.2						
20.0%	25.0%	2.003	125.6	18.98	1117.3						
20.0%	25.0%	1.985	125.4	20.14	854.5						
20.0%	25.0%	2.000	124.6	20.23	803.8						
20.0%	25.0%	2.000	124.6	20.23	803.8						
22.5%	20.0%	2.000	128.4	15.67	2049.7						
22.5%	20.0%	2.003	127.4	15.38	1959.4						
22.5%	20.0%	1.955	128.1	16.50	1611.1						
22.5%	22.5%	1.985	126.4	18.23	1386.1						
22.5%	22.5%	1.985	125.9	16.63	1502.2						
22.5%	22.5%	1.992	126.6	16.52	1526.9						
22.5%	25.0%	1.960	126.1	20.40	1005.2						
22.5%	25.0%	1.980	125.6	19.56	1096.6						
22.5%	25.0%	1.980	125.4	20.30	1043.7						
25.0%	20.0%	1.855	123.9		2495.0						
25.0%	20.0%	1.945	121.7		1883.6						
27.5%	22.5%	1.980	127.7	16.13	1901.1						
27.5%	25.0%	1.990	127.8	18.04	1590.5						
27.5%	25.0%	1.985	127.3	18.13	1514.6						

Final Report Contract #BC354 RPWO #13

Table A.2 Modulus Tests of Gatorock Trial Mix

Trial Mix Cement	Trial Mix Water	q _u psi	E _i psi	E _s psi	E _{25%} psi	ε _f %	ε _{25%} %
10.0%	11.0%	122.1	13420	7408	12860	1.648	0.412
10.0%	11.0%	103.0	21600	16490	21600	0.625	0.156
10.0%	15.0%	302.5	114900	85300	114420	0.355	0.089
10.0%	15.0%	295.6	80870	40650	60000	0.833	0.208
10.0%	15.0%	273.9	102000	77100	101300	0.355	0.089
10.0%	15.0%	207.6	138000	72410	136700	0.287	0.072
10.0%	20.0%	407.8	93000	62540	88940	0.007	0.002
10.0%	20.0%	395.4	165700	67130	131700	0.006	0.001
10.0%	20.0%	478.6	338900	118300	282200	0.404	0.101
10.0%	20.0%	449.4	231600	90160	210200	0.498	0.125
10.0%	25.0%	342.6	910900	55600	188200	0.616	0.154
10.0%	25.0%	336.2	508100	61840	206000	0.544	0.136
10.0%	25.0%	327.8	141250	41410	126340	0.792	0.198
10.0%	25.0%	309.6	80820	38000	76117	0.815	0.204
15.0%	12.8%	108.1	2063	3874	9029	2.791	0.698
15.0%	12.8%	693.9	106300	66780	103900	1.039	0.260
15.0%	15.0%	417.4	666400	180800	524000	0.214	0.053
15.0%	15.0%	747.3	500000	221600	432900	0.337	0.084
15.0%	15.0%	488.2	117200	39340	99260	1.241	0.310
15.0%	15.0%	552.3	182100	146100	179900	0.378	0.094
15.0%	15.0%	588.9	232300	143600	200000	0.410	0.102
15.0%	20.0%	998.6	528700	212700	400500	0.469	0.117
15.0%	20.0%	873.0	477400	274000	473300	0.319	0.080
15.0%	25.0%	525.2	242600	92200	242300	0.570	0.142
15.0%	25.0%	577.7	315900	100700	265000	0.574	0.143
17.6%	15.0%	792.5	257500	109000	200300	0.727	0.182
17.5%	17.5%	776.0	272800	135200	255100	0.574	0.143
17.5%	17.5%	573.9	195100	116500	186800	0.493	0.123
17.5%	17.5%	461.0	212300	98270	212300	0.469	0.117
17.5%	20.0%	1219.0	517600	204800	456400	0.595	0.149
17.5%	20.0%	722.7	341600	132300	203600	0.548	0.137
17.5%	20.0%	1158.3	699000	273400	604200	0.424	0.106
17.5%	20.0%	1192.9	280000	220800	260600	0.540	0.135
17.5%	25.0%	876.3	319900	135500	259800	0.647	0.162
17.5%	25.0%	877.9	500000	167100	468300	0.525	0.131
17.5%	25.0%	828.2	365300	137800	332900	0.601	0.150
20.0%	20.8%	1327.4	527400	94700	225400	1.402	0.351
20.0%	20.8%	1467.4	387000	277600	354700	0.529	0.132
20.0%	20.8%	1536.9	725400	330400	481500	0.465	0.116
20.0%	25.0%	1052.0	353000	166400	272100	0.632	0.158
20.0%	25.0%	1010.7	289200	147900	225300	0.684	0.171
20.0%	25.0%	1381.5	497000	279200	436500	0.495	0.124
20.0%	25.0%	1309.8	380000	280300	376700	0.467	0.117

Table A.2 (cont.) Modulus Tests of Gatorock Trial Mix

Trial Mix Cement	Trial Mix Water	q _u psi	E _i psi	E _s psi	E _{25%} psi	ε _f %	ε _{25%} %
20.0%	25.0%	1092.3	1502200	262500	759300	0.416	0.104
20.0%	25.0%	828.2	1645800	223800	765200	0.370	0.093
20.0%	25.0%	803.8	634600	192200	655300	0.418	0.105
20.0%	25.0%	908.1	1347000				
22.5%	20.0%	2043.7	621200	423300	724900	0.483	0.121
22.5%	20.0%	1939.4	614000	571000	500500	0.340	0.085
22.5%	20.0%	1617.7	958800	300400	779800	0.539	0.135
22.5%	20.0%	1867.0	1565200				
22.5%	22.5%	1365.3	698900	248700	603100	0.549	0.137
22.5%	22.5%	1483.6	1111000	322500	862600	0.460	0.115
22.5%	22.5%	1509.6	1936000	390200	1106500	0.387	0.097
22.5%	22.5%	1452.8	1582900				
22.5%	25.0%	986.7	747800	246500	599500	0.400	0.100
22.5%	25.0%	1078.0	620100	287700	507200	0.375	0.094
22.5%	25.0%	1016.9	1037200	235600	764600	0.432	0.108
22.5%	25.0%	1027.2	1261750				
25.0%	20.0%	2518.4	706500	567900	672000	0.443	0.111
25.0%	20.0%	1886.0	586900	519600	584100	0.363	0.091
27.5%	22.5%	1876.4	691800	366900	681300	0.511	0.128
27.5%	25.0%	1565.5	1442300	424700	955600	0.369	0.092
27.5%	25.0%	1436.0	689500	308500	685300	0.466	0.116

Final Report Contract #BC354 RPWO #13

Table A.3 Unconfined Compressive and Modulus Tests of Gatorock PMT Cores

Core Sample	Cast Date	Coring Date	Test Date	Elapsed Time days	w %	q _u psi	Average q _u psi	Modulus, E _i psi	Average E _i psi
1UC1	8/31/01	10/23/01	12/13/01	104	15.7	2677.5	2757.8	2,300,726	2,226,465
1UC2	8/31/01	10/23/01	12/14/01	105	8.6	2888.5			
1UC3	8/31/01	10/23/01	12/14/01	105	12.7	2528.1			
1UC4	8/31/01	10/23/01	12/14/01	105	13.0	3028.0			
1UC5	8/31/01	10/23/01	12/13/01	104	14.1	2666.8			
2UC1	9/1/01	10/24/01	11/27/01	87	13.9	2735.9	3213.0	2,858,731	3,517,500
2UC2	9/1/01	10/24/01	11/27/01	87	9.7	3176.0			
2UC3	9/1/01	10/24/01	11/27/01	87	10.7	3863.8			
2UC4	9/1/01	10/24/01	11/27/01	87	14.4	3076.5			
3UC1	10/30/01	11/13/01	12/14/01	45	16.8	2098.6	2241.7	2,587,237	2,395,838
3UC2	10/30/01	11/13/01	12/16/01	47	15.4	2617.1			
3UC3	10/30/01	11/13/01	12/16/01	47	14.1	2340.0			
3UC4	10/30/01	11/13/01	12/14/01	45	16.6	1911.2			
4UC1	11/6/01	11/20/01	12/14/01	38	18.3	1572.1	2158.7	2,044,161	2,041,564
4UC2	11/6/01	11/20/01	12/16/01	40	14.9	2184.7			
4UC3	11/6/01	11/20/01	12/16/01	40	12.8	2385.8			
4UC4	11/6/01	11/20/01	12/14/01	38	15.8	2492.4			
5UC1	12/13/01	12/27/01	12/28/01	15	15.3	1798.4	2091.2	2,074,111	2,079,708
5UC2	12/13/01	12/27/01	12/28/01	15	14.7	1661.8			
5UC3	12/13/01	12/27/01	12/28/01	15	15.9	2403.0			
5UC4	12/13/01	12/27/01	12/28/01	15	15.2	2501.8			
6UC1	12/14/01	12/28/01	12/29/01	15	-	2218.8	1948.8	2,077,350	2,042,554
6UC2	12/14/01	12/28/01	12/29/01	15	15.3	1070.0			
6UC3	12/14/01	12/28/01	12/29/01	15	16.7	2215.3			
6UC4	12/14/01	12/28/01	12/29/01	15	-	2291.1			
7UC1	1/14/02	1/29/02	1/29/02	15	17.0	1603.4	1659.6	1,743,500	1,764,000
7UC2	1/14/02	1/29/02	1/29/02	15	19.0	1486.1			
7UC3	1/14/02	1/29/02	1/29/02	15	18.0	1726.8			
7UC4	1/14/02	1/29/02	1/29/02	15	16.5	1821.9			
8UC1	1/25/02	2/13/02	2/13/02	19	14.8	1509.0	1629.8	1,616,500	1,625,000
8UC2	1/25/02	2/13/02	2/13/02	19	-	1412.8			
8UC3	1/25/02	2/13/02	2/13/02	19	15.6	1820.8			
8UC4	1/25/02	2/13/02	2/13/02	19		1776.6			

Final Report Contract #BC354 RPWO #13

Table A.4 Splitting Tensile Tests of Gatorock PMT Cores

Core Sample	Cast Date	Coring Date	Test Date	Elapsed Time days	w %	q _t psi	Average q _t psi
1ST1	08/31/01	10/23/01	02/07/02	160	6.41	808.9	545.1
1ST2	08/31/01	10/23/01	02/07/02	160	5.12	494.7	
1ST3	08/31/01	10/23/01	02/07/02	160	-	331.7	
2ST1	09/01/01	10/24/01	02/07/02	159	4.61	223.2	451.6
2ST2	09/01/01	10/24/01	02/07/02	159	5.22	825.2	
2ST3	09/01/01	10/24/01	02/07/02	159	7.87	429.5	
2ST4	09/01/01	10/24/01	02/07/02	159	7.87	429.1	
2ST5	09/01/01	10/24/01	02/07/02	159	6.11	350.8	
3ST1	10/30/01	11/13/01	02/07/02	100	12.42	401.5	384.1
3ST2	10/30/01	11/13/01	02/07/02	100	13.76	390.8	
3ST3	10/30/01	11/13/01	02/07/02	100	13.86	362.8	
3ST4	10/30/01	11/13/01	02/07/02	100	13.54	293.8	
3ST5	10/30/01	11/13/01	02/07/02	100	14.35	454.8	
3ST6	10/30/01	11/13/01	02/07/02	100	12.07	401.2	
4ST1	11/06/01	11/20/01	03/12/02	126	5.75	184.6	217.4
4ST2	11/06/01	11/20/01	03/12/02	126	7.95	194.3	
4ST3	11/06/01	11/20/01	03/12/02	126	10.36	277.1	
4ST4	11/06/01	11/20/01	03/12/02	126	-	157.3	
4ST5	11/06/01	11/20/01	03/12/02	126	10.27	240.1	
4ST6	11/06/01	11/20/01	03/12/02	126	-	250.8	
5ST1	12/13/01	12/27/01	03/12/02	89	11.38	213.3	224.7
5ST2	12/13/01	12/27/01	03/12/02	89	11.36	235.2	
5ST3	12/13/01	12/27/01	03/12/02	89	8.35	204.5	
5ST4	12/13/01	12/27/01	03/12/02	89	-	289.9	
5ST5	12/13/01	12/27/01	03/12/02	89	10.76	169.8	
5ST6	12/13/01	12/27/01	03/12/02	89	-	235.6	
6ST1	12/14/01	12/28/01	03/12/02	88	14.56	199.8	146.0
6ST2	12/14/01	12/28/01	03/12/02	88	14.18	215.2	
6ST3	12/14/01	12/28/01	03/12/02	88	-	146.1	
6ST4	12/14/01	12/28/01	03/12/02	88	12.96	81.2	
6ST5	12/14/01	12/28/01	03/12/02	88	10.49	87.9	
7ST1	01/14/02	01/29/02	03/12/02	57	4.71	114.2	163.6
7ST2	01/14/02	01/29/02	03/12/02	57	4.48	209.1	
7ST3	01/14/02	01/29/02	03/12/02	57	7.46	148.3	
7ST4	01/14/02	01/29/02	03/12/02	57	6.56	166.3	
7ST5	01/14/02	01/29/02	03/12/02	57	-	179.8	
8ST1	01/25/02	02/13/02	03/19/02	53	-	145.1	191.2
8ST2	01/25/02	02/13/02	03/19/02	53	16.77	214.8	
8ST3	01/25/02	02/13/02	03/19/02	53	17.14	254.9	
8ST4	01/25/02	02/13/02	03/19/02	53	17.28	177.6	
8ST5	01/25/02	02/13/02	03/19/02	53	16.64	163.4	

Final Report Contract #BC354 RPWO #13

Table A.5 Unconfined Compressive and Modulus Tests of FDOT Cores

Site	Sample No.	Core No.	Pier	Shaft	Depth ft	L/D Ratio	q _u psi	E _i psi
SR10	2B	b3-2	6	1	55.36	1.966	499.7	954,056
SR10	2F	b3-2	6	1	57.62	2.067	688.0	902,193
SR10	2A	b3-2	6	1	54.78	1.758	859.3	
SR10	2E	b3-2	6	1	54.93	1.695	945.5	
SR10	1B	b3-1	6	1	50.66	2.249		1,532,233
SR10	1D	b3-1	6	1	52.18	2.025	455.7	1,121,218
SR10	1A	b4-1	20	1	84.48	2.051	1034.1	798,209
SR10	1B	b4-1	20	1	85.19	2.066	1174.9	1,450,737
SR10	1F	b4-1	20	1	87.39	1.797	899.9	1,507,607
SR10	2D	b4-2	20	1	91.10	2.031		
SR10	2F	b4-2	20	1	92.27	2.029	910.9	
SR10	2B	b4-2	20	1	89.93	1.562		
SR10	1B	b6-2	2	2		1.875	397.6	503,637
SR10	1A	b6-2	2	2		2.024		1,399,376
SR10	1G	b6-2	2	2		1.669	854.3	-
Hallandale	1B	hbb-r1	3	3	63.14	1.749	2396.9	-
Hallandale	3B	hbb-r3	3	1	81.01	2.104	3064.8	3,676,182
Hallandale	3C	hbb-r3	3	1	81.60	2.070	6172.7	7,538,934
Hallandale	3D	hbb-r3	3	1	82.18	2.010	4704.2	5,666,636
Hallandale	3E	hbb-r3	3	1	82.93	2.062	9339.4	914,287
Hallandale	3F	hbb-r3	3	1	83.68	2.056	10214.2	1,094,361
Hallandale	4C	hbb-r4	3	1	87.14	2.053	5625.2	9,222,758

Table A.6 Splitting Tensile Tests of FDOT Cores

Site	Sample No.	Core No.	Pier	Shaft	Depth ft	L/D Ratio	q _t psi
SR10	1c	b3-1	6	1	51.4	0.503	259.2
SR10	1e	b3-1	6	1	52.6	0.506	20.0
SR10	1f	b3-1	6	1	53.1	0.473	
SR10	2g	b3-2	6	1	58.1	0.505	130.0
SR10	2d	b3-2	6	1	56.4	0.488	72.6
SR10	2c1	b3-2	6	1	55.8	0.539	49.8
SR10	2c2	b3-2	6	1	56.0	0.510	115.6
SR10	1a1	b4-1	20	1	84.1	0.409	133.0
SR10	1c1	b4-1	20	1	85.6	0.474	89.9
SR10	1c2	b4-1	20	1	85.9	0.442	73.7
SR10	1d1	b4-1	20	1	86.2	0.535	41.7
SR10	1d2	b4-1	20	1	86.5	0.504	64.4
SR10	1g	b4-1	20	1	87.8	0.476	69.0
SR10	1e1	b4-1	20	1	86.8	0.474	78.6
SR10	2a1	b4-2	20	1	89.3	0.441	79.6
SR10	2a2	b4-2	20	1	89.6	0.504	66.9
SR10	2c1	b4-2	20	1	90.4	0.506	49.3
SR10	2c2	b4-2	20	1	90.6	0.505	15.7
SR10	2e1	b4-2	20	1	91.5	0.537	81.4
SR10	2e2	b4-2	20	1	91.7	0.536	76.2
SR10	2g1	b4-2	20	1	92.9	0.503	81.0
SR10	2g2	b4-2	20	1	93.1	0.521	63.3
SR10	1d1	b6-2	2	2		0.509	20.1
SR10	1d2	b6-2	2	2		0.525	15.9
SR10	1f1	b6-2	2	2		0.540	52.0
SR10	1f2	b6-2	2	2		0.476	40.9
SR10	1f3	b6-2	2	2		0.524	48.5
SR10	1a1	b6-2	2	2		0.525	40.5
SR10	1a2	b6-2	2	2		0.477	37.9
SR10	1c	b6-2	2	2		0.605	14.6
SR10	1e1	b6-2	2	2		0.477	50.9
SR10	1e2	b6-2	2	2		0.443	103.8

Table A.6 (cont.) Splitting Tensile Tests of FDOT Cores

Site	Sample No.	Core No.	Pier	Shaft	Depth ft	L/D Ratio	q _t psi
Hallandale	1a1	hbb-r1	3	3	62.4	0.477	805.7
Hallandale	1a2	hbb-r1	3	3	62.7	0.538	616.2
Hallandale	1c	hbb-r1	3	3	63.6	0.417	93.9
Hallandale	1d	hbb-r1	3	3	64.7	0.510	233.1
Hallandale	1e1	hbb-r1	3	3	65.1	0.637	114.4
Hallandale	1e2	hbb-r1	3	3	65.4	0.527	82.1
Hallandale	1f1	hbb-r1	3	3	65.7	0.447	448.5
Hallandale	1f2	hbb-r1	3	3	66.0	0.415	132.9
Hallandale	2a1	hbb-r2	3	3	67.4	0.474	662.1
Hallandale	2a2	hbb-r2	3	3	67.6	0.381	250.6
Hallandale	2a3	hbb-r2	3	3	67.9	0.475	261.3
Hallandale	2b	hbb-r2	3	3	68.9	0.576	61.2
Hallandale	2c1	hbb-r2	3	3	69.0	0.418	416.5
Hallandale	2c2	hbb-r2	3	3	69.2	0.449	197.2
Hallandale	2c3	hbb-r2	3	3	69.5	0.485	42.4
Hallandale	3a	hbb-r3	3	1	80.6	0.446	275.1
Hallandale	3g	hbb-r3	3	1	84.2	0.477	493.0
Hallandale	4a1	hbb-r4	3	1	85.8	0.558	661.8
Hallandale	4a2	hbb-r4	3	1	85.9	0.479	870.7
Hallandale	4a3	hbb-r4	3	1	86.2	0.447	737.7
Hallandale	4b	hbb-r4	3	1	86.6	0.479	722.4

Final Report Contract #BC354 RPWO #13

Table A.7 Unconfined Compressive and Modulus Tests of SR20 PMT Cores

Pier	Shaft	Test Hole	Core	Sample	Top Elev. ft	Rec. %	RQD %	L/D Ratio	q _u psi	E psi
62	5	1	2	A	-30.97	45.0	13.3	1.770	87.3	21,822
62	5	1	2	B	-30.97	45.0	13.3	1.917	91.7	14,145
62	5	1	3	A	-35.86	61.7	29.2	2.120	87.1	23,047
62	5	1	5	A	-45.89	60.0	35.0	1.991	1104.5	448,380
62	5	1	5	B	-45.89	60.0	35.0	1.973	2905.0	1,231,851
62	5	1	5	C	-45.89	60.0	35.0	1.967	2573.7	1,462,966
62	5	1	5	D	-45.89	60.0	35.0	1.986	3278.3	1,433,409
62	5	1	6	A	-50.86	41.7	17.5	1.997	1422.2	687,769
62	5	1	6	B	-50.86	41.7	17.5	1.971	1410.9	684,281
62	5	2	4	A	-44.30	50.0	15.0	1.996	2447.4	1,425,235
62	5	2	4	B	-44.30	50.0	15.0	1.994	1661.7	1,204,239
62	5	2	5	A	-49.50	45.8	9.2	1.783	1702.1	1,204,536
62	7	3	4	A	-38.90	35.0	9.2	2.007	374.4	466,372
62	7	3	7	A	-53.82	73.3	22.5	2.015	65.3	57,178
62	7	4	1	A	-28.65	30.0	8.3	2.194	14.4	3,875
62	7	4	4	A	-43.75	48.8	20.8	2.079	127.8	86,069
62	7	4	4	B	-43.75	48.8	20.8	2.110	86.8	62,193
62	7	4	4	C	-43.75	48.8	20.8	1.658	112.2	51,265
62	7	4	6	A	-54.02	65.8	53.6	2.006	316.9	30,992
62	7	4	6	B	-54.02	65.8	53.6	1.747	101.9	64,455
62	7	4	6	C	-54.02	65.8	53.6	1.993	182.7	130,179
62	7	4	6	D	-54.02	65.8	53.6	2.014	110.8	84,411
62	7	4	6	E	-54.02	65.8	53.6	2.069	157.1	128,456

Table A.8 Splitting Tensile Tests of SR20 PMT Cores

Pier	Shaft	Test Hole	Core	Sample	Top Elev. ft	Rec. %	RQD %	L/D Ratio	q _t psi
62	5	1	3	A	-35.86	61.7	29.2	0.609	12.5
62	5	1	3	B	-35.86	61.7	29.2	0.595	147.9
62	5	1	3	C	-35.86	61.7	29.2	0.641	4.4
62	5	1	5	A	-45.86	60.0	35.0	0.644	414.8
62	5	1	5	B	-45.86	60.0	35.0	0.575	860.4
62	5	1	5	C	-45.86	60.0	35.0	0.676	593.9
62	5	1	6	A	-50.86	41.7	17.5	0.682	477.6
62	5	1	6	B	-50.86	41.7	17.5	0.684	583.0
62	5	1	6	C	-50.86	41.7	17.5	0.747	417.8
62	5	1	6	D	-50.86	41.7	17.5	0.563	274.2
62	5	1	6	E	-50.86	41.7	17.5	0.559	19.8
62	5	1	6	F	-50.86	41.7	17.5	0.619	24.4
62	5	2	2	A	-34.26	30.0	0.0	0.605	129.0
62	5	2	4	B	-44.30	50.0	15.0	0.562	589.2
62	5	2	4	C	-44.30	50.0	15.0	0.521	460.1
62	5	2	4	D	-44.30	50.0	15.0	0.624	775.0
62	5	2	4	E	-44.30	50.0	15.0	0.567	276.4
62	5	2	5	A	-49.50	45.8	9.2	0.546	413.0
62	5	2	5	B	-49.50	45.8	9.2	0.627	862.4
62	5	2	5	C	-49.50	45.8	9.2	0.594	1040.3
62	5	2	5	D	-49.50	45.8	9.2	0.506	296.6
62	5	2	5	E	-49.50	45.8	9.2	0.592	559.7
62	5	2	5	F	-49.50	45.8	9.2	0.507	181.8

Final Report Contract #BC354 RPWO #13

Table A.8 (cont.) Splitting Tensile Tests of SR20 PMT Cores

Pier	Shaft	Test Hole	Core	Sample	Top Elev. ft	Rec. %	RQD %	L/D Ratio	q _t psi
62	7	3	3	A	-33.82	12.5	0.0	0.568	117.8
62	7	3	4	A	-38.90	35.0	9.2	0.621	8.1
62	7	3	5	A	-43.82	18.3	0.0	0.605	8.9
62	7	3	6	A	-48.90	18.3	0.0	0.651	14.2
62	7	3	7	A	-53.82	73.3	22.5	0.605	1313.3
62	7	3	7	B	-53.82	73.3	22.5	0.681	464.6
62	7	3	7	C	-53.82	73.3	22.5	0.697	432.9
62	7	3	7	D	-53.82	73.3	22.5	0.697	43.3
62	7	3	7	E	-53.82	73.3	22.5	0.691	8.7
62	7	3	7	F	-53.82	73.3	22.5	0.727	8.2
62	7	4	1	A	-28.65	30.0	8.3	0.717	79.8
62	7	4	3	A	-38.65	27.5	0.0	0.665	7.5
62	7	4	4	A	-43.75	48.8	20.8	0.764	4.4
62	7	4	4	B	-43.75	48.8	20.8	0.678	7.2
62	7	4	5	A	-49.00	26.7	6.7	0.628	10.4
62	7	4	5	C	-49.00	26.7	6.7	0.559	10.8
62	7	4	5	D	-49.00	26.7	6.7	0.576	166.5
62	7	4	6	A	-54.02	65.8	53.6	0.669	14.8
62	7	4	6	B	-54.02	65.8	53.6	0.640	18.5
62	7	4	6	C	-54.02	65.8	53.6	0.630	21.6
62	7	4	6	D	-54.02	65.8	53.6	0.598	12.0
62	7	4	6	E	-54.02	65.8	53.6	0.584	8.5
62	7	4	6	F	-54.02	65.8	53.6	0.609	12.0
62	7	4	6	G	-54.02	65.8	53.6	0.640	12.7

Final Report Contract #BC354 RPWO #13

Table A.9 Summary Comparison of Unconfined Compressive and Tensile Strength

Site	Pier No.	Shaft/ Core No.	Sample No.	Station	Boring No.	Surf. Elev. ft	Core Elev. ft	qu psi	qt psi	Rec. %	RQD %	qu Avg. psi	qt Avg. psi
SR20	43	1	a	121+00	TH-43B	46.30	-39.00	1148.6	55.6	90	78	1148.6	55.6
SR20	44	1	a	122+11	TH-44A	44.40	-20.00	38.9	11.1	95	58	38.9	11.1
SR20			b			44.40	-28.00	877.8	237.5	83	56	877.8	237.5
SR20	45	1	a	123+21	TH-45B	45.20	-22.00	70.8	13.9	95	72	70.8	13.9
SR20			b			45.20	-26.00	47.2	15.3	95	72	47.2	15.3
SR20	46	1	a	124+32	TH-46A	45.30	-25.00	80.6	15.3	60	30	80.6	15.3
SR20			b			45.30	-32.00	86.1	11.1	80	40	86.1	11.1
SR20	46	2	a	124+32	TH-46B	44.80	-24.00	87.5	8.3	100	75	87.5	8.3
SR20			b			44.80	-26.00	186.8	25.0	100	75	186.8	25.0
SR20			b			45.00	-21.00	44.4	9.7	100	75	44.4	9.7
SR20			c			45.00	-27.00	62.5	18.1	80	26	62.5	18.1
SR20			b			45.50	-25.00	158.3	26.4	100	67	158.3	26.4
SR20	48	1	a	126+52	TH-48A	44.90	-16.00	50.0	18.1	100	60	50.0	18.1
SR20			b			44.90	-24.00	72.2	11.8	80	41	72.2	11.8
SR20	48	2	a	126+52	TH-48B	45.90	-20.00	55.6	29.2	100	57	55.6	29.2
SR20			b			45.90	-25.00	1169.4	73.6	100	70	1169.4	73.6
SR20	49	1	a	127+63	TH-49A	45.20	-19.00	40.3	12.5	85	45	40.3	12.5
SR20			b			45.20	-23.00	61.1	11.1	95	45	61.1	11.1
SR20			c			45.20	-33.00	119.4	19.4	100	85	119.4	19.4
SR20			d			45.20	-35.00	2898.6	56.9	35	25	2898.6	56.9
SR20	49	2	a	127+63	TH-49B	45.50	-15.00	56.9	9.7	60	21	56.9	9.7
SR20			b			45.50	-29.00	505.6	51.4	70	45	505.6	51.4
SR20			b			45.30	-27.00	358.3	94.4	95	70	358.3	94.4
SR20	50	2	a	128+73	TH-50B	45.60	-24.00	16.7	25.0	100	67	16.7	25.0
SR20			b			45.60	-25.00	223.6	30.6	100	67	223.6	30.6
SR20	51	1	a	129+84	TH-51A	46.10	-24.00	118.1	11.1	90	40	118.1	11.1
SR20	51	2	a	129+84	TH-51B	46.30	-24.00	81.9	8.3	100	60	81.9	8.3
SR20			b			46.30	-33.00	111.1	8.3	90	50	111.1	8.3
SR20	53	1	a	132+05	TH-53A	46.40	-24.00	81.9	13.9	80	50	81.9	13.9
SR20			b			46.40	-29.00	102.8	8.3	95	73	102.8	8.3
SR20			b			44.10	-28.00	212.5	83.3	100	70	212.5	83.3
SR20	54	2	a	133+15	TH-54B	44.70	-20.00	50.0	15.3	100	50	50.0	15.3
SR20			b			44.70	-24.00	94.4	13.9	63	50	94.4	13.9
SR20	55	2	a	134+26	TH-55B	45.10	-21.00	83.3	16.7	100	66	83.3	16.7
SR20			b			45.10	-43.00	1425.0	144.4	80	80	1425.0	144.4
SR20	56	1	a	135+36	TH-56A	45.80	-24.00	59.7	12.5	100	50	59.7	12.5
SR20			b			46.30	-22.00	76.4	9.7	100	45	76.4	9.7
SR20			c			46.30	-33.00	1238.9	12.5	100	26	1238.9	12.5
SR20	57	1	a		P57-1	47.40	-33.00	49.3	13.9	30	20	49.3	13.9
SR20			b			47.40	-39.00	919.4	304.2	30	22	919.4	304.2
SR20	57	2	a		P57-2	47.60	-26.00	43.1	4.9	62	37	43.1	4.9
SR20	57	4	a		P57-4	47.50	-27.00	54.9	20.1	80	42	54.9	20.1
SR20			c			47.50	-34.00	134.0	16.7	33	22	134.0	16.7
SR20	58	2	a		P58-2	37.00	-33.00	27.8	2.8	63	47	27.8	2.8

Final Report Contract #BC354 RPWO #13

Table A.9 Summary Comparison of Unconfined Compressive and Tensile Strength

Site	Pier No.	Shaft/ Core No.	Sample No.	Station	Boring No.	Surf. Elev. ft	Core Elev. ft	qu psi	qt psi	Rec. %	RQD %	qu Avg. psi	qt Avg. psi
SR20	58	3	a		P58-3	41.00	-26.00	43.1	8.3	73	68	43.1	8.3
SR20	58	4	a		P58-4	42.00	-44.00	514.6	104.2	37	25	514.6	104.2
SR20	59	1	a		P59-1	40.00	-27.00	13.9	2.8	65	37	13.9	2.8
SR20	59	3	a		P59-3	42.00	-30.00	44.4	3.5	85	67	44.4	3.5
SR20	59	4	a		P59-4	41.00	-27.00	43.8	4.2	50	45	43.8	4.2
SR20	60	1	a		P60-1	45.00	-39.00	235.4	79.9	35	8	235.4	79.9
SR20			d			45.00	-55.00	86.8	13.2	100	83	86.8	13.2
SR20	60	2	a		P60-3	39.80	-55.00	2186.1	220.8	50	0	2186.1	220.8
SR20	61	1	a	144+86	TH-61A	48.70	-28.00	79.2	12.5	100	86	79.2	12.5
SR20			b			48.70	-29.00	62.5	11.1	100	86	62.5	11.1
SR20			c			48.70	-38.00	80.6	16.7	90	63	80.6	16.7
SR20	61	2	a	144+86	TH-61B	49.50	-26.00	73.6	11.1	100	59	73.6	11.1
SR20			b			49.50	-31.00	48.6	5.6	100	88	48.6	5.6
SR20	62	1	a	145+96	TH-62A	47.50	-27.00	47.2	5.6	90	50	47.2	5.6
SR20			b			47.50	-37.00	138.9	6.9	70	35	138.9	6.9
SR20	62	2	a	145+96	TH-62B	47.30	-27.00	68.1	13.9	68	57	68.1	13.9
SR20	63	1	a	147+86	TH-63A	47.00	-34.00	177.8	4.2	60	25	177.8	4.2
SR20	63	2	a	147+86	TH-63B	47.20	-34.00	41.7	15.3	75	45	41.7	15.3
SR20	64	1	a	149+15	TH-64A	48.20	-26.00	79.2	11.1	66	41	79.2	11.1
SR20			c			48.20	-38.00	83.3	2.8	45	33	83.3	2.8
SR20	65	1	a	149+25	TH-65A	47.80	-27.00	36.1	4.2	82	50	36.1	4.2
SR20	65	2	a	149+25	TH-65B	48.30	-42.00	81.9	9.7	73	50	81.9	9.7
SR20	66	1	a	150+34	TH-66A	47.10	-28.00	72.2	11.1	100	56	72.2	11.1
SR20	66	2	a	150+34	TH-66B	47.60	-28.00	62.5	4.2	100	75	62.5	4.2
SR20			b			47.60	-35.00	161.1	27.8	83	62	161.1	27.8
SR20	67	2	a	151+44	TH-67B	47.30	-27.00	90.3	15.3	62	35	90.3	15.3
SR20	69	1	a	153+62	TH-69A	46.60	-29.00	52.8	11.1	82	66	52.8	11.1
SR20			b			46.60	-34.00	87.5	30.6	58	26	87.5	30.6
SR20	69	2	a	153+62	TH-69B	46.50	-31.00	54.2	5.6	13	0	54.2	5.6
SR20	70	1	a	154+74	TH-70A	46.50	-30.00	16.7	5.6	100	69	16.7	5.6
SR20			b			46.10	-37.00	113.9	44.4	57	13	113.9	44.4
SR20			b			46.20	-42.00	93.1	11.1	100	61	93.1	11.1
SR20	71	2	a	155+63	TH-71B	45.70	-33.00	70.8	16.7	60	32	70.8	16.7
SR20	72	2	a	156+93	TH-72B	45.80	-30.00	76.4	8.3	80	67	76.4	8.3
SR20	73	1	a	157+91	TH-73A	45.50	-34.00	47.2	2.8	90	42	47.2	2.8
SR20	59	8 / 2-2	1t, 3t, 4u				-74.00	839.7	162.8			839.7	162.8
SR20	60	3 / 2A	2t, 4u				-56.00	365.6	306.4			365.6	306.4
SR20	73	2 / 1	1u, 2t				-33.00	128.6	35.1			128.6	35.1
SR20	69		1				-26.00					352.1	19.4
SR20	69		1				-30.00					336.6	22.9
SR20	69		2				-31.80					348.4	22.2
SR20	69		3				-32.50					322.7	22.2
SR20	69		1				-35.00					195.7	82.5
SR20	69		2				-38.00					143.7	13.2
SR20	69		1				-40.00					164.5	15.3

Final Report Contract #BC354 RPWO #13

Table A.9 Summary Comparison of Unconfined Compressive and Tensile Strength

Site	Pier No.	Shaft/ Core No.	Sample No.	Station	Boring No.	Surf. Elev. ft	Core Elev. ft	qu psi	qt psi	Rec. %	RQD %	qu Avg. psi	qt Avg. psi
SR20	69		2				-41.50					164.5	12.5
SR20	69		1				-45.00					199.9	30.5
SR20	69		2				-46.30					200.6	30.5
SR20	69		3				-48.00					200.6	10.4
SR20	69		1				-50.00					187.4	13.2
SR20	69		2				-52.00					187.4	50.0
SR20	69		3				-52.80					179.8	50.0
SR20	62		1				-27.30					309.5	18.0
SR20	62		2				-28.50					309.5	20.1
SR20	62		1				-31.00					157.5	33.3
SR20	62		2				-33.00					157.5	13.2
SR20	62		1				-41.00					202.6	17.4
SR20	62		1				-46.50					560.8	350.5
Broadway	TH4	4 / 3		103+64				822.4	136.8	40	27	822.4	136.8
Broadway	TH5	5 / 3-4		108+84				3195.4	35.2	68	15	3195.4	187.7
Broadway	TH5	5 / 4-5		108+84					340.1	33	8		
Broadway	TH6	6 / 3		112+54				1547.5	235.8	75	37	1547.5	208.8
Broadway	TH6	6 / 3		112+54					181.8	75	37		
Broadway	TH7	7 / 1		104+90				4117.3	558.8	47	27	4117.3	558.8
Broadway	FS2E	1 / 1		104+29				367.4	291.9	78	53	367.4	291.9
Broadway	FS2E	2 / 1		104+29				6263.7	291.9	78	53	6263.7	230.1
Broadway	FS2E	2 / 1		104+29					168.3	78	53		
Broadway	FS2W	2 / 1		104+29				3572.6	282.0	72	40	3572.6	282.0
Broadway	FS3E	2 / 1		104+29				4125.4	298.6	72	50	4125.4	298.6
Broadway	FS3W	1 / 1		104+41				5132.7	115.2	57	37	5132.7	115.2
Broadway	FS3W	2 / 1		104+41				3730.0	146.6	88	70	3730.0	146.6
Broadway	FS3W	2A / 1		104+41				4145.5	243.4	50	38	5348.3	243.4
Broadway	FS3W	2A / 1		104+41				6551.0		50	38		
Broadway	FS4E	1 / 1		104+53				2886.0	176.8	58	22	2886.0	176.8
Broadway	FS4E	2 / 1		104+53				4480.4	513.1	37	17	4480.4	513.1
Broadway	FS4W	1 / 1		104+53				1136.2	205.0	40	18	1136.2	205.0
Broadway	FS4W	2 / 1		104+53				4626.4	323.1	40	35	4626.4	323.1
Broadway	FS5E	2 / 1		104+65				534.8	134.9	83	58	534.8	134.9
Broadway	FS5W	1 / 1		104+65				2760.9	215.0	75	47	2760.9	155.9
Broadway	FS5W	1 / 1		104+65					96.8	75	47		
Broadway	FS5W	2 / 1		104+65				965.8	33.9	72	52	746.9	139.3
Broadway	FS5W	2 / 1		104+65				528.0	211.8	72	52		
Broadway	FS5W	2 / 1		104+65					172.2	72	52		
Broadway	FS6E	1 / 1		104+65				1231.9	93.3	63	35	1231.9	93.3
Broadway	FS6E	2 / 1		104+77				698.8	164.7	62	32	698.8	164.7
Broadway	FS6W	1 / 1		104+77				2410.9	54.8	68	33	2410.9	129.1
Broadway	FS6W	1 / 1		104+77					203.3	68	33		
Broadway	FS7E	2 / 1		104+90				1064.7	174.8	72	55	819.0	97.3
Broadway	FS7E	2 / 1		104+90				573.2	19.7	72	55		
Broadway	FS7W	1 / 1		104+90				1666.2	181.3	57	53	1666.2	170.8

Final Report Contract #BC354 RPWO #13

Table A.9 Summary Comparison of Unconfined Compressive and Tensile Strength

Site	Pier No.	Shaft/ Core No.	Sample No.	Station	Boring No.	Surf. Elev. ft	Core Elev. ft	qu psi	qt psi	Rec. %	RQD %	qu Avg. psi	qt Avg. psi
Broadway	FS7W	1 / 1		104+90					160.3	57	53		
Broadway	FS7W	2 / 1		104+90				3705.7	203.4	100	70	3705.7	351.3
Broadway	FS7W	2 / 1		104+90					499.2	100	70		
Broadway	FS8E	2 / 1		104+90				1548.3	169.6	100	70	1548.3	169.3
Broadway	FS8E	2 / 1		104+90					169.0	100	70		
Broadway	2	2 / 1		105+44				4622.7	267.2	53	25	4622.7	223.3
Broadway	2	2 / 1		105+44					179.4	53	25		
Broadway	2	4 / 1		105+44				8184.9	336.4	53	35	8184.9	336.4
Broadway	2	5 / 1		105+44				7426.3	814.1	53	32	7426.3	814.1
Broadway	2	5 / 1		105+44				7426.3	261.8	53	32	7426.3	261.8
Broadway	3	1 / 1		105+44				1556.8	145.6	80	57	1208.3	190.5
Broadway	3	1 / 1		105+44				859.7	235.3	80	57		
Broadway	3	2 / 1		105+44				984.9	140.3	67	23	984.9	140.3
Broadway	4	1 / 1		106+54				790.9	342.6	72	33	790.9	230.2
Broadway	4	1 / 1		106+54					117.7	72	33		
Broadway	4	2 / 1		106+54				2568.7	326.8	57	28	2568.7	326.8
Broadway	4	3 / 1		106+54				6062.3	307.4	72	63	6062.3	314.5
Broadway	4	3 / 1		106+54					496.8	72	63		
Broadway	4	3 / 1		106+54					139.2	72	63		
Broadway	5	4 / 1		107+24				731.8	4.9	55	37	731.8	224.7
Broadway	5	4 / 1		107+24					444.4	55	37		
Broadway	5	7 / 1		107+24				2259.4	6.9	42	33	2259.4	6.9
Broadway	6	1 / 1		108+04				4234.8	220.6	62	40	4234.8	220.6
Broadway	6	2 / 1		108+04				804.5	286.6	68	38	804.5	231.3
Broadway	6	2 / 1		108+04					175.9	68	38		
Broadway	6	4 / 1		108+04				4458.9	27.7	67	30	4458.9	27.7
Broadway	6	5 / 1		108+04				680.5	30.9	32	23	680.5	59.5
Broadway	6	5 / 1		108+04					88.1	32	23		
Broadway	6	7 / 1		108+04				1991.8	128.6	68	45	1991.8	249.2
Broadway	6	7 / 1		108+04					369.8	68	45		
Broadway	7	2 / 1		108+84				3152.2	274.5	43	25	3152.2	274.5
Broadway	7	3 / 1		108+84				2332.5	36.4	73	38	2332.5	131.3
Broadway	7	3 / 1		108+84					226.1	73	38		
Broadway	7	3 / 2		108+84				1208.2	237.7	78	60	760.3	237.7
Broadway	7	3 / 2		108+84				312.3		78	60		
Broadway	7	5 / 1		108+84				3550.9	82.8	47	23	3550.9	82.8
Broadway	7	8 / 1		108+84				2460.3	370.6	63	43	2460.3	188.6
Broadway	7	8 / 1		108+84					6.6	63	43		
Broadway	8	TS / 1		109+64				2295.9	476.5	63	63	2364.8	408.5
Broadway	8	TS / 1		109+64				2433.7	491.8	63	63		
Broadway	8	TS / 1		109+64					257.1	63	63		
Broadway	8	6 / 1		109+64				7458.5	194.2	52	33	7458.5	161.8
Broadway	8	6 / 1		109+64					129.3	52	33		
Broadway	9	1 / 1		110+44				2963.9	435.6	38	27	2963.9	435.6
Broadway	9	7 / 1		110+44				4099.9	122.2	45	22	4099.9	122.2

Final Report Contract #BC354 RPWO #13

Table A.9 Summary Comparison of Unconfined Compressive and Tensile Strength

Site	Pier No.	Shaft/ Core No.	Sample No.	Station	Boring No.	Surf. Elev. ft	Core Elev. ft	qu psi	qt psi	Rec. %	RQD %	qu Avg. psi	qt Avg. psi
Broadway	10	1 / 1		111+24				1353.4	308.8	70	70	1353.4	252.5
Broadway	10	1 / 1		111+24					196.2	70	70		
Broadway	10	2 / 1		111+24				1356.5	443.0	60	47	1356.5	238.0
Broadway	10	2 / 1		111+24					67.3	60	47		
Broadway	10	2 / 1		111+24					203.8	60	47		
Broadway	10	3 / 1		111+24				3881.9	317.4	70	48	3881.9	317.4
Broadway	10	4 / 1		111+24				2311.5	229.7	68	52	2311.5	192.6
Broadway	10	4 / 1		111+24					154.0	68	52		
Broadway	10	4 / 1		111+24				2311.5	194.2	68	52		
Broadway	10	5 / 1		111+24				1456.1	118.1	73	63	1456.1	116.6
Broadway	10	5 / 1		111+24					115.0	73	63		
Broadway	10	8 / 1		111+24				1775.5	350.3	63	37	1775.5	350.3
Broadway	12	6 / 1		112+54				547.3	134.9	70	53	547.3	180.1
Broadway	12	6 / 1		112+54					225.2	70	53		
Broadway	EB1	2 / 1		113+34				1124.0	338.7	47	38	1124.0	190.9
Broadway	EB1	2 / 1		113+34					41.3	47	38		
Broadway	EB1	2 / 1		113+34					192.7	47	38		
Broadway	EB1			113+34				1632.2	260.9	62	55	1077.9	345.1
Broadway	EB1			113+34				523.6	429.2	62	55		
Broadway				5+19	TB-1			422.9	640.9	68	44	422.9	640.9
Broadway				5+19	TB-1			124.0	79.0	50	50	124.0	48.0
Broadway				5+19	TB-1				17.0	50	50		
Broadway				5+19	TB-1			161.0	17.0	50	50	161.0	99.0
Broadway				5+19	TB-1				181.0				
Broadway				5+19	TB-1			6859.7	181.0	33	26	1815.9	158.5
Broadway				5+19	TB-1				136.0				
Broadway				5+19	TB-1			1815.9	136.0	38	15	1815.9	136.0
Broadway				6+74	TB-2			7658.6	687.9	100	70	7658.6	687.9
Broadway				6+74	TB-2			1024.0	222.1	100	70	1024.0	222.1
Broadway				6+74	TB-2			7658.6	429.0	60	37	998.4	429.0
Broadway				6+74	TB-2			1903.9	429.0	60	37		
Broadway				6+74	TB-2			93.0	430.9	68	34	1792.9	408.9
Broadway				6+74	TB-2			93.0	387.0	68	34		
Broadway				6+74	TB-2			3492.8	387.0	68	34		
Broadway				12+22	TB-6			138.9	39.0	38	25	138.9	35.5
Broadway				12+22	TB-6			138.9	32.1	38	25		
Broadway				12+22	TB-6			493.0	87.0	46	17	493.0	87.0
Broadway				12+22	TB-6			646.0	355.1	66	51	646.0	355.1
Broadway				12+22	TB-6			165.1	117.0	58	49	165.1	117.0
Broadway				10+50	TB-7			105.0	13.1	47	37	122.0	13.1
Broadway				10+50	TB-7			138.9	13.1	47	37		
Broadway				10+50	TB-7			92.0	32.1	73	47	62.3	32.1
Broadway				10+50	TB-7			32.6	32.1	73	47		
Broadway				10+50	TB-7			1034.0	364.9	88	72	1034.0	339.0
Broadway				10+50	TB-7			1034.0	313.0	88	72		

Final Report Contract #BC354 RPWO #13

Table A.9 Summary Comparison of Unconfined Compressive and Tensile Strength

Site	Pier No.	Shaft/ Core No.	Sample No.	Station	Boring No.	Surf. Elev. ft	Core Elev. ft	qu psi	qt psi	Rec. %	RQD %	qu Avg. psi	qt Avg. psi
Broadway				10+50	TB-7			446.0	180.0	49	41	285.0	109.0
Broadway				10+50	TB-7			446.0	136.0	49	41		
Broadway				10+50	TB-7			124.0	136.0	49	41		
Broadway				10+50	TB-7			124.0	11.0	49	41		
Broadway				4+16	TB-8			1848.8	154.3	74	66	1848.8	154.3
Broadway				4+16	TB-8			517.9	63.4	67	43	517.9	63.4
Broadway				4+16	TB-8			1109.8	116.8	55	47	3459.8	458.5
Broadway				4+16	TB-8			5809.8	116.8	55	47		
Broadway				4+16	TB-8			5809.8	800.2	55	47		
Broadway				4+41	TB-9			1156.7	115.9	19	15	1156.7	115.9
Broadway				4+41	TB-9			472.0	148.7	59	47	472.0	148.7
Broadway				4+41	TB-9			628.9	491.7	53	41	628.9	491.7
Broadway				4+41	TB-9			551.9	298.6	53	41	551.9	298.6
Broadway				4+65	TB-10			4846.4	825.0	43	25	4846.4	825.0
Broadway				5+14	TB-12			3831.6	572.0	33	12	3831.6	572.0
Broadway				5+14	TB-12			657.9	258.7	56	49	657.9	258.7
Broadway				5+14	TB-12			2845.6	394.1	34	18	2845.6	394.1
Broadway				5+44	TB-13			407.0	57.0	64	48	407.0	57.0
Broadway				5+44	TB-13			518.9	432.2	44	10	518.9	432.2
Broadway				5+94	TB-14			831.9	169.7	68	56	831.9	169.7
Broadway				5+94	TB-14			469.9	77.3	73	53	469.9	77.3
Broadway				5+94	TB-14			697.9	337.9	68	30	666.4	479.9
Broadway				5+94	TB-14			635.0	621.9	68	30		
Broadway				6+54	TB-15			781.9	124.2	40	13	781.9	124.2
Broadway				6+54	TB-15			3583.6	54.8	62	17	3583.6	54.8
Broadway				7+24	TB-16			275.0	35.7	55	51	275.0	35.7
Broadway				8+04	TB-17			11231.7	946.5	61	58	11231.7	946.5
Broadway				8+04	TB-17			646.9	186.5	32	7	899.4	186.5
Broadway				8+04	TB-17			1151.9	186.5	18	7		
Broadway				8+84	TB-18			320.0	56.7	39	15	320.0	56.7
Broadway				9+64	TB-19			914.9	1316.9	69	30	2844.7	1316.9
Broadway				9+64	TB-19			4774.5	1316.9	69	30		
Broadway				9+64	TB-19			686.9	112.1	27	17	686.9	112.1
Broadway				9+64	TB-19			1059.9	102.1	25	8	1059.9	102.1
Broadway				10+44	TB-20			1405.9	83.4	38	17	1405.9	732.5
Broadway				10+44	TB-20			1405.9	1381.6	38	17		
Broadway				10+44	TB-20			1256.9	395.7	55	28	1256.9	395.7
Broadway				11+24	TB-21			551.9	351.7	79	54	551.9	351.7
Broadway				11+24	TB-21			843.0	237.1	77	37	1706.4	237.1
Broadway				11+24	TB-21			2569.8	237.1	77	37		
Broadway				11+94	TB-22			1237.9	352.7	43	7	1237.9	426.0
Broadway				11+94	TB-22			1237.9	499.4	58	23		
Broadway				11+94	TB-22			2980.7	245.4	58	23	2980.7	245.4
Broadway				12+54	TB-23			444.0	774.1	65	53	444.0	774.1
Broadway				12+54	TB-23			1428.9	768.8	51	32	1428.9	768.8

Final Report Contract #BC354 RPWO #13

Table A.9 Summary Comparison of Unconfined Compressive and Tensile Strength

Site	Pier No.	Shaft/ Core No.	Sample No.	Station	Boring No.	Surf. Elev. ft	Core Elev. ft	qu psi	qt psi	Rec. %	RQD %	qu Avg. psi	qt Avg. psi
Broadway				13+34	TB-25			923.9	140.7	63	51	923.9	140.7
SR10	3	1c	1d					146.9	259.2			146.9	139.6
SR10	3	1e	1d						20.0				
SR10	3	2c1	2a					279.8	49.8			241.9	88.9
SR10	3	2c2	2a						115.6				
SR10	3	2g	2f					221.1	130.0				
SR10	3	2d	2e					305.2	72.6				
SR10	3	2c1	2b					161.4	49.8				
SR10	3	2c2	2b						115.6				
SR10	4	1a1	1a					332.3	133.0			332.9	78.6
SR10	4	1c1	1b					377.5	89.9				
SR10	4	1c2	1b						73.7				
SR10	4	1d1	1b						41.7				
SR10	4	1d2	1b						64.4				
SR10	4	1g	1f					289.0	69.0				
SR10	4	1e1	1f						78.6				
SR10	4	2a1	1f					289.0	79.6			290.4	64.2
SR10	4	2a2	1f						66.9				
SR10	4	2c1	2f					291.9	49.3				
SR10	4	2c2	2f						15.7				
SR10	4	2e1	2f						81.4				
SR10	4	2e2	2f						76.2				
SR10	4	2g1	2f						81.0				
SR10	4	2g2	2f						63.3				
SR10	6	1a1	1b					128.7	42.5			202.6	43.4
SR10	6	1a2	1b						36.2				
SR10	6	1d1	1b						20.4				
SR10	6	1d2	1b						16.7				
SR10	6	1c	1b						17.7				
SR10	6	1f1	1g					276.6	56.1				
SR10	6	1e1	1g						50.9				
SR10	6	1e2	1g						103.8				
SR10	6	1f2	1g						39.0				
SR10	6	1f3	1g						50.8				
SR10	b-1	1	2	118+25			1.70	671.5	26.6	75	53	671.5	120.8
SR10	b-1	1	2	118+25			1.70		31.4	75	53		
SR10	b-1	1	2	118+25			1.70		200.8	75	53		
SR10	b-1	1	2	118+25			1.70		181.0	75	53		
SR10	b-1	1	2	118+25			1.70		164.4	75	53		
SR10	b-1	1	6	118+25			-29.30	361.9	148.8	97	67	361.9	112.4
SR10	b-1	1	6	118+25			-29.30		159.9	97	67		
SR10	b-1	1	6	118+25			-29.30		68.7	97	67		
SR10	b-1	1	6	118+25			-29.30		72.1	97	67		
SR10	b-1	1	8	118+25			-42.30	187.7	64.9	72	28	187.7	64.9
SR10	b-1	1	9	118+25			-48.80	315.5	210.5	92	28	315.5	168.2

Final Report Contract #BC354 RPWO #13

Table A.9 Summary Comparison of Unconfined Compressive and Tensile Strength

Site	Pier No.	Shaft/ Core No.	Sample No.	Station	Boring No.	Surf. Elev. ft	Core Elev. ft	qu psi	qt psi	Rec. %	RQD %	qu Avg. psi	qt Avg. psi
SR10	b-1	1	9	118+25			-53.80		125.9	92	28		
SR10	b-1	1	10	118+25			-54.80	1201.8	228.2	87	33	1201.8	151.6
SR10	b-1	1	10	118+25			-54.80		74.9	87	33		
SR10	b-6	6	1	120+15			23.10	387.4	110.9	60	27	285.8	110.9
SR10	b-6	6	1	120+15			18.10	184.1		60	27		
SR10	b-6	6	2	120+15			11.00	246.4	17.4	90	43	246.4	26.6
SR10	b-6	6	2	120+15			11.00		41.9	90	43		
SR10	b-6	6	2	120+15			11.00		24.3	90	43		
SR10	b-6	6	2	120+15			11.00		22.7	90	43		
SR10	b-6	6	3	120+15			9.00	374.1	25.0	77	43	310.2	30.8
SR10	b-6	6	3	120+15			8.00	246.2	32.4	77	43		
SR10	b-6	6	3	120+15			7.00		35.1	77	43		
SR10	b-6	6	8	120+15			-22.40	731.3	221.0	58	42	1485.3	274.2
SR10	b-6	6	8	120+15			-27.40	2239.3	327.4	58	42		
SR10	b-6	6	12	120+15			-47.40	230.3	68.6	100	75	230.3	99.3
SR10	b-6	6	12	120+15			-47.40		115.7	100	75		
SR10	b-6	6	12	120+15			-47.40		105.4	100	75		
SR10	b-6	6	12	120+15			-47.40		107.4	100	75		
SR10	b-7	7	1	120+53			4.40	295.1	78.6	100	100	319.3	77.7
SR10	b-7	7	1	120+53			3.00	303.1	89.7	100	100		
SR10	b-7	7	1	120+53			2.00	359.8	64.8	100	100		
SR10	b-7	7	2	120+53			-2.10	593.4	46.1	82	48	746.2	168.3
SR10	b-7	7	2	120+53			-4.00	611.0	57.6	82	48		
SR10	b-7	7	2	120+53			-5.00	1034.3	260.0	82	48		
SR10	b-7	7	2	120+53			-7.10		309.5	82	48		
SR10	b-7	7	3	120+53			-8.60	268.6	46.7	92	92	340.4	42.7
SR10	b-7	7	3	120+53			-10.00	354.8	34.5	92	92		
SR10	b-7	7	3	120+53			-11.00	479.2	46.8	92	92		
SR10	b-7	7	3	120+53			-12.00	258.9		92	92		
SR10	b-7	7	4	120+53			-15.10	401.2	91.9	67	58	413.6	68.1
SR10	b-7	7	4	120+53			-16.00	372.4	41.7	67	58		
SR10	b-7	7	4	120+53			-18.00	467.3	70.8	67	58		
SR10	b-7	7	5	120+53			-26.60	1630.5	155.8	42	33	1630.5	163.5
SR10	b-7	7	5	120+53			-26.60		171.1	42	33		
SR10	b-7	7	6	120+53			-27.60	941.5	144.6	88	88	698.3	101.3
SR10	b-7	7	6	120+53			-28.00	455.0	126.3	88	88		
SR10	b-7	7	6	120+53			-28.50		47.0	88	88		
SR10	b-7	7	6	120+53			-29.50		87.2	88	88		
SR10	b-7	7	9	120+53			-47.10	371.2	52.6	93	78	373.6	68.0
SR10	b-7	7	9	120+53			-48.00	317.6	62.7	93	78		
SR10	b-7	7	9	120+53			-49.00	552.6	88.8	93	78		
SR10	b-7	7	9	120+53			-50.00	252.9		93	78		
SR10	b-7	7	10	120+53			-52.60	375.7	51.1	85	80	395.3	56.5
SR10	b-7	7	10	120+53			-53.00	439.1	57.9	85	80		
SR10	b-7	7	10	120+53			-53.00	381.8	60.6	85	80		

Final Report Contract #BC354 RPWO #13

Table A.9 Summary Comparison of Unconfined Compressive and Tensile Strength

Site	Pier No.	Shaft/ Core No.	Sample No.	Station	Boring No.	Surf. Elev. ft	Core Elev. ft	qu psi	qt psi	Rec. %	RQD %	qu Avg. psi	qt Avg. psi
SR10	b-7	7	10	120+53			-55.00	415.4		85	80		
SR10	b-7	7	10	120+53			-56.00	364.6		85	80		
SR10	b-7-2	7	2	120+53			26.90	167.3	15.4	97	67	167.3	15.4
SR10	b-7-2	7	3	120+53			20.00	12.8	1.2	100	92	12.8	1.6
SR10	b-7-2	7	3	120+53			16.90		2.0	100	92		
SR10	b-8	8	1	120+91			4.00	205.8	52.0	98	85	290.8	52.9
SR10	b-8	8	1	120+91			2.00	252.2	45.3	98	85		
SR10	b-8	8	1	120+91			1.00	414.5	45.1	98	85		
SR10	b-8	8	1	120+91			1.00		46.7	98	85		
SR10	b-8	8	1	120+91			1.00		75.6	98	85		
SR10	b-8	8	2	120+91			-2.50	731.9	34.1	95	95	731.9	116.9
SR10	b-8	8	2	120+91			-5.00		100.5	95	95		
SR10	b-8	8	2	120+91			-5.00		94.5	95	95		
SR10	b-8	8	2	120+91			-5.00		211.0	95	95		
SR10	b-8	8	2	120+91			-5.00		208.8	95	95		
SR10	b-8	8	2	120+91			-5.00		131.4	95	95		
SR10	b-8	8	2	120+91			-5.00		38.0	95	95		
SR10	b-8	8	3	120+91			-7.90	391.2	240.4	83	75	319.8	132.7
SR10	b-8	8	3	120+91			-8.50	214.4	216.6	83	75		
SR10	b-8	8	3	120+91			-9.50	353.9	61.0	83	75		
SR10	b-8	8	3	120+91			-10.00		84.7	83	75		
SR10	b-8	8	3	120+91			-11.00		61.0	83	75		
SR10	b-8	8	4	120+91			-15.00	325.7	49.3	77	72	317.1	82.6
SR10	b-8	8	4	120+91			-16.00	336.9	91.8	77	72		
SR10	b-8	8	4	120+91			-17.00	288.7	132.6	77	72		
SR10	b-8	8	4	120+91			-18.00		56.8	77	72		
SR10	b-8	8	5	120+91			-20.90	142.4	23.6	93	93	857.7	124.3
SR10	b-8	8	5	120+91			-20.90	338.0	195.7	93	93		
SR10	b-8	8	5	120+91			-24.00	783.8	153.6	93	93		
SR10	b-8	8	5	120+91			-25.90	2166.5		93	93		
SR10	b-8	8	6	120+91			-29.00	1028.8	354.8	80	75	645.0	236.1
SR10	b-8	8	6	120+91			-31.40	413.8	117.3	80	75		
SR10	b-8	8	6	120+91			-31.40	513.5		80	75		
SR10	b-8	8	6	120+91			-31.40	623.8		80	75		
SR10	b-8	8	7	120+91			-34.00	350.4	272.2	95	73	578.2	149.5
SR10	b-8	8	7	120+91			-34.00	732.9	108.1	95	73		
SR10	b-8	8	7	120+91			-36.00	651.3	112.8	95	73		
SR10	b-8	8	7	120+91			-37.90		104.7	95	73		
SR10	b-8	8	8	120+91			-39.00	591.0	73.4	98	92	438.0	55.6
SR10	b-8	8	8	120+91			-40.00	463.0	68.3	98	92		
SR10	b-8	8	8	120+91			-41.00	260.0	24.9	98	92		
SR10	b-8	8	8	120+91			-42.00		55.8	98	92		
SR10	b-8	8	9	120+91			-45.40	441.2	132.0	72	22	410.7	132.0
SR10	b-8	8	9	120+91			-45.40	380.1		72	22		
SR10	b-8	8	10	120+91			-50.90	672.6	144.3	88	73	511.4	109.9

Final Report Contract #BC354 RPWO #13

Table A.9 Summary Comparison of Unconfined Compressive and Tensile Strength

Site	Pier No.	Shaft/ Core No.	Sample No.	Station	Boring No.	Surf. Elev. ft	Core Elev. ft	qu psi	qt psi	Rec. %	RQD %	qu Avg. psi	qt Avg. psi
SR10	b-8	8	10	120+91			-52.00	403.5	230.6	88	73		
SR10	b-8	8	10	120+91			-53.00	458.0	43.6	88	73		
SR10	b-8	8	10	120+91			-54.00		56.4	88	73		
SR10	b-8	8	10	120+91			-55.00		74.7	88	73		
SR10	b-8	8	1	120+91			30.60	356.2	5.8	55	17	356.2	7.9
SR10	b-8	8	1	120+91			32.00		10.0	55	17		
SR10	b-8	8	3	120+91			17.00	271.4	25.2	100	52	271.4	33.3
SR10	b-8	8	3	120+91			15.60		33.1	100	52		
SR10	b-8	8	3	120+91			15.60		41.7	100	52		
SR10	b-8	8	5	120+91			9.00	197.7	122.1	100	85	209.3	80.5
SR10	b-8	8	5	120+91			8.00	237.7	156.1	100	85		
SR10	b-8	8	5	120+91			7.00	192.4	11.6	100	85		
SR10	b-8	8	5	120+91			5.60		56.4	100	85		
SR10	b-8	8	5	120+91			5.60		56.4	100	85		
SR10	b-9	9	1	121+29			-8.90	235.7	44.5	80	80	263.6	55.7
SR10	b-9	9	1	121+29			-9.50	250.7	35.5	80	80		
SR10	b-9	9	1	121+29			-10.00	246.6	33.7	80	80		
SR10	b-9	9	1	121+29			-11.00	321.5	52.3	80	80		
SR10	b-9	9	1	121+29			-13.00		112.3	80	80		
SR10	b-9	9	2	121+29			-15.40	316.2	39.3	97	97	388.1	67.7
SR10	b-9	9	2	121+29			-16.00	217.1	91.0	97	97		
SR10	b-9	9	2	121+29			-17.00	396.3	76.0	97	97		
SR10	b-9	9	2	121+29			-17.50	552.1	64.3	97	97		
SR10	b-9	9	2	121+29			-18.00	458.8		97	97		
SR10	b-9	9	3	121+29			-23.00	766.8	75.5	83	67	864.2	139.1
SR10	b-9	9	3	121+29			-24.00	471.8	127.0	83	67		
SR10	b-9	9	3	121+29			-25.00	1354.1	153.7	83	67		
SR10	b-9	9	3	121+29			-26.00		63.2	83	67		
SR10	b-9	9	3	121+29			-26.90		276.0	83	67		
SR10	b-9	9	4	121+29			-28.40	527.1	128.0	90	67	407.2	83.4
SR10	b-9	9	4	121+29			-29.00	508.5	45.1	90	67		
SR10	b-9	9	4	121+29			-29.50	261.5	103.1	90	67		
SR10	b-9	9	4	121+29			-30.00	331.8	57.3	90	67		
SR10	b-9	9	5	121+29			-34.90	241.5	102.9	92	50	383.6	83.7
SR10	b-9	9	5	121+29			-36.00	284.1	62.1	92	50		
SR10	b-9	9	5	121+29			-36.50	504.9	65.9	92	50		
SR10	b-9	9	5	121+29			-37.00	503.7	103.7	92	50		
SR10	b-9	9	6	121+29			-41.40	454.7	61.5	97	83	334.1	44.3
SR10	b-9	9	6	121+29			-42.00	262.2	31.4	97	83		
SR10	b-9	9	6	121+29			-42.50	306.9	32.3	97	83		
SR10	b-9	9	6	121+29			-43.00	288.3	52.0	97	83		
SR10	b-9	9	6	121+29			-44.00	358.3		97	83		
SR10	b-9	9	7	121+29			-47.90	452.7	72.8	92	85	370.9	59.4
SR10	b-9	9	7	121+29			-48.50	476.6	50.3	92	85		
SR10	b-9	9	7	121+29			-49.50	183.5	55.2	92	85		

Final Report Contract #BC354 RPWO #13

Table A.9 Summary Comparison of Unconfined Compressive and Tensile Strength

Site	Pier No.	Shaft/ Core No.	Sample No.	Station	Boring No.	Surf. Elev. ft	Core Elev. ft	qu psi	qt psi	Rec. %	RQD %	qu Avg. psi	qt Avg. psi
SR10	b-9	9	8	121+29			-53.40	597.5	254.6	92	92	536.9	118.5
SR10	b-9	9	8	121+29			-54.00	625.9	76.9	92	92		
SR10	b-9	9	8	121+29			-54.50	489.6	92.6	92	92		
SR10	b-9	9	8	121+29			-56.00	434.7	49.7	92	92		
SR10	b-9	9	9	121+29			-59.90	771.0	138.1	75	67	1120.5	198.6
SR10	b-9	9	9	121+29			-62.00	1469.9	157.6	75	67		
SR10	b-9	9	9	121+29			-64.00		81.9	75	67		
SR10	b-9	9	9	121+29			-64.00		416.9	75	67		
SR10	b-9	9	10	121+29			-66.40	354.7	75.9	92	80	593.3	116.0
SR10	b-9	9	10	121+29			-67.00	638.5	176.7	92	80		
SR10	b-9	9	10	121+29			-68.00	550.6	47.7	92	80		
SR10	b-9	9	10	121+29			-69.00	775.4	163.6	92	80		
SR10	b-9	9	10	121+29			-70.00	647.3		92	80		
SR10	b-9	9	11	121+29			-71.90	809.3	225.7	93	87	708.5	155.4
SR10	b-9	9	11	121+29			-72.50	790.3	187.3	93	87		
SR10	b-9	9	11	121+29			-73.00	786.6	180.3	93	87		
SR10	b-9	9	11	121+29			-73.50	447.9	119.6	93	87		
SR10	b-9	9	11	121+29			-74.00		64.0	93	87		
SR10	b-9-2	9	3	121+29			20.00	225.4	29.7	100	97	225.2	36.2
SR10	b-9-2	9	3	121+29			19.00	133.0	22.3	100	97		
SR10	b-9-2	9	3	121+29			18.00	234.8	49.8	100	97		
SR10	b-9-2	9	3	121+29			17.00	275.7	43.0	100	97		
SR10	b-9-2	9	3	121+29			16.00	256.9		100	97		
SR10	b-9-2	9	4	121+29			15.00	153.0	23.9	100	68	205.7	53.3
SR10	b-9-2	9	4	121+29			14.00	229.8	25.4	100	68		
SR10	b-9-2	9	4	121+29			13.00	234.3	21.0	100	68		
SR10	b-9-2	9	4	121+29			13.00		120.2	100	68		
SR10	b-9-2	9	4	121+29			13.00		76.0	100	68		
SR10	b-9-2	9	5	121+29			10.00	193.1	18.5	100	93	189.2	57.7
SR10	b-9-2	9	5	121+29			9.00	195.6	96.8	100	93		
SR10	b-9-2	9	5	121+29			9.00	189.3		100	93		
SR10	b-9-2	9	5	121+29			9.00	62.9		100	93		
SR10	b-9-2	9	5	121+29			8.00	305.1		100	93		
SR10	b-9-2	9	6	121+29			6.10	198.9	118.5	100	77	198.9	90.2
SR10	b-9-2	9	6	121+29			6.10		2.1	100	77		
SR10	b-9-2	9	6	121+29			6.10		70.4	100	77		
SR10	b-9-2	9	6	121+29			6.10		169.6	100	77		
SR10	b-10	10	1	121+67			-9.20	178.1	27.3	75	58	255.4	36.1
SR10	b-10	10	1	121+67			-10.00	322.5	49.0	75	58		
SR10	b-10	10	1	121+67			-11.00	265.5	32.1	75	58		
SR10	b-10	10	2	121+67			-15.70	442.3	48.9	90	88	477.5	79.1
SR10	b-10	10	2	121+67			-17.00	572.9	132.2	90	88		
SR10	b-10	10	2	121+67			-18.00	471.6	69.4	90	88		
SR10	b-10	10	2	121+67			-19.00	423.2	65.9	90	88		
SR10	b-10	10	3	121+67			-22.20	375.2	71.8	80	45	375.2	115.3

Final Report Contract #BC354 RPWO #13

Table A.9 Summary Comparison of Unconfined Compressive and Tensile Strength

Site	Pier No.	Shaft/ Core No.	Sample No.	Station	Boring No.	Surf. Elev. ft	Core Elev. ft	qu psi	qt psi	Rec. %	RQD %	qu Avg. psi	qt Avg. psi
SR10	b-10	10	3	121+67			-23.00		41.9	80	45		
SR10	b-10	10	3	121+67			-23.00		232.2	80	45		
SR10	b-10	10	5	121+67			-37.00	349.8	66.5	88	67	384.3	86.0
SR10	b-10	10	5	121+67			-37.00	418.7	128.5	88	67		
SR10	b-10	10	5	121+67			-37.00		62.9	88	67		
SR10	b-10	10	6	121+67			-43.00	288.9	43.5	93	67	391.3	46.3
SR10	b-10	10	6	121+67			-44.00	493.7	56.9	93	67		
SR10	b-10	10	6	121+67			-45.00		41.4	93	67		
SR10	b-10	10	6	121+67			-45.00		43.3	93	67		
SR10	b-10	10	7	121+67			-49.00	358.9	75.1	98	83	404.9	75.2
SR10	b-10	10	7	121+67			-49.50	391.1	46.2	98	83		
SR10	b-10	10	7	121+67			-51.00	547.8	75.3	98	83		
SR10	b-10	10	7	121+67			-53.00	321.8	104.2	98	83		
SR10	b-10	10	8	121+67			-53.70	603.3	296.8	92	83	584.2	184.6
SR10	b-10	10	8	121+67			-54.00	597.6	249.9	92	83		
SR10	b-10	10	8	121+67			-54.50	551.7	186.0	92	83		
SR10	b-10	10	8	121+67			-55.00		88.7	92	83		
SR10	b-10	10	8	121+67			-55.50		101.4	92	83		
SR10	b-10	10	9	121+67			-55.50	698.4	193.9	92	83	714.5	226.2
SR10	b-10	10	9	121+67			-55.50	730.5	235.5	92	83		
SR10	b-10	10	9	121+67			-55.50		249.2	92	83		
SR10	b-10	10	10	121+67			-65.70	1464.4	212.4	93	83	846.5	214.9
SR10	b-10	10	10	121+67			-67.00	434.1	196.8	93	83		
SR10	b-10	10	10	121+67			-67.50	937.4	235.6	93	83		
SR10	b-10	10	10	121+67			-68.00	586.5		93	83		
SR10	b-10	10	10	121+67			-69.00	810.3		93	83		
SR10	b-10	10	11	121+67			-71.20	452.0	63.3	92	90	602.5	128.3
SR10	b-10	10	11	121+67			-72.00	245.8	122.0	92	90		
SR10	b-10	10	11	121+67			-73.00	443.1	203.5	92	90		
SR10	b-10	10	11	121+67			-74.00	903.4	124.3	92	90		
SR10	b-10	10	11	121+67			-74.50	968.3		92	90		
SR10	b-10-2	10	1	121+67			8.80	76.8	36.8	92	32	161.0	36.8
SR10	b-10-2	10	1	121+67			8.80	245.1		92	32		
SR10	b-10-2	10	3	121+67			-2.00	50.7	6.0	97	70	39.5	5.9
SR10	b-10-2	10	3	121+67			-3.00	28.3	4.0	97	70		
SR10	b-10-2	10	3	121+67			-4.00		7.7	97	70		
SR10	b-11	11	1	122+05			-13.00	369.3	27.5	72	63	369.3	84.1
SR10	b-11	11	1	122+05			-14.10		192.8	72	63		
SR10	b-11	11	1	122+05			-14.10		48.8	72	63		
SR10	b-11	11	1	122+05			-14.10		67.3	72	63		
SR10	b-11	11	4	122+05			-28.60	553.5	53.8	90	83	394.2	80.6
SR10	b-11	11	4	122+05			-29.50	241.8	96.5	90	83		
SR10	b-11	11	4	122+05			-30.00	480.6	101.6	90	83		
SR10	b-11	11	4	122+05			-30.50	300.9	70.3	90	83		
SR10	b-11	11	5	122+05			-35.10	569.1	139.8	92	75	406.5	99.4

Final Report Contract #BC354 RPWO #13

Table A.9 Summary Comparison of Unconfined Compressive and Tensile Strength

Site	Pier No.	Shaft/ Core No.	Sample No.	Station	Boring No.	Surf. Elev. ft	Core Elev. ft	qu psi	qt psi	Rec. %	RQD %	qu Avg. psi	qt Avg. psi
SR10	b-11	11	5	122+05			-36.00	426.2	131.4	92	75		
SR10	b-11	11	5	122+05			-38.00	224.3	70.5	92	75		
SR10	b-11	11	5	122+05			-39.00		55.8	92	75		
SR10	b-11	11	6	122+05			-40.60	452.0	93.1	83	55	331.2	97.6
SR10	b-11	11	6	122+05			-42.00	210.4	102.0	83	55		
SR10	b-11	11	7	122+05			-49.00	597.9	75.8	93	75	597.9	132.8
SR10	b-11	11	7	122+05			-51.00		104.1	93	75		
SR10	b-11	11	7	122+05			-51.00		86.8	93	75		
SR10	b-11	11	7	122+05			-51.00		264.5	93	75		
SR10	b-11	11	8	122+05			-54.00	368.4	220.1	90	83	382.9	149.3
SR10	b-11	11	8	122+05			-54.50	409.9	106.3	90	83		
SR10	b-11	11	8	122+05			-55.00	370.5	165.2	90	83		
SR10	b-11	11	8	122+05			-56.00		105.5	90	83		
SR10	b-11	11	10	122+05			-66.10	790.3	62.8	98	88	734.4	179.6
SR10	b-11	11	10	122+05			-67.00	193.2	274.0	98	88		
SR10	b-11	11	10	122+05			-68.00	948.9	230.7	98	88		
SR10	b-11	11	10	122+05			-69.50	1005.3	151.0	98	88		
SR10	b-11	11	11	122+05			-72.10	462.4	162.2	97	97	711.0	167.9
SR10	b-11	11	11	122+05			-73.00	875.8	148.7	97	97		
SR10	b-11	11	11	122+05			-74.00	590.5	192.9	97	97		
SR10	b-11	11	11	122+05			-77.10	915.3		97	97		
SR10	b-11-2	11	3	122+05			-4.10	906.7	304.7	87	47	906.7	304.7
Hallandale	7	1a1	1b					776.6	768.4			776.6	311.3
Hallandale	7	1a2	1b						662.8				
Hallandale	7	1c	1b						78.3				
Hallandale	7	1d	1b						237.7				
Hallandale	7	1e1	1b						145.9				
Hallandale	7	1e2	1b						86.4				
Hallandale	7	1f1	1b						401.0				
Hallandale	7	1f2	1b						110.2				
Hallandale	7	2a1	1b					776.6	628.1			776.6	243.5
Hallandale	7	2a2	1b						191.0				
Hallandale	7	2a3	1b						248.1				
Hallandale	7	2b	1b						70.5				
Hallandale	7	2c1	1b						348.4				
Hallandale	7	2c2	1b						177.3				
Hallandale	7	2c3	1b						41.1				
Hallandale	8	3a	3b					994.9	245.2			2176.6	357.9
Hallandale	8	3a	3c					2002.4					
Hallandale	8	3a	3d					1528.7					
Hallandale	8	3g	3d						470.7				
Hallandale	8	3g	3e					3041.2					
Hallandale	8	3g	3f					3315.9					
Hallandale	8	4a1	4c					1823.8	739.2			1823.8	731.3
Hallandale	8	4a2	4c						834.2				

Final Report Contract #BC354 RPWO #13

Table A.9 Summary Comparison of Unconfined Compressive and Tensile Strength

Site	Pier No.	Shaft/ Core No.	Sample No.	Station	Boring No.	Surf. Elev. ft	Core Elev. ft	qu psi	qt psi	Rec. %	RQD %	qu Avg. psi	qt Avg. psi
Hallandale	8	4a3	4c						659.2				
Hallandale	8	4b	4c						692.5				
Gatorock	1							2677.5	808.9			2757.8	545.1
Gatorock	1							2888.5	494.7				
Gatorock	1							2528.1	331.7				
Gatorock	1							3028.0					
Gatorock	1							2666.8					
Gatorock	2							2735.9	223.2			3213.0	451.6
Gatorock	2							3176.0	825.2				
Gatorock	2							3863.8	429.5				
Gatorock	2							3076.5	429.1				
Gatorock	2								350.8				
Gatorock	3							2098.6	401.5			2241.7	384.1
Gatorock	3							2617.1	390.8				
Gatorock	3							2340.0	362.8				
Gatorock	3							1911.2	293.8				
Gatorock	3								454.8				
Gatorock	3								401.2				
Gatorock	4							1572.1	184.6			2158.7	217.4
Gatorock	4							2184.7	194.3				
Gatorock	4							2385.8	277.1				
Gatorock	4							2492.4	157.3				
Gatorock	4								240.1				
Gatorock	4								250.8				
Gatorock	5							1798.4	213.3			2091.2	224.7
Gatorock	5							1661.8	235.2				
Gatorock	5							2403.0	204.5				
Gatorock	5							2501.8	289.9				
Gatorock	5								169.8				
Gatorock	5								235.6				
Gatorock	6							2218.8	199.8			1948.8	146.0
Gatorock	6							1070.0	215.2				
Gatorock	6							2215.3	146.1				
Gatorock	6							2291.1	81.2				
Gatorock	6								87.9				
Gatorock	7							1603.4	114.2			1659.6	163.6
Gatorock	7							1486.1	209.1				
Gatorock	7							1726.8	148.3				
Gatorock	7							1821.9	166.3				
Gatorock	7								179.8				
Gatorock	8							1509.0	145.1			1629.8	191.2
Gatorock	8							1412.8	214.8				
Gatorock	8							1820.8	254.9				
Gatorock	8							1776.6	177.6				
Gatorock	8								163.4				

Final Report Contract #BC354 RPWO #13

Table A.9 Summary Comparison of Unconfined Compressive and Tensile Strength

Site	Pier No.	Shaft/ Core No.	Sample No.	Station	Boring No.	Surf. Elev. ft	Core Elev. ft	qu psi	qt psi	Rec. %	RQD %	qu Avg. psi	qt Avg. psi
Gatorock	C15-W15							272.3	59.4			272.3	59.4
Gatorock	C20-W20							432.7	71.2			432.7	71.2
Gatorock	C25-W25							328.2	20.3			328.2	20.3
Gatorock	C15-W15							557.2	127.5			557.2	127.5
Gatorock	C20-W20							935.3	89.1			935.3	89.1
Gatorock	C25-W25							550.4	47.7			550.4	47.7
Gatorock	C17-W17							611.1	79.3			611.1	79.3
Gatorock	C20-W20							1068.4	169.1			1068.4	169.1
Gatorock	C25-W25							859.6	108.8			859.6	108.8
Gatorock	C25-W25							1075.4	158.1			1075.4	158.1
SR30	th-1	1	1	21+10.4			27.50	5944.9	349.6	80	63	5944.9	681.0
SR30	th-1	1	1	21+10.4			27.50		1046.0	80	63		
SR30	th-1	1	1	21+10.4			27.50		647.5	80	63		
SR30	th-1	1	2	21+10.4			33.00	1876.7	750.9	100	82	1465.3	423.2
SR30	th-1	1	2	21+10.4			35.00	1053.8	95.6	100	82		
SR30	th-1	1	3	21+10.4			41.00	2289.7	399.9	83	62	2289.7	587.9
SR30	th-1	1	3	21+10.4			41.00		303.6	83	62		
SR30	th-1	1	3	21+10.4			41.00		295.7	83	62		
SR30	th-1	1	3	21+10.4			41.00		1172.4	83	62		
SR30	th-1	1	3	21+10.4			42.00		767.9	83	62		
SR30	th-1	1	4	21+10.4			44.00	2274.9	474.8	90	78	2274.9	584.5
SR30	th-1	1	4	21+10.4			44.00		694.3	90	78		
SR30	th-1	1	5	21+10.4			51.00	4361.2	658.8	98	98	3771.3	666.0
SR30	th-1	1	5	21+10.4			52.00	3181.3	728.6	98	98		
SR30	th-1	1	5	21+10.4			53.00		610.5	98	98		
SR30	th-1	1	6	21+10.4			54.00	6375.2	934.1	93	73	4389.9	660.5
SR30	th-1	1	6	21+10.4			57.00	2404.5	608.5	93	73		
SR30	th-1	1	6	21+10.4			59.00		439.0	93	73		
SR30	th-1	1	7	21+10.4			63.00	982.4	451.0	100	55	2513.9	446.9
SR30	th-1	1	7	21+10.4			63.00	4045.4	351.8	100	55		
SR30	th-1	1	7	21+10.4			63.00		537.9	100	55		
SR30	th-1	1	8	21+10.4			65.00	2299.2	339.0	80	68	2715.2	303.4
SR30	th-1	1	8	21+10.4			66.00	3131.2	310.9	80	68		
SR30	th-1	1	8	21+10.4			66.00		260.4	80	68		
SR30	th-2	2	2	21+39.5			43.00	475.6	1015.5	100	77	668.1	573.8
SR30	th-2	2	2	21+39.6			48.00	860.5	132.2	100	77		
SR30	th-2	2	3	21+39.7			48.00	895.5	72.3	85	78	895.5	78.8
SR30	th-2	2	3	21+39.8			50.00		66.5	85	78		
SR30	th-2	2	3	21+39.9			52.00		86.6	85	78		
SR30	th-2	2	3	21+39.9			52.00		89.8	85	78		
SR30	th-2	2	4	21+39.1			58.00	291.7	9.6	95	68	291.7	20.0
SR30	th-2	2	4	21+39.1			58.00		30.4	95	68		
SR30	th-2	2	5	21+39.1			58.00	1027.1	184.2	92	60	1217.0	244.8
SR30	th-2	2	5	21+39.1			63.00	1406.9	306.5	92	60		
SR30	th-2	2	5	21+39.1			63.00		243.6	92	60		

Final Report Contract #BC354 RPWO #13

Table A.9 Summary Comparison of Unconfined Compressive and Tensile Strength

Site	Pier No.	Shaft/ Core No.	Sample No.	Station	Boring No.	Surf. Elev. ft	Core Elev. ft	qu psi	qt psi	Rec. %	RQD %	qu Avg. psi	qt Avg. psi
SR30	th-3	3	1	21+68.4			33.00	1128.0	100.2	88	82	1128.0	222.5
SR30	th-3	3	1	21+68.4			33.00		135.1	88	82		
SR30	th-3	3	1	21+68.4			33.00		432.1	88	82		
SR30	th-3	3	3	21+68.4			41.00	3610.2	792.1	93	55	4045.4	899.4
SR30	th-3	3	3	21+68.4			46.00	4480.5	1006.7	93	55		
SR30	th-3	3	4	21+68.4			46.00	2562.7	353.7	73	67	2230.1	472.3
SR30	th-3	3	4	21+68.4			51.00	1897.4	590.9	73	67		
SR30	th-3	3	5	21+68.4			51.60	4171.9	423.6	87	62	4171.9	370.2
SR30	th-3	3	5	21+68.4			51.60		316.9	87	62		
SR30	th-3	3	6	21+68.4			57.50	4102.4	864.4	73	35	4102.4	864.4
SR30	th-3	3	7	21+68.4			62.50	4155.5	614.8	100	88	2887.5	432.5
SR30	th-3	3	7	21+68.4			66.00	1619.4	250.2	100	88		
SR30	th-4	4	1	21+97.4			23.00	1380.7	181.9	100	73	794.2	174.6
SR30	th-4	4	1	21+97.4			28.00	207.6	167.4	100	73		
SR30	th-4	4	1	21+97.4			28.00		174.6	100	73		
SR30	th-4	4	2	21+97.4			28.00	1008.2	47.3	93	53	898.0	44.7
SR30	th-4	4	2	21+97.4			33.00	787.8	42.0	93	53		
SR30	th-4	4	3	21+97.4			33.00	962.2	136.7	100	70	1899.5	113.8
SR30	th-4	4	3	21+97.4			38.00	2836.7	91.0	100	70		
SR30	th-4	4	4	21+97.4			38.00	3351.9	1086.2	95	75	3351.9	611.1
SR30	th-4	4	4	21+97.4			40.00		426.7	95	75		
SR30	th-4	4	4	21+97.4			40.00		320.4	95	75		
SR30	th-4	4	5	21+97.4			43.00	2466.8	1034.2	100	100	2466.8	1034.2
SR30	th-4	4	6	21+97.4			48.00	6322.3	77.2	100	100	6322.3	330.7
SR30	th-4	4	6	21+97.4			48.00		584.1	100	100		
SR30	th-5	5	1	21+13.3			9.50	601.7	56.3	97	97	573.1	61.8
SR30	th-5	5	1	21+13.3			11.00	544.4	61.2	97	97		
SR30	th-5	5	1	21+13.3			13.00		67.7	97	97		
SR30	th-6	6	1	21+13.3			6.00	739.4	58.4	97	92	732.0	68.1
SR30	th-6	6	1	21+13.3			7.00	724.6	93.0	97	92		
SR30	th-6	6	1	21+13.3			9.00		52.8	97	92		
SR30	th-7	7	1	21+97.4			9.50	1716.9	163.2	97	83	1126.9	126.4
SR30	th-7	7	1	21+97.4			11.00	536.8	150.3	97	83		
SR30	th-7	7	1	21+97.4			13.00		65.8	97	83		
SR30	th-8	8	1	21+97.4			7.00	1029.8	162.8	95	67	1167.1	145.5
SR30	th-8	8	1	21+97.4			8.00	1304.4	128.2	95	67		
Victory	TB-4						39.60	726.0	711.0	21	8	726.0	711.0
Victory	TB-6						48.50	3026.0	351.0	67	36	3026.0	351.0
Victory	TB-7						14.50	221.0	164.0	93	58	221.0	164.0
Victory	TB-15						25.00	1325.0	238.0	100	100	1736.0	344.0
Victory								2813.0	450.0				
Victory								1070.0					
Victory	TB-15						16.50	1191.0	586.0	92	45	798.0	586.0
Victory								405.0					
Victory	TB-18						27.30	419.0	218.0	100	83	419.0	218.0

Final Report Contract #BC354 RPWO #13

Table A.9 Summary Comparison of Unconfined Compressive and Tensile Strength

Site	Pier No.	Shaft/ Core No.	Sample No.	Station	Boring No.	Surf. Elev. ft	Core Elev. ft	qu psi	qt psi	Rec. %	RQD %	qu Avg. psi	qt Avg. psi
Victory	TB-18						25.30	806.0	40.0	82	42	806.0	162.0
Victory									284.0				
Victory	TB-19						20.50	1957.0	275.0	97	73	1957.0	275.0
Victory	TB-20						30.30	133.0	94.0	75	61	171.5	94.0
Victory								210.0					
Victory	TB-23						10.00	1260.0	120.0	97	70	1259.0	113.5
Victory								1258.0	107.0				
Victory	TB-24						12.00	553.0	453.0	94	94	553.0	453.0
Victory	TB-26						4.00	663.0	550.0	83	60	663.0	550.0
Victory	TB-27						20.00	1768.0	722.0	25	17	1768.0	722.0
Victory	TB-1						39.90	1459.0	353.0	98	62	1459.0	353.0
Victory	TB-1						24.90	1920.0	666.0	80	13	1920.0	666.0
Victory	TB-3						34.30	2231.0	686.0	40	8	2231.0	686.0
Victory	TB-3						24.30	1345.0	512.0	30	23	1345.0	512.0
Victory	TB-3						19.30	1279.0	580.0	50	20	1279.0	580.0
Victory	TB-16						22.00	2995.0	927.0	94	89	2995.0	927.0
Victory	TB-16						4.00	2362.0	153.0	65	50	2362.0	167.5
Victory									182.0				
Victory	TB-18						27.80	1568.0	443.0	100	83	1568.0	443.0
Victory	TB-19						22.50	2242.0	216.0	97	73	2242.0	216.0
Victory	TB-23						11.00	578.0	81.0	97	70	578.0	81.0
Victory	19-1	3					15.80	337.9	196.8	48	45	1484.1	313.5
Victory								2459.2	367.3				
Victory								1655.1	376.3				
Victory	19-1	4					9.80	1329.9	377.6	98	53	922.5	262.7
Victory								515.1	147.7				
Victory	19-2	3					11.20	1798.5	187.4	83	28	1798.5	155.3
Victory									109.8				
Victory									168.8				
Victory	T-4	1					25.50	1384.2	96.9	83	73	1384.2	314.5
Victory									532.1				
Victory	T-4	4					7.00	350.0	152.6	97	35	350.0	152.6
Victory	T-4	5					0.50	180.6	14.9	100	93	280.5	33.0
Victory								380.4	51.0				
Victory	T-4	6					-4.80	1447.6	169.6	93	83	1336.5	169.6
Victory								1225.3					
Victory	T-5	1					25.00	899.2	99.9	92	57	899.2	99.9
Victory	T-5	2					19.50	1220.2	151.9	95	38	1220.2	151.9
Victory	T-5	3					13.00	1466.1	341.4	82	50	1466.1	341.4
Victory	3-1	1					37.10	1744.9	216.5	77	43	1744.9	216.5
Victory	3-1	3					26.10	1924.8	378.6	100	82	1924.8	378.6
Victory	3-1	4					20.60	782.5	533.7	87	40	782.5	533.7
Victory	3-2	1					35.90	1130.6	217.8	97	40	1130.6	217.8
Victory	3-2	3					23.90	2390.4	258.8	100	68	2423.2	258.8
Victory								2456.0					

Final Report Contract #BC354 RPWO #13

Table A.9 Summary Comparison of Unconfined Compressive and Tensile Strength

Site	Pier No.	Shaft/ Core No.	Sample No.	Station	Boring No.	Surf. Elev. ft	Core Elev. ft	qu psi	qt psi	Rec. %	RQD %	qu Avg. psi	qt Avg. psi
Victory	TH-1	1					39.00	71.3	78.7	60	18	71.3	78.7
Victory	TH-1	3					26.00	370.4	280.9	80	62	370.4	280.9
Victory	TH-2	1					38.10	1609.2	140.0	75	20	1609.2	140.0
Victory	TH-2	2					32.60	800.1	341.1	73	40	800.1	341.1
Victory	TH-2	3					27.10	676.5	297.1	97	52	676.5	297.1
Victory	TH-2	4					21.60	1127.5	649.0	97	62	1127.5	649.0
Victory	1-1	1					27.98	1220.9	392.8	87	68	1220.9	435.7
Victory									587.6				
Victory									326.7				
Victory	1-2	1					29.06	529.0	367.3	92	50	529.0	367.3
Victory	1-3	1					30.29	3949.2	257.6	88	73	3949.2	253.7
Victory									249.7				
Victory	5-1	1					26.57	3441.2	527.4	93	70	3441.2	527.4
Victory	6-1	1					11.24	2047.7	131.0	87	52	1461.3	131.0
Victory								874.9					
Victory	6-2	1					21.72	4593.0	420.2	52	42	4593.0	420.2
Victory	10-2	5					-6.20	1047.1	63.3	68	47	1047.1	190.9
Victory									318.5				
Victory	12-1	1					12.01	1976.6	185.1	70	53	1976.6	330.1
Victory									475.1				
Victory	12-2	1					-3.91	987.1	163.8	83	65	895.2	163.8
Victory								803.2					
Victory	13-1	1					14.70	3104.9	619.4	63	23	3104.9	619.4
Victory	15-1	1					10.73	3544.1	375.3	90	72	3544.1	552.7
Victory									730.0				
Victory	16-1	1					12.10	818.3	304.3	100	70	818.3	381.4
Victory									292.7				
Victory									547.3				
Victory	17-1	1&2					8.60	1630.6	205.0	67	25	1630.6	205.0
Victory	17-2	1					10.96	1664.2	247.4	67	37	1664.2	247.4
Victory	18-1	1					18.00	645.5	175.5	80	58	645.5	175.5
Victory	18-2	2					9.09	1539.8	120.9	87	52	1539.8	169.8
Victory									218.6				
Victory	20-1	2					10.22	1084.4	337.8	52	52	1084.4	278.3
Victory									218.8				
Victory	20-2	1					19.06	1752.1	197.5	65	52	1752.1	318.6
Victory									439.7		1		
Victory	21-2	2					18.18	2245.8	110.0	63	7	2245.8	110.0
Victory	22-1	1					16.57	4474.7	68.3	92	52	4474.7	98.2
Victory									128.0				
Victory	23-2	1					18.81	908.4	194.9	50	27	908.4	194.9
Victory	24-2	1					14.32	296.6	338.9	63	43	296.6	187.5
Victory									36.0				
Victory	24-2	2					9.82	1689.5	181.3	90	77	1689.5	181.3
Victory	25-2	1					7.87	1257.5	104.7	68	55	1257.5	104.7

Final Report Contract #BC354 RPWO #13

Table A.9 Summary Comparison of Unconfined Compressive and Tensile Strength

Site	Pier No.	Shaft/ Core No.	Sample No.	Station	Boring No.	Surf. Elev. ft	Core Elev. ft	qu psi	qt psi	Rec. %	RQD %	qu Avg. psi	qt Avg. psi
SR20-PMT	62	5			1		-35.90					88.7	54.9
SR20-PMT	62	5			1		-46.60					2466.4	622.7
SR20-PMT	62	5			1		-49.90					2116.3	407.0
SR20-PMT	62	5			1		-52.20					1416.0	309.2
SR20-PMT	62	5			2		-47.50					2054.4	525.0
SR20-PMT	62	5			2		-48.50					1936.9	543.3
SR20-PMT	62	5			2		-50.50					1702.1	555.4
SR20-PMT	69	7			3		-42.92					374.4	8.1
SR20-PMT	69	7			3		-54.65					65.3	326.3
SR20-PMT	69	7			4		-29.90					14.4	79.8
SR20-PMT	69	7			4		-31.92					14.4	79.8
SR20-PMT	69	7			4		-46.00					108.9	5.8
SR20-PMT	69	7			4		-49.00					108.9	39.9
SR20-PMT	69	7			4		-54.65					199.7	15.1
SR20-PMT	69	7			4		-58.60					173.4	14.3

Table A.10 Summary Comparison of Unconfined Compressive and Modulus Tests

Site	Test No.	Q _u (psi)	E _i (psi)
Victory	V1	1,130.6	3,125,000
Victory	V2	2,397.8	3,041,900
Victory	V3	2,858.6	4,651,200
Victory	V4	370.0	1,299,000
Victory	V5	622.6	2,222,000
Victory	V6	1,744.9	3,625,000
Victory	V7	1,943.0	3,333,300
Victory	V8	1,735.2	4,286,000
Victory	V9	1,396.6	2,186,000
Victory	V16	380.4	1,923,000
Victory	V17	350.0	1,800,000
Victory	V18	87.0	715,500
Victory	V20	1,329.8	3,496,000
Victory	V21	1,703.0	2,200,000
Victory	V22	2,484.0	2,216,912
Victory	V28	1,225.3	3,073,508
Victory	V29	180.6	479,000
Victory	V30	350.0	1,429,000
Victory	V31	1,380.0	3,226,000
Victory	V32	1,393.4	3,896,000
Victory	V33	1,220.2	2,985,000
Victory	V34	910.1	2,325,600
Victory	V35	515.1	2,294,000
Victory	V36	1,806.0	4,396,000
SR20	Blt11	424.2	114,300
SR20	Blt21	603.7	251,000
SR20	Blt210	863.6	212,100
SR20	Blt212	737.5	715,000
SR20	Blt213	566.7	435,421
SR20	Blt215	365.6	250,000
SR20	Blt216	389.2	107,120
SR20	Blt217	149.6	46,800
SR20	Blt218	128.6	24,300
SR20	Blt219	151.3	50,000
SR20	Blt22	265.5	86,000
SR20	Blt222	839.7	467,500
SR20	Blt271	252.1	29,000
SR20	Blt57	547.4	59,800
SR20	Blt570	288.1	48,900
SR20	Blt571	252.1	35,600
SR20	Blt572	166.6	15,200

Final Report Contract #BC354 RPWO #13

Table A.10 Summary Comparison of Unconfined Compressive and Modulus Tests

Site	Test No.	Q _u (psi)	E _i (psi)
SR20	Blt573	313.9	168,300
SR20	Blt574	389.2	238,267
SR20	Blt575	359.8	333,300
SR20	Blt577	189.0	181,200
SR20	Blt578	126.3	17,800
SR20	Blt579	129.8	40,000
Broadway	Broad265	1,053.0	326,300
Broadway	Broad268	938.0	2,195,000
Broadway	Broad269	1,515.9	703,900
Broadway	Broad270	782.8	167,800
Broadway	Broad271	449.5	251,400
Broadway	Broad272	1,577.6	946,700
Broadway	Broad81	358.4	553,200
Broadway	Broad86	591.7	44,000
Broadway	Broad221	364.7	62,500
Gatorock	C10-W11	122.1	13,420
Gatorock		103.0	21,600
Gatorock		302.5	114,900
Gatorock	C10-W15	295.6	80,870
Gatorock		273.9	102,000
Gatorock		207.6	138,000
Gatorock		407.8	93,000
Gatorock	C10-W20	395.4	165,700
Gatorock		478.6	338,900
Gatorock		449.4	231,600
Gatorock	C10-W25	342.6	910,900
Gatorock		336.2	508,100
Gatorock		327.8	141,250
Gatorock		309.6	80,820
Gatorock	C15-W13	108.1	2,063
Gatorock		693.9	106,300
Gatorock		417.4	666,400
Gatorock	C15-W15	747.3	500,000
Gatorock		488.2	117,200
Gatorock		552.3	182,100
Gatorock		588.9	232,300
Gatorock	C15-W20	998.6	528,700
Gatorock		873.0	477,400
Gatorock	C15-W25	525.2	242,600
Gatorock		577.7	315,900
Gatorock	C18-W15	792.5	257,500

Table A.10 Summary Comparison of Unconfined Compressive and Modulus Tests

Site	Test No.	Q _u (psi)	E _i (psi)
Gatorock		776.0	272,800
Gatorock	C17-W17	573.9	195,100
Gatorock		461.0	212,300
Gatorock		1,219.0	517,600
Gatorock	C17-W20	722.7	341,600
Gatorock		1,158.3	699,000
Gatorock		1,192.9	280,000
Gatorock		876.3	319,900
Gatorock	C17-W25	877.9	500,000
Gatorock		828.2	365,300
Gatorock		1,327.4	527,400
Gatorock	C20-W21	1,467.4	387,000
Gatorock		1,536.9	725,400
Gatorock		1,052.0	353,000
Gatorock	C20-W25	1,010.7	289,200
Gatorock		1,381.5	497,000
Gatorock		1,309.8	380,000
Gatorock		1,092.3	1,502,200
Gatorock	C20-W25	828.2	1,645,800
Gatorock		803.8	634,600
Gatorock		908.1	1,347,000
Gatorock		2,043.7	621,200
Gatorock	C22-W20	1,939.4	614,000
Gatorock		1,617.7	958,800
Gatorock		1,867.0	1,565,200
Gatorock		1,365.3	698,900
Gatorock	C22-W22	1,483.6	1,111,000
Gatorock		1,509.6	1,936,000
Gatorock		1,452.8	1,582,900
Gatorock		986.7	747,800
Gatorock	C22-W25	1,078.0	620,100
Gatorock		1,016.9	1,037,200
Gatorock		1,027.2	1,261,750
Gatorock	C25-W20	2,518.4	706,500
Gatorock		1,886.0	586,900
Gatorock	C27-W22	1,876.4	691,800
Gatorock	C27-W25	1,565.5	1,442,300
Gatorock		1,436.0	689,500
Gatorock	1uc2	2,888.5	2,300,726
Gatorock	1uc3	2,528.1	2,319,529
Gatorock	1uc4	3,028.0	2,059,139

Table A.10 Summary Comparison of Unconfined Compressive and Modulus Tests

Site	Test No.	Q _u (psi)	E _i (psi)
Gatorock	2uc2	3,176.0	2,858,731
Gatorock	2uc3	3,863.8	4,176,269
Gatorock	3uc2	2,617.1	2,587,237
Gatorock	3uc3	2,340.0	2,204,438
Gatorock	4uc2	2,184.7	2,044,161
Gatorock	4uc3	2,385.8	2,038,967
Gatorock	5uc2	1,661.8	2,074,111
Gatorock	5uc3	2,403.0	2,085,305
Gatorock	6uc2	1,070.0	2,077,350
Gatorock	6uc3	2,215.3	2,007,757
Gatorock	7uc2	1,486.1	1,743,500
Gatorock	7uc3	1,726.8	1,784,500
Gatorock	8uc2	1,412.8	1,616,500
Gatorock	8uc3	1,820.8	1,633,500
SR10	b3-2	161.4	953,059
SR10	b3-2	221.1	898,064
SR10	b3-1	146.9	1,115,551
SR10	b4-1	332.3	781,804
SR10	b4-1	377.5	1,463,230
SR10	b4-1	289.0	1,498,580
SR10	b6-2	128.7	507,169
Hallandale	hbb-r3	994.9	3,803,962
Hallandale	hbb-r3	2,002.4	7,514,171
Hallandale	hbb-r3	1,528.7	5,620,766
Hallandale	hbb-r3	3,041.2	928,537
Hallandale	hbb-r3	3,315.9	1,074,008
Hallandale	hbb-r4	1,823.8	9,194,685
SR20-PMT	th1_c2_A	87.3	21,821.9
SR20-PMT	th1_c2_B	91.7	14,145.1
SR20-PMT	th1_c3_A	87.1	23,047.0
SR20-PMT	th1_c5_A	1,104.5	448,379.6
SR20-PMT	th1_c5_B	2,905.0	1,231,851.0
SR20-PMT	th1_c5_C	2,573.7	1,462,965.9
SR20-PMT	th1_c5_D	3,278.3	1,433,408.8
SR20-PMT	th1_c6_A	1,422.2	687,768.9
SR20-PMT	th1_c6_B	1,410.9	684,281.0
SR20-PMT	th2_c4_A	2,447.4	1,425,235.3
SR20-PMT	th2_c4_B	1,661.7	1,204,239.2
SR20-PMT	th2_c5_A	1,702.1	1,204,536.3
SR20-PMT	th3_c4_A	374.4	466,372.2
SR20-PMT	th3_c7_A	65.3	57,177.8

Table A.10 Summary Comparison of Unconfined Compressive and Modulus Tests

Site	Test No.	Q _u (psi)	E _i (psi)
SR20-PMT	th4_c1_A	14.4	3,875.5
SR20-PMT	th4_c4_A	127.8	86,069.0
SR20-PMT	th4_c4_B	86.8	62,193.2
SR20-PMT	th4_c4_C	112.2	51,264.8
SR20-PMT	th4_c6_A	316.9	30,991.8
SR20-PMT	th4_c6_B	101.9	64,455.4
SR20-PMT	th4_c6_C	182.7	130,178.8
SR20-PMT	th4_c6_D	110.8	84,410.7
SR20-PMT	th4_c6_E	157.1	128,455.6